The daily temperature amplitude
and
surface solar radiation

Knut Makowski

The daily temperature amplitude and surface solar radiation

Knut Makowsk

DISS. ETH NO. 18319

The daily temperature amplitude
and
surface solar radiation

A dissertation submitted to

ETH ZURICH

for the degree of

DOCTOR OF SCIENCES

presented by

Knut Makowski

dipl. Geogr., University of Zurich

born 2 October 1979

citizen of Germany

accepted on the recommendation of

Prof. Dr. Thomas Peter, examiner
Prof. Dr. Atsumu Ohmura, co-examiner
Dr. Martin Wild, co-examiner
Dr. Beate G. Liepert, co-examiner

Zurich 2009

Abstract

The surface solar radiation (SSR) is an important factor influencing the local and global energy budget. Since it has varied measurably over the last decades, the question concerning the impact of these changes arises. An important measure reflecting those changes is the diurnal temperature range (DTR). The DTR is defined as the difference between daily maximum and minimum temperature. From this definition stems a particular suitability of the DTR for investigating changes in SSR. The changes are due mostly to changes in the daily maximum temperature. However, the daily maximum temperature always depends on the preceding daily minimum temperature which, in turn, is influenced by the cooling which occurs between noon and the subsequent sunrise. By subtracting the daily minimum temperature from the daily maximum temperature, the signal of a short and long-term change of SSR is found in the DTR.

It has been widely accepted that DTR decreased on a global scale during the second half of the twentieth century. In this thesis it is shown, however, that the long-term trend of annual DTR has reversed from a decrease to an increase during the 1970s in Western Europe and during the 1980s in Eastern Europe. The trend analysis, performed using polynomial regression analysis and standardized statistical tests, is based on the high-quality dataset of the European Climate Assessment and Dataset Project. It incorporates approximately 200 stations covering the area bordered by Iceland, Algeria, Turkey and Russia for the period 1950 to 2005. National and regional annual means, as well as the pan-European mean have been investigated with respect to trends and reversal periods. Good agreement was found between trends in SO2 emissions, radiation and DTR in areas affected by high pollution. Consequently, it can be inferred that the trends in DTR were influenced by changes in emissions and the associated changes in incoming solar radiation.

Furthermore, this thesis reveals strong correlations between SSR and DTR in Europe between 1970 and 2005, which is the period with the best data availability on seasonal and decadal scales. For this purpose a subset of 31 pairs of stations (31 DTR and 31 SSR) in Europe were used with collocated long term SSR and DTR measurements. When comparing the European mean anomaly time series of SSR and DTR, composed of all 31 individual SSR and DTR records, a correlation coefficient of 0.87 was found in the annual mean and between 0.61 and 0.92 in the seasonal mean anomalies. When investigating the pairs of SSR and DTR individually it was found that most local correlations are lower than the European mean which is potentially due to the local influence of advected air masses, as discussed in the final section of this thesis. The correlations between the pairwise investigated sites decrease with a decrease of the average solar incident angle which decreases either due to season or latitude or both. At high alpine altitude the correlations

are generally lower, again most likely due to an advective influence, as discussed in the last section. The highest correlation on local and seasonal scales seems to be connected to the variability of the large scale circulation in Europe. The output of eleven simulations of current generation regional climate models over Europe confirms the strong relationship between SSR and DTR. The seasonal dependence of the relationship is well reproduced but the absolute values of DTR and SSR are mostly too low. The pattern of decrease (dimming) and increase (brightening) in SSR and DTR was not reproduced in the modeled time series. In summary, there is strong evidence from both models and observations that DTR is a reliable representative of SSR.

Finally, the connection between SSR and two different measures of daily temperature amplitude for twenty sites around the globe is analyzed. One is the previously used DTR and the other is the periodic amplitude (PerAmp). The latter is defined as the monthly average of the warmest hour of the day minus the monthly average of the coldest hour of the day. The averaging causes a reduction of the influences of advected air masses in the PerAmp. Consequently, PerAmp should be more closely connected to SSR than DTR. Comparing the mean annual cycles, the smallest possible difference between the PerAmp and SSR curves is about 10% less than between SSR and DTR. At Arctic sites PerAmp explains 84% of the SSR variability, in the best case, while DTR explains a maximum of 50%. In the mid-latitudes, annual cycles of both temperature amplitude measures and SSR are closely related at individual sites; the perennial variability of DTR and PerAmp is in most cases significant and positively correlated with SSR. Correlations between SSR and PerAmp are higher than between SSR and DTR in more than 60% of the cases. In the long term development the highest agreement between SSR and the daily temperature amplitudes was found in the Asian subtropics and in the Arctic. It can be concluded that PerAmp is indeed more strongly related to SSR than DTR. The substantially larger amount of data which has to be processed to derive PerAmp is, however, a major drawback that needs to be considered.

Summarizing the conclusions of the individual subsections it can be stated that changes in SSR influence the diurnal temperature cycle and thereby mean temperature over both short and long time scales. Due to this strong connection, the diurnal temperature amplitude holds the key to understanding past changes of SSR and disentangle surface solar and greenhouse influences on global warming.

Zusammenfassung

Die solare Einstrahlung an der Erdoberfläche (surface solar radiation - SSR) ist eine der wichtigsten Komponenten der Energiebilanz. Da die SSR sich im Verlauf der letzten Jahrzehnte messbar verändert hat, drängt sich die Frage nach dem Einfluss dieser Veränderungen auf. Eine wichtige Messgrösse, welche diese Veränderungen potentiell widerspiegelt, ist die tägliche Amplitude der Lufttemperatur (diurnal temperature range - DTR). Die DTR ist definiert als Differenz zwischen dem absoluten Tagesmaximum und dem absoluten Tagesminimum der Temperatur. Aus dieser Definition lässt sich direkt die gute Anwendbarkeit der DTR zur Untersuchung der Veränderung der SSR ableiten. Veränderungen der SSR schlagen sich grösstenteils in der täglichen Maximaltemperatur nieder. Diese ist jedoch immer abhängig von der erreichten Minimaltemperatur des vorangegangenen Tages. Die Minimaltemperatur ihrerseits hängt von der Abkühlung zwischen der Mittagszeit und dem darauffolgenden Sonnenaufgang ab. Durch die Reduktion der Maximaltemperatur um die Minimaltemperatur wird sowohl das Signal der kurzfristigen, wie auch der langfristigen Variationen der SSR in der DTR manifestiert.

Es wird allgemein als zutreffend betrachtet, dass die DTR global gesehen während der zweiten Hälfte des zwanzigsten Jahrhunderts abgenommen hat. In der vorgelegten Arbeit wird jedoch für Europa eine Trendumkehr bezüglich der Langzeittrends aufgezeigt. Die Umkehr findet während der 70er Jahre in Westeuropa und während der 80er Jahre in Osteuropa statt. Die Trendanalyse, welche unter Anwendung polynomialer Regressionsverfahren und standardisierten statistischen Tests durchgeführt wurde, basiert auf dem qualitativ hochwertigen Datensatz des European Climate Assessment and Dataset Projektes. Sie beinhaltet Daten von rund 200 Stationen, für den Zeitraum 1950 bis 2005. Die Stationen sind auf ein Gebiet verteilt, welches von Island, Algerien, der Türkei und Russland umschlossen wird. Im Rahmen der Analyse wurden nationale, überregionale und ein gesamteuropäisches Mittel der DTR bestimmt, welche bezüglich Trendverlauf und Trendumkehr untersucht wurden. Beim Vergleich der gemittelten DTR - Zeitreihen mit der langfristigen Entwicklung von SSR und SO_2-Emissionen konnten in den Regionen mit hohen Emissionen Übereinstimmungen im Trendverlauf identifiziert werden. Demzufolge kann geschlussfolgert werden, dass die Entwicklung der DTR teilweise von der Entwicklung der Emissionen und den damit verbundenen Veränderungen der SSR abhängt.

Im Weiteren werden in der vorgelegten Arbeit die hohen Korrelationen zwischen SSR und DTR zwischen 1970 und 2005 in Europa auf saisonaler und mehrdekadischer Basis aufgezeigt. Zur Bearbeitung dieses Themenbereichs wurde ein Datensatz bestehend aus 31 Stationspaaren (31 DTR und 31 SSR) mit Langzeitmessungen in Europa verwendet. Beim Vergleich der gemittelten europäischen DTR und SSR Zeitreihen, welche aus den

Anomalien aller 31 Einzelzeitreihen bestehen, wurden Korrelationskoeffizient von 0.87 für die Jahresmittel und zwischen 0.61 und 0.92 für die saisonalen Mittel bestimmt. Bei der individuellen Untersuchung der Stationspaare zeigte sich, dass die lokalen Korrelationen zumeist niedriger sind als jene des europäischen Mittels, was durch den lokalen advektiven Einfluss verursacht wird, wie im abschliessenden Kapitel dieser Arbeit diskutiert. Die Korrelation zwischen den paarweise untersuchten Stationen nehmen in Jahreszeiten und Breiten mit geringerem Einstrahlungswinkel sowie in alpinen Hochlagen rasch ab. Hohe Korrelationskoeffizienten auf regionaler und saisonaler Ebene scheinen mit der Variabilität der grossräumlichen Zirkulation über Europa zusammen zu hängen. Die Ergebnisse von elf aktuellen Regionalen Klimasimulationen für den Raum Europa bestätigen den starken Zusammenhang zwischen DTR und SSR. Die saisonale Abhängigkeit der Übereinstimmung zwischen DTR und SSR wird in den Modellen ebenfalls richtig reproduziert, jedoch sind die berechneten absoluten Werte meist zu tief. Das für die SSR und DTR bekannte Entwicklungsmuster von Abnahme (dimming) und Zunahme (brightening) wurde in den modellierten Zeitreihen zumeist nicht reproduziert. Sowohl die modellierten wie auch die gemessenen Daten geben jedoch Grund zu der Annahme, dass die DTR ein zuverlässiger Indikator für die Entwicklung der SSR ist.

Abschliessend wurde in dieser Arbeit der Zusammenhang zwischen der SSR und zwei unterschiedlichen Masszahlen der täglichen Temperaturamplitude für zwanzig global verteilte Stationen beleuchtet. Eine der beiden Masszahlen ist die bereits zuvor verwendete DTR die andere ist die Periodische Amplitude (PerAmp). Letztere ist definiert als Differenz der im Monatsmittel wärmsten und kältesten Stunde des Tages. Die Mittelung verursacht eine Reduktion des advektiven Einflusses auf die PerAmp. Folglich sollte die PerAmp in engerem Zusammenhang mit der SSR stehen als die DTR. Beim Vergleich der mittleren Jahreszyklen zeigt sich, dass die kleinstmögliche Differenz zwischen der PerAmp und der SSR etwa 10% geringer ist als jene zwischen SSR und DTR. An den arktischen Stationen erfasst die PerAmp im besten Fall 84% der SSR Variabilität während die DTR maximal 50% widerspiegelt. An jeweiligen Stationen der mittleren Breiten sind die Jahreszyklen beider Messgrössen eng mit der SSR verbunden. Die mehrjährige Variabilität von DTR und PerAmp ist meist signifikant und positiv mit der SSR korreliert. Die Korrelationen zwischen SSR und PerAmp sind in mehr als 60% der Fälle höher als zwischen SSR und DTR. Die höchsten Korrelationen bezüglich der Langzeitentwicklung zwischen der SSR und den Masszahlen der Amplitude Tagestemperatur sind in den Subtropen Asiens und in der Arktis zu finden. Gesamthaft kann daraus geschlussfolgert werden, dass die PerAmp tatsächlich stärker mit der SSR verbunden ist als die DTR. Die deutlich grössere Datenmenge welche zur Bestimmung der PerAmp verarbeitet werden muss, ist jedoch ein grosser Nachteil bei der Analyse, der mit in Betracht gezogen werden muss.

Zusammenfassend kann auf Basis der Schlussfolgerungen aus den einzelnen Teilabschnitten festgehalten werden, dass Veränderungen in der SSR langfristiger und kurzfristiger Natur, Einfluss auf die tägliche Temperaturamplitude und damit die Durchschnittstemperatur haben. Infolge des starken Zusammenhangs mit der SSR

beinhaltet die tägliche Temperaturamplitude das Potential, die zurückliegende Entwicklung der SSR zu untersuchen und damit den Einfluss von Veränderungen in der kurzwelligen Einstrahlung und der langwelligen Ausstrahlung auf die globale Erwärmung zu trennen.

Table of contents

1 Introduction

1.1 Motivation

The fact that the presence or absence of sunshine alters the temperature on the Earth's surface is self-evident since it is easily perceptible to everyone. The amount of sunlight that reaches the surface is influenced by different factors on many different timescales. At a given place it varies within seconds when clouds block the sun's rays from directly reaching the surface. For the entire globe it can vary during thousands of years as the Earth's mean distance from the sun is altered by its changing orbit.

Changes in the amount of sunlight reaching the Earth altered the living conditions during the late Holocene enormously. During the Medieval Warm Period wine could be cultivated all over England. In contrast, the Little Ice Age caused famines due to poor harvests, which exacerbated survival in many parts of the world. In preindustrial times changes in the amount of sunlight reaching the Earth's surface were caused by natural processes. These changes originated either from the Earth, for e.g., volcanic eruptions, or came from the Sun, altering its output by the number of sunspots and faculae, or from changes in the orbital parameters (also termed Milanković parameters). During the last two centuries humans, however, have gained the power to alter the input (output) of energy to (from) their planet. So far, unfortunately, mankind has altered the climate system only incidentally and has worsened living conditions.

Today, the best-known anthropogenic change of the climate system happens through emissions of carbon dioxide and other greenhouse gases. The increase of the carbon dioxide concentration in the atmosphere causes additional retention of energy within the system. Most of the emitted anthropogenic carbon dioxide originates from the combustion of fossil fuels which are used to produce energy. Fossil fuels also contain sulfur which is emitted during combustion in gaseous form, as sulfur dioxide. Further, when combustion takes place under suboptimal conditions precursor gases of carbonaceous aerosols and solid soot particles are emitted.

Carbonaceous and sulfuric acid aerosols, which stem from sulfur dioxide emissions, alter the radiative properties of the atmosphere in different ways than carbon dioxide. While carbon dioxide retains energy in the troposphere by absorbing the emitted longwave radiation emitted from the surface, carbonaceous and sulfurous particles prevent the incoming shortwave radiation from reaching the Earth's surface by absorbing and reflecting it and thus, as an immediate response, cooling the surface. In contrast to carbon dioxide, which as a gas lasts for a long time in the atmosphere, carbonaceous and sulfuric

acid aerosols are washed out of the atmosphere rather quickly. This means when emissions stop, the atmospheric concentration will decrease within days to months.

Both carbonaceous aerosols and sulfuric acid have a rather drastic influence on human living conditions. Carbonaceous aerosols, on the one hand, blur the atmosphere; a frequent phenomenon during special weather situations in London in the middle of the last century was the well-known London-smog. On the other hand, it was discovered that it can cause serious damage to the lungs. In most extreme cases it can be responsible for lung cancer. Sulfur dioxide emissions lead in the presence of oxidants in the formation of sulfuric acid. When sulfuric acid is washed out of the atmosphere by precipitation it can acidify and degrade soil, which can lead to forest dieback and crop loss. Buildings made from sand- and limestone can be damaged by enhanced erosion.

As a consequence of the negative effects of sulfuric and carbonaceous emissions, technologies were developed to reduce the sulfur content of fossil fuels and to improve the combustion process which reduces carbonaceous emissions. While the build up of emissions had led to a reduction of the amount of sunlight reaching the surface (dimming), its politically regulated reduction led to in increase of the same (brightening). The overall change in incoming radiation that was actually measured during the last decades is small if still significant. It is in general not uniform and can be altered by many factors. Despite this, it should still have a measurable influence on the long term temperature development.

Investigating only the mean temperature with respect to dimming and brightening would, however, makes little sense, since it incorporates all the influences during a 24-hour day. A much better measure might be the daily maximum temperature, which is predominantly caused by the short heating period after dawn. Thus, it embodies changes of the incoming radiation over longer time scales. The absolute maximum of each day however is dependent on the amount of cooling taking place in the afternoon and during the previous night. Ideally the minimum temperature which is normally reached shortly before or after dawn contains this information. So by reducing the maximum temperature by the amount of the minimum temperature one restores most of the imprint of the solar signal on the daily temperature development. The difference between daily maximum and the daily minimum temperature is a measure of the overall amplitude or range of temperatures, which have been reached during a 24 hour period, or a diurnal cycle. Subsequently, it is called the diurnal temperature range. The relationship between the surface solar radiation and the diurnal temperature range are the subject of the presented thesis.

1.2   Outline

Chapter 2 [*Makowski et al.*, 2008] presents the results of a detailed trend analysis for the greater European area, between 1950 and 2005. Further the connections between diurnal temperature range, surface solar radiation and sulfurous emissions are discussed.

Chapter 3 [*Makowski et al.*, 2009] deals with the quantitative connection between diurnal temperature range and surface solar radiation. The investigated period is 1970-2005. Besides station data, gridded datasets and regional climate model output for the overall European domain is analyzed. Further various aspects of short variability and long term development are light and attributed to potential forcings such as large scale circulation.

Chapter 4 [*Makowski and Ohmura*, 2009] focuses on the influence of advected air masses on the diurnal temperature cycle at stations in different climatological regions and various altitudes. The focus is put on the deeper examination of the potential advantages of an alternate diurnal temperature measure, the periodic amplitude.

Chapter 5 summarizes briefly the main issues of the chapters 2-4 and points towards emerging issues based on the findings in this thesis.

Appendix A [*Wild et al.*, 2007] completes the overall picture, showing the close connection between diurnal temperature range and surface solar radiation by presenting global scale results derived from a gridded dataset. The focus in this article is put on large scale, long term connections during the second half of the last century.

2   European DTR trends

Diurnal temperature range over Europe between 1950 and 2005

K. Makowski, M. Wild, A. Ohmura

Institute for Atmospheric and Climate Science, ETH Zurich, Switzerland

Abstract

It has been widely accepted that diurnal temperature range (DTR) decreased on a global scale during the second half of the twentieth century. Here we show however, that the long-term trend of annual DTR has reversed from a decrease to an increase during the 1970s in Western Europe and during the 1980s in Eastern Europe. The analysis is based on the high-quality dataset of the European Climate Assessment and Dataset Project, from which we selected approximately 200 stations covering the area bordered by Iceland, Algeria, Turkey and Russia for the period 1950 to 2005. We investigate national and regional annual means as well as the pan-European mean with respect to trends and reversal periods. 17 of the 24 investigated regions including the pan-European mean show a statistical significant increase of DTR since 1990 at the latest. Of the remaining 7 regions, 2 show a non-significant increase, 3 a significant decrease and 2 no significant trend. Changes in DTR are affected by both surface shortwave and longwave radiation, the former of which has undergone a change from dimming to brightening in the period considered. Consequently, we discuss the connections between DTR, shortwave radiation and sulfur emissions which are thought to be amongst the most important factors influencing the incoming solar radiation through the primary and secondary aerosol effect. We find reasonable agreement between trends in SO_2 emissions, radiation and DTR in areas affected by high pollution. Consequently, we conclude that the trends in DTR could be mostly determined by changes in emissions and the associated changes in incoming solar radiation.

2.1 Introduction

Satellite and ground based measurements for Europe show that the mean surface air temperature has increased overall during the second half of the last century [*Trenberth et al.*, 2007]. For the 1950s and 1960s, a characteristic phase of roughly no increase or even decrease is apparent. Since the late 1970s an accelerated increase in the mean temperature was observed. The slow increase of the mean temperature followed by a rapid increase is especially evident during the summer months [*Trenberth et al.*, 2007] where the incoming shortwave radiation is one of the most dominant factors for the daily temperature development. This leads to the hypothesis that changes in the incoming solar flux at the surface had a discernible influence on the mean temperature development between 1950 and 2000 [*Wild et al.*, 2007]. Measurements of shortwave radiation at the surface, from stations around the globe, have shown that the incoming flux has significantly decreased and subsequently increased in many of the investigated stations within the last 4 to 5 decades [*Ohmura and Lang*, 1989; *Liepert and Kukla*, 1997; *Gilgen et al.*, 1998; *Stanhill and Cohen*, 2001; *Roderick and Farquhar*, 2002; *Pinker et al.*, 2005; *Wild et al.*, 2005]
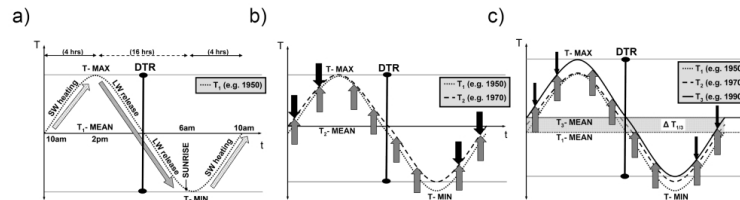

Figure 2.1 *Sketch of mean diurnal temperature (T) cycle under a) weak anthropogenic radiative influence, dominant radiative processes are denoted by arrows, b) enhanced shortwave radiative cooling – "global dimming" (represented by the black arrows) and long-wave radiative warming (represented by the grey arrows), and c) weakening shortwave radiative cooling – "global brightening" (thinner black arrows) and continued long-wave radiative warming.*

(DTR: diurnal temperature range; T-MAX/-MIN: daily mean maximum/minimum; T-MEAN: daily mean temperature, SW: shortwave, LW: longwave, Δ T1/3: overall amount of warming from state a) to c) or e.g. 1950 to 1990 respectively)

The diurnal temperature range (DTR) is considered a suitable measure to investigate the counteracting effects of longwave and shortwave radiative forcing, because the diurnal minimum is closely related to the longwave radiative flux, while the diurnal maximum is predominantly determined by shortwave radiation (Figure 2.1a). It is known that the DTR has been decreasing since the 1950s on a global scale due to a strong increase of the diurnal minimum [*Karl et al.*, 1984; *Karl et al.*, 1993; *Kukla and Karl*, 1993]. Comparison of GCM simulations with observations have shown that the DTR decrease has been underestimated due to a strong increase in the modeled maximum temperature. However, a change in aerosol burden was not included [*Braganza et al.*, 2004]. The change in DTR has

formerly been addressed mainly as consequence of cloud cover development, precipitation, change in irrigation and surface albedo or water vapor feedback [*Stenchikov and Robock*, 1995; *Dai et al.*, 1997; *Easterling et al.*, 1997; *Dai et al.*, 1999; *Stone and Weaver*, 2003; *Englehart and Douglas*, 2005; *Vose et al.*, 2005]. Many of the cited publications have concluded that neither of these factors alone is likely to be the unique explanation of the observed changes in DTR [*Easterling et al.*, 1997]. We argue that shortwave radiation directly or via feedbacks is a major factor for the changes in DTR since only the shortwave radiation – modulated by the atmospheric aerosol burden – could exert a strong and sufficiently homogeneous effect to change DTR on a global scale [*Liu et al.*, 2004b; *Wild et al.*, 2007].

The decrease of the solar flux and its relative cooling effect can been seen as a blocking action against the increase of temperature caused by the greenhouse effect. Consequently the diurnal maximum temperature remains constant while the diurnal minimum is forced to increase (Figure 2.1b). The recovery of surface solar radiation results in a removal of the blocking on diurnal temperature development thus leading to an increase of DTR and daily maximum respectively, thereby revealing the full extent of global warming [*Wild et al.*, 2007] (Figure 2.1c).

In the present study a detailed investigation of this issue is conducted focusing on the European area where the best coverage with observational data can be found.

2.2 Data and Methods

We chose the data products of the European Climate Assessment and Dataset Project (ECA&D-P) for an internally consistent investigation of the DTR evolution during the recent decades. It contains freely available data for more than 600 stations with minimum and maximum temperature measurements in daily resolution for different periods between about 1800 and today [*Tank et al.*, 2002].

Because the change of incoming radiative flux at the surface is considered very important to DTR development and is measured since the 1950s, the complete second half of the last century is investigated in this study. From the ECA&D-P dataset, all stations with data for the period 1951 up to 2003 (or up to 2005 where available) were selected and national means were calculated. The time series of a station was dismissed if it had more than five years with data gaps or if two or more consecutive years were affected by these gaps. In addition, each time series was checked for jumps in the DTR. If jumps of more than half degree were caused by filled data (from neighboring stations, performed during ECA&D-P), then the value was replaced by an interpolated value, on monthly basis, if the measurement from the original site was available in the previous and following year. In total less than 0.5% of the monthly values used in this study were interpolated due to missing data. Systematic errors probably due to data submission were found in all stations in Iceland, Denmark and Romania. For Iceland all data after 1998, for Denmark all data after 2002 and for Romania all data had to be discarded and these were replaced by data
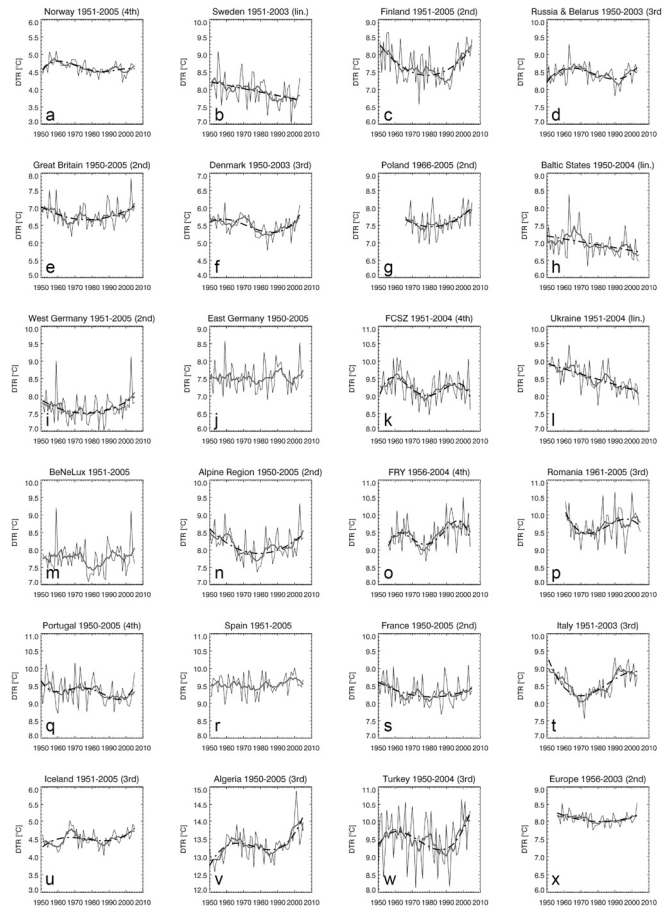
Figure 2.2 *Time series of annual mean DTR for each investigated region. All y-axes are scaled to 3 degrees Celsius for a better comparability. Graphs from row 1-5 are geographically arranged – except: surrounding regions of Europe as well as European mean are in the last row. The order of the best suitable polynomial trend model according to Table 2.1 is indicated in brackets next to the name of the region and the investigated period. Thick, grey, solid line presents 7 year running mean. The thick, black, dashed line shows the fitted trend model, if no black line is plotted none of the models was significant above the 90% level.*

FCZS – former Czechoslovakia, FRY – Former Republic of Yugoslavia

which we obtained directly from the respective national meteorological service. For the region of the former Republic of Yugoslavia (FRY) all data prior to 1956 had to be dismissed due to quality issues. For Poland, data are available only since 1966. The temporal coverage was still considered sufficient to investigate decadal changes in DTR.

To obtain a sufficient number of stations for the calculation of regional annual means (Figure 2.2), station measurements were grouped either nationally or by averaging over several small nations. Netherlands, Luxembourg and Belgium were drawn together as BeNeLux, likewise the states of the FRY; Estonia, Lithuania and Latvia were grouped as Baltic States, Slovakia and the Czech Republic to former Czechoslovakia (FCZS).

Conversely, Germany was divided into an eastern and a western part according to the border line from the pre-1989 period. This is to take account of the different development of atmospheric aerosol burden in the two countries, which depends mainly on the industrial emissions within the range of some tens to hundreds of kilometers upstream. The overall resulting data coverage is indicated by the small blue crosses shown in Figure 2.3, identifying 189 (168 with coverage 1956-2003) out of the original 604 ECA&D-P stations satisfying the criteria described above.

Subsequently these national annual mean time series were fitted by polynomials up to fourth order, to facilitate the characterization and quantification of the DTR trend (Figure 2.2). The rational for fitting polynomial trend models was investigated by applying multiple regression analysis and control of lagged autocorrelation within the residuals to assure stationary white noise. The regression analysis, followed by calculation of statistical significance level (1 – P-values; given in %) based on a standard T-test was performed for every coefficient for fits between first order (linear) and fourth order polynomials as summarized in Table 2.1 (for further details see reading example, section 2.6.1).

For most regions R^2 increased together with the statistical significance of the fitted model, hence making it easy to decide which of the investigated models performs best. If the comparison of R^2 and p-values (significance levels) showed an ambiguous result (see e.g. Table 2.1, line 5, Denmark), the residuals were checked in more detail and the model with the lowest autocorrelations in the residuals was selected (not shown). Note that only models with no significant autocorrelations were accepted. The annual mean time series together with the fitted trend curve and the seven year running mean trend for all investigated regions as well as the European mean are shown in Figure 2.2.

Further information for each time series was obtained by estimating the year of reversal from decreasing to increasing DTR (applies not to regions with linear trends). The estimation was performed by calculating the minimum in the seven year running mean (Figure 2.2) for the period 1965 to 1995. For the example of Finland (Figure 2.2c), the running mean given as gray bold line shows a clear local minimum in 1989 (compare year given in Figure 2.3 and diamond at the row "Finland" in Figure 2.4). The particular period 1965 to 1995 was chosen since it embraces the whole era of reversal from dimming to brightening [*Wild et al.*, 2005].

Table 2.1 *Data for each investigated region, including overall Europe and each trend type. Order: Western Europe N–S; Eastern N–S, surrounding regions, Europe; Columns from left to right: (1) Name of the region, (2) R^2 and significance codes for each coefficient (- < 90%, o 90%-95%, x 95% - 99%, xx 99% - 99.999%, xxx > 99.999%), columns (3) to (5) equal to column (2) but for higher order polynomial fits, (6) number of stations for the mean calculations, and (7) data period (for more details see example in section 2.6.1). R^2's in bold denote the best suitable model according to R^2, significance and residuals (not shown), which was subsequently used in Figure 2.2.*

FCZS – former Czechoslovakia, FRY – Former Republic of Yugoslavia

	1st		2nd		3rd		4th		No.	Period
Norway	0.15	xx	0.17	-	0.26	o x x	**0.32**	x x x o	4	51-05
Sweden	**0.15**	xx	0.15	-	0.16	-	0.20	-	5	51-03
Finland	0.01	-	**0.25**	xxx xxx	0.27	-	0.28	-	3	51-05
Great Britain	<0.01	-	**0.14**	xx xx	0.14	-	0.14	-	3	50-05
Denmark	0.06	o	0.18	xx x	**0.30**	x xx	0.33	-	5	50-03
East Germany (DDR)	<0.01	-	<0.01	-	<0.01	-	<0.01	-	12	50-05
West Germany (BRD)	<0.01	-	**0.12**	x x	0.12	-	0.12	-	13	51-05
BeNeLux	<0.01	-	0.02	-	0.04	-	0.06	-	9	51-05
Alpine	0.01	-	**0.24**	xxx xxx	0.25	-	0.25	-	2	50-05
France	0.02	-	**0.11**	x x	0.11	-	0.11	-	25	50-05
Italy	0.03	-	0.42	xxx xxx	**0.52**	xxx xxx xx	0.59	x xx	4	51-03
Spain	0.02	-	0.05	-	0.05	-	0.08	-	9	51-05
Portugal	0.05	o	0.05	-	0.06	-	**0.12**	o o o	3	50-05
Russia & Belarus	0.02	-	0.02	-	**0.22**	xx xxx xxx	0.22	-	36	50-03
Baltic States	**0.13**	xx	0.15	-	0.16	-	0.17	-	9	50-04
Poland	0.07	o	**0.17**	o x	0.17	-	0.17	-	2	66-05
FCZS	0.02	-	0.03	-	0.04	-	**0.16**	x xx xx x	3	51-04
Ukraine	**0.37**	xxx	0.37	-	0.37	-	0.37	-	9	51-05
FRY	0.08	x	0.11	-	0.13	-	**0.26**	x x xx	4	56-04
Romania	0.01	-	0.05	-	**0.13**	x x o	0.16	-	19	61-05
Iceland	0.07	o	0.07	-	**0.18**	x x	0.22	-	4	51-05
Algeria	0.17	xx	0.19	-	**0.37**	xx xxx xxx	0.37	o -	3	50-05
Turkey	<0.01	-	0.04	-	**0.13**	o x	0.13	-	3	50-04
Europe	0.01	-	**0.14**	x x	0.21	-	0.21	- o	168	56-03

The results are presented in Figure 2.3 and Figure 2.4. The numbers displayed in Figure 2.3 give the year of the minimum of DTR. If they are printed in brackets no significant trend could be estimated (compare Table 2.1).

In addition to the minimum DTR value between 1965 and 1995, all values within the lowest 10% of the difference between maximum and minimum (7 year running mean) value within that period have been calculated to give additional information on the distinctness of the reversal. In Figure 2.4 the years below and equal to the 10th-percentile are marked with dashes, diamonds show the minimum (for further details on the method see detailed example, section 2.6.2).

2.3　Results

In the following section we discuss annual means of the DTR records, starting with the regional averages as described above, followed by a description of the European mean. The data records and polynomial fits determined in this analysis are compiled in Figure 2.2. By the use of regional averages we aim to underline the hypothesis that DTR is affected by changes in regional emissions influencing shortwave radiation reaching the ground. Detailed information for each country or region can be found in Table 2.1 and Figure 2.2-Figure 2.4. A complete descriptions of all regions (except the European mean, see below) shown in Figure 2.2 is provided in section 2.7.

For most of Western Europe a distinct reversal from decreasing to increasing DTR is visible. The fitted polynomial trends are significant in the Great Britain, Germany, Poland, Finland, France, Italy and Switzerland/Austria. For Spain and the Benelux an alike development of decrease and increase in DTR can be seen from the running mean but the fitted polynomial trends miss the 90% significance level.

Circumjacent countries, as Portugal, FRY, FCZS and Norway show trends significant at the fourth order polynomial with pronounced periods of increasing DTR in recent decades. In North-Eastern Europe a region covering Sweden, the Baltic States and the Ukraine, with a continued decrease in DTR can be identified. All decreasing linear trends are significant at the 99% level.

The countries located farther away from central Europe, namely Russia, Belarus, Turkey, Algeria and Iceland show trends which are best described by a third order polynomial. All coefficients for all trends are significant at the 95% level except for the first (not significant) and second coefficient (90% level) of Turkey. In addition to the presently increasing DTR a prominent feature in the annual mean time series of the above mentioned countries is a second, earlier increase in DTR between 1950 and 1960 which is addressed in more detail in the discussion section.
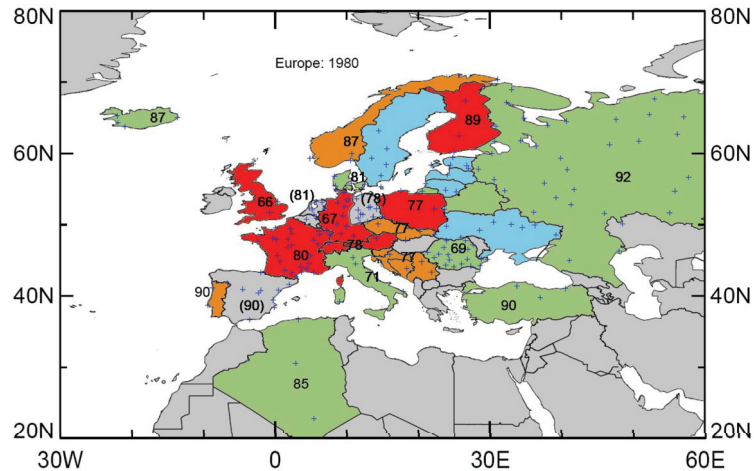

Figure 2.3 *Distribution of statistical significant, fitted DTR trend models. Blue - linear (all trends are negative), red - second order (all trends show first a decrease, then an increase), green - third order (all trends show first an increase, then a decrease, then an increase) orange – forth order polynomial. Numbers are the year of reversal from decrease to increase in the 7 year running mean, derived from the annual mean DTR of region/country where denoted. The uncertainty of the actual year of reversal can be inferred from Figure 2.4. The trend model is not significant (>90%) if the numbers are in brackets, consequently the investigated region is also not color-coded (Spain, Eastern-Germany, Benelux). Blue crosses represent stations investigated.*

Overall, the farther away the country is located from central Europe the more recent is the time of reversal from decrease to increase of DTR. The earliest can be found in the UK (1967) and Germany (1967), the latest in Iceland (1987), Turkey (1990) and Russia (1992).

From Figure 2.4 extended periods of reversal can be seen in Romania, Norway and Denmark. For Romania, which is an outlier compared to the surrounding nations, the early appearing of the lowest value in the 7 year running mean is put more into perspective by the "error bars" in Figure 2.4, equally true for the late reversal in Norway and the early one in Denmark.

For the European geographical mean between 1956 and 2003, 168 stations were used. To avoid biases, series shorter than this period have been excluded. The European trend is best described by a second order polynomial (Figure 2.2x). Both coefficients are significant at the 95% level. The reversal from decrease to increase takes place in the early 1980s. This overall character of the averaged European DTR is even strengthened if shorter data series such as those from Romania and Poland were included (alternative mean not shown).

2.4   Discussion

The extent of the DTR is determined by many different factors, such as surface solar radiation or sunshine duration, cloud cover connected with changes in large scale circulation or aerosols, soil moisture and water vapor content of the atmosphere.

Change in water vapor for example leads to an asymmetry in the DTR [*Stenchikov and Robock*, 1995] by changing longwave and shortwave downwelling fluxes. A continued increase in water vapor due to anthropogenic influence would lead to a slightly reduced downwelling shortwave and increased downwelling longwave radiation at the surface. This would consequently lead to a continued reduction of DTR which, however, we did not observe in the investigated area, and therefore do not consider water vapor as a major factor influencing DTR in Europe.

Soil moisture plays an important role by damping the DTR as energy is consumed by evaporation during the daytime and released by condensation during the nighttime. However, according to Robock and Li [2006], long-term changes in soil moisture are coupled to changes in solar radiation and tropospheric air pollution respectively at least on regional scale in Russia and the Ukraine, where long-term records of soil moisture data are available.

For the inter-annual variability of DTR the total amount of cloud cover as well as the cloud optical properties play an important role again by altering longwave and shortwave downwelling fluxes [*Karl et al.*, 1993]. Clouds alter DTR mostly by damping the daytime maximum via a strong reduction of surface solar radiation, while the influence on the nighttime minimum seems to be rather small [*Dai et al.*, 1999]. Apart from local convection, long-term changes in cloud cover can be connected to large scale circulation patterns and aerosols. However, the correlation between DTR and cloud cover in Europe for the period 1910 to 1990 is only 0.35 according to Dai et al. [1997].

For the long-term influence of changes in large scale circulation [*Sanchez-Lorenzo et al.*, 2008] show that in Western Europe on a seasonal scale, circulation may have an influence on the long-term development of sunshine duration, which can be used as proxy for surface solar radiation [*Stanhill and Cohen*, 2005]. Still for the overall annual mean long-term trend in sunshine duration, they identified changes in surface solar radiation from anthropogenic aerosol emissions as a more likely explanation.

To sum up, factors influencing surface solar radiation and factors that are influenced by surface solar radiation seem to account for the most of the changes in DTR in Europe. Consequently, we consider changing surface solar radiation as a major cause for the different types of DTR development.
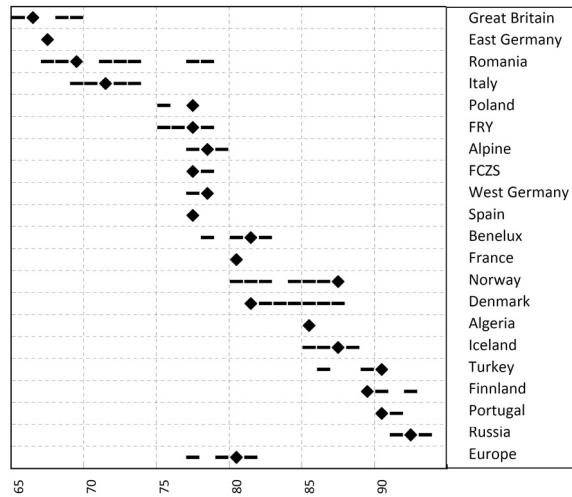

Figure 2.4 *Reversal of 7 year running mean DTR trends. Diamonds represent the year of reversal of DTR as calculated from 7 year running mean trend. Dashed lines show additionally the period covered by values within the lowest 10% of the amplitude of maximum DTR minus minimum DTR (of seven year running mean values) for the period 1965-1995. For more details see example in section 2.6.2.*

FCZS – former Czechoslovakia, FRY – Former Republic of Yugoslavia

Since solar radiation incident at the top of atmosphere has not changed substantially during the investigated period [*Beer et al.*, 2000], two different candidates are likely to have influenced surface shortwave radiation, namely clouds and aerosols (first and secondary effect). Norris and Wild [2007] showed that by removing the cloud cover influence from

surface solar radiation data, the reversal from dimming to brightening becomes even more pronounced for most of Europe. Consequently cloud coverage changes acted as a disguise rather than a cause for the variations in surface solar radiation.

A much more likely candidate for the varying surface solar radiation and DTR trend types and their time shifted reversals are different patterns of emissions, leading to regionally differentiated backscattering of solar radiation by aerosols. A reduction of incoming radiation has been reported by Liepert and Kukla [1997], Gilgen et al. [1998] and Abakumova et al. [1996]. Wild et al. [2005] reported a reversal from global dimming to brightening in mid to late 1980s at widespread locations throughout the world. From Abakumova et al. [1996], a reduction in incoming shortwave radiation until at least 1990 is evident for the specific region of Russia. These results indicate that changes in surface solar radiation were found in many regions though they do not have to be necessarily simultaneous. The global background signal and forcing from aerosol as presented by Mishchenko et al. [2007], showing a general decrease during the 1990s, can be dominated by local influence as described by Alpert et al. [2005]. Publications from Stern [2006] and Lefohn et al. [1999] assume that a reversal from increase to decrease of Eastern European emissions (dominated by Russia) took place in the late 1980s or early 1990s. In contrast, Western European emissions are peaking already during the early 1970s according to Smith et al. [2005], Streets et al. [2006] and Stern [2006]. This is confirmed in Mylona [1996] and Vestreng et al. [2007] who have shown that the maximum in SO_2 emissions from fossil fuel for early industrialized countries, such as the UK or the former Federal Republic of Germany, can be as early as the second half of the 1960s.

2.4.1   DTR, Radiation and Emissions - the biggest European emitters

In the following section we discuss the qualitative connection between trends in SO_2 emissions, sunshine duration, radiation and DTR in several examples. We included the annual sunshine duration in this section as a proxy for surface solar radiation [*Stanhill and Cohen*, 2005], which is only available for a sufficient number of sites since the 1960s. Sanchez-Lorenzo et al. [2007] and [2008] provide data for sunshine duration in Western Europe between 1938 and 2004. SO2 emissions at land level are available from Mylona [1996] and Vestreng et al. [2007]. Vestreng et al. [2007] is partially a succeeding work of Mylona [1996] and both provide SO_2 emission estimates for every fifth year. Therefore, we combined the estimates to one time series if they cover the same source region. Data from Mylona [1996] are available between 1880 and 1990, Vestreng et al. [2007] provide data between 1980 and 2004. For the overlapping period between 1980 and 1990 the data from Vestreng et al. [2007] were favored for the following analysis. Further SO_2 estimates can be derived from Lefohn et al. [1999]. They provide annual estimates of sulfur emissions between 1850 and 1990. Obviously not all sulfurous emissions will be in the form of SO_2 but still we converted all sulfur into SO_2 for the gain of a much simpler comparison against the Mylona [1996] and Vestreng et al. [2007] data. Valuable information on transboundary fluxes and trend development of SO_2 since 1980 can be

obtained from Klein and Benedictow [2006]. Data from long-term surface solar radiation measurement can be found in Ohmura [2006]. A recently submitted paper from Gilgen et al. [2009] provides additional information on reversal years and overall trends from gridded data of the Global Energy Balance Archive. To make the characteristics of the DTR time series more easily comparable against the rather slow changes of emissions and the low pass filter data of sunshine duration, we calculated the eleven year running mean of the annual DTR time series. The miss weighting at the edges was indicated by using dashed lines (Figure 2.5 and Figure 2.6). The emissions of SO_2 were plotted upside down to indicate the potential sulfate aerosol forcing on DTR.
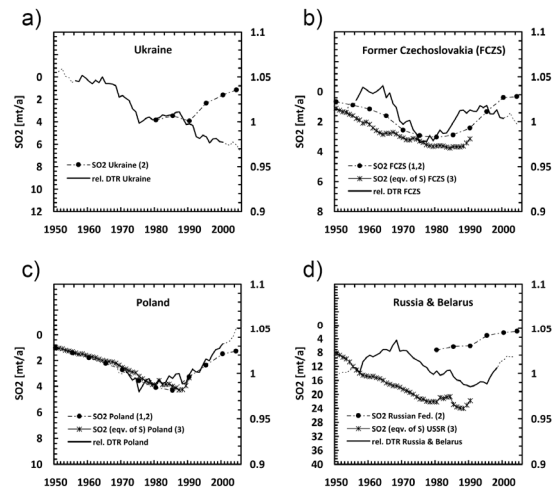

Figure 2.5 *Time series of annual mean DTR and SO_2 emissions. Eleven-year running means of DTR, expressed as relative (rel.) deviations from the 1971-2000 mean, are plotted as solid black line. Differently weighted first and last five years of the time series are denoted as dashed black lines. SO_2 emissions from Mylona [1996] (1) and Vestreng et al. [2007] (2) were plotted up side down, to indicate the presumed forcing. Estimated sulfur emissions from Lefohn et al. [1999] (3) were converted to SO_2 equivalent and also plotted upside down. All SO_2 estimates are expressed in megatons per year.*

According to Berge et al. [1999] the 10 biggest emitters (in total t/a) in Europe are: Bulgaria, France, Germany, Italy, Poland, Spain, Great Britain, Ukraine, Russia and the Czech Republic (or FCZS). Except for Bulgaria all countries above were analyzed with respect to their DTR trends and will be discussed subsequently in more detail beginning with the Eastern European countries, from south to north.

The best fitting trend for the Ukrainian DTR time series is a linear trend with a slope of -0.014°C/a, emphasizing a continuous decrease (Figure 2.2l). A more detailed inspection of the running mean in Figure 2.2l and Figure 2.5 a reveals, however, a tendency towards an increase around 1978 which is reverses to a continued decrease from 1987 onward. Data for emissions are available from 1980 [*Mylona*, 1996] and Lefohn et al. [1999] estimated their values for the Union of Soviet Socialist Republics - USSR), showing a distinct decrease since 1990 which is not reflected in the DTR data. However, the previously described short increase and decrease of DTR is reflected in a short decreasing and increasing period of SO_2 emissions. Surface solar radiation measurements for Odessa show a decrease from 1960 until 1987 (end of data). The described short increase in DTR between 1978 and 1987 is mirrored as well in the radiation time series plot [*Abakumova et al.*, 1996, Figure 4], most evident between 1977 and 1983. To summarize, the continued decrease in DTR since 1980 cannot be explained by a continued increase of national emissions. However, the findings are not contradictory with respect to the connection between DTR and radiation (for further details on the Ukraine, as an example for linear decreasing trends, see section 2.4.3).

For the FCZS, data of emissions are available for the whole period from Mylona [1996] and Vestreng et al. [2007]. The highest values occur around 1980 in line with the reversal of DTR from decrease to increase which is calculated around 1977 (Figure 2.4 and Figure 2.5b). In Gilgen et al. [2009] the reversal of surface solar radiation from dimming to brightening is estimated between 1978 and 1983.

Daily maximum and minimum temperature for Poland is available since 1966. The reversal from decrease to increase is calculated at 1977 in the seven year running mean. The running mean of the Polish time series (Figure 2.2g and Figure 2.5c) shows a short increasing and subsequently decreasing period between 1975 and 1986. The reversal of the second order polynomial fit to DTR which omits the described hump is between 1980 and 1985, which this is close to the peaking of emissions in 1985. Consequently, both reversals are consistent with the reversal in incoming shortwave radiation in 1980.

Russian emissions peak at 1975 according to Vestreng et al. [2007]. Other emission estimates as e.g. from Stern [2006] and Lefohn et al. [1999] suggest that the decrease of emissions started much later namely in the late 1980s (Figure 2.5d) with the breakdown of the former Soviet Union. However, the significant decrease of emissions after the collapse of the Eastern Bloc is reflected in all cited emission estimates. The DTR decrease for Russia lasts until 1990 consistent with the decrease in surface solar radiation [*Abakumova et al.*, 1996] measured at Moscow. Likewise, the observed increase of surface solar radiation at Moscow [*Wild et al.*, 2005] is mirrored in an increasing DTR. Both are potentially caused by the strong decrease of SO_2 emissions reported from various estimates.
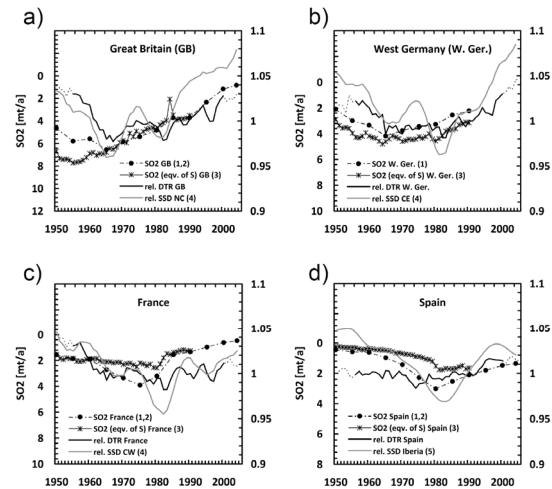
Figure 2.6 *As Figure 2.5. In addition, sunshine duration series from Sanchez-Lorenzo et al. [2008] (4) and Sanchez-Lorenzo et al. [2007] (5) are plotted as solid grey line. Plotted data are low-pass filtered values (11-year window 3 year σ Gaussian low-pass filter) expresses as relative deviations from the 1961-1990 mean.*

In Western Europe the biggest emitters during 1985 and 1995 are France, [*Tank et al.*] Germany, Great Britain and Spain [*Berge et al.*, 1999]. The DTR for all four regions is best described with a second order polynomial trend, significant above 95% except for Spain with p-values of 0.35, (1st coefficient) and 0.21 (2nd coefficient) (not shown). For the comparison of DTR against SO_2 emissions and sunshine duration we used in addition the low-pass filter time-series from Sanchez-Lorenzo et al. [2007] for Iberia to compare it to our DTR data of Spain. In Sanchez-Lorenzo et al. [2008] the same authors provided annual means of sunshine duration for most of Western Europe, split into six regions. Here we also used the low pass filtered data of sunshine duration for the regions NC (north central), CW (central west) and CE (central east). We compared NC to Great Britain, CW to France and CE to West Germany according to their spatial coverage given in Figure 1 of Sanchez-Lorenzo et al. [2008].

For Great Britain a reversal in DTR is apparent around 1965 simultaneously to the emissions from Mylona [1996] of SO_2 which are peaking in 1965, according to Lefohn et al. [1999] emissions reach their maximum already around 1960. The annual sunshine duration from Sanchez-Lorenzo et al. [2008], which covers the central to south-eastern part of the UK, shows a reversal from decrease to increase in the late 1960s. Subsequently, sunshine duration increases along with DTR and the decreasing emissions until the present (Figure 2.6a).

In the former Federal Republic of Germany, the DTR reversal is calculated at 1967 by the 7-year-running mean. Reversal of SO_2 emissions is in 1965 according to Mylona [1996]. The most dominant increase of DTR and decrease of SO_2 respectively, however begins during the 1980s which is in line with the end of the decrease in surface solar radiation in Germany [*Liepert and Kukla*, 1997, Figure 2] and a strong increase in sunshine duration (Figure 2.6b). Notably the horizontal visibility increased already since the second half of the 1960s in most of the Western German stations investigated by [*Liepert and Kukla*, 1997]. These results point to a decrease of turbidity and thus a reduction of aerosol burden of the troposphere.

In France the DTR reversal is calculated at 1980 while SO_2 emissions estimated by Mylona [1996] start to decrease from 1975, Lefohn et al. [1999] in contrast determine the highest value of emissions not until 1980 (Figure 2.6c). The reversal in shortwave incoming radiation is between 1980 and 1986 according to Gilgen et al. [2009]. Sunshine duration reverses between 1980 and 1985. The maximum lag of about one decade between radiation and SO_2 emission [from *Mylona*, 1996] reversals can be explained by the method used to determine the year of reversal. Gilgen et al. [2009] used a second order polynomial fit to define the period of reversal. The reversal in the DTR retrieved from the fitted second order polynomial would be similar, namely around 1980 to 1982 (Figure 2.2s).

Spain as the most southern representative of the largest emitters in Europe has reduced its emissions remarkably since 1980 [*Mylona*, 1996]. The reversal of DTR derived from the 7 year-running mean is at 1977 (Figure 2.2r and Figure 2.4). According to Sanchez-Lorenzo et al. [2007] the reversal for sunshine duration for the whole Iberia Peninsula is in 1982 most evident during spring and summer, with mostly clear sky situations. The period where all three independently investigated measures (namely emissions, DTR and sunshine duration) show a reversal in their long-term behavior lies consequently within 5 years (Figure 2.6d).

To summarize on the section with the biggest emitters in Europe we would like to point to the good qualitative agreement between the low frequency trends in DTR and SO_2 emission estimates in six (four in Western, two in Eastern Europe) of the eight regions analyzed.

The long-term evolution of sunshine duration from Sanchez-Lorenzo et al. [2007] and [2008] supports our conclusions for Western Europe. The biggest disagreement between DTR and SO_2 emissions can be found for Eastern Europe, namely in Russia and the Ukraine. However, trends in surface solar radiation from Abakumova et al. [1996] for these regions support our results for long-term DTR development. To conclude that though we found good agreement, more work involving chemistry climate models with an appropriate input and transport of pollutants is required in order to improve our understanding of the relation between DTR and air pollution in the future.

2.4.2   Long range effects on DTR and Radiation

According to the previous section a further feature which has to be discussed is the inconsistency in the DTR reversal compared to the reversal in emissions in a number of regions such as Finland. The running-mean curve for the DTR in Finland (Figure 2.2c) shows a reversal in the early 1990s, in line with the surface solar radiation measurements, taken in Sodankyla in the north of Finland [*Ohmura*, 2006, Figure 9]. According to Gilgen et al. [2009] 1990 is the year of reversal from dimming to brightening, for the mean of seven stations in southern Finland. Emissions, however, peaked around 1975 [*Vestreng et al.*, 2007]. It can be seen from the EMEP (Co-operative program for monitoring and evaluation of the long-range transmission of air pollutants in Europe) Report 1/06 [*Klein and Benedictow*, 2006] for Finland that for 2004 about 80% of the oxidized sulphur deposition originates from outside Finland. Biggest contributor is Russia with as much as 23% for overall Finland. This implies that the influence on DTR especially for stations in the North and East of Finland is likely to be dominated by Russian emissions, thus giving a possible explanation for the reversal in DTR and surface solar radiation as late as 1989 (Figure 2.4).

Similar to Finland, other countries in Northern Europe, such as Sweden, Norway, Iceland, Latvia, Lithonia and Denmark contribute no more than 10% to their total of oxidized sulphur deposition, leaving these regions as dependent on neighboring countries such as Great Britain, Germany, Poland, Estonia, Ukraine and Russia and their patterns in matters of emissions [*Klein and Benedictow*, 2006].

2.4.3   Linear downward trends of DTR

Another interesting feature is the linear downward trend of the DTR in Sweden, the Baltic States and Ukraine. It is noteworthy that they seem to build a north-west, south-east orientated zone between Eastern and Western Europe (Figure 2.3). The linear decreasing DTR trend is not explainable by the national emission trends of the corresponding regions, since the emissions for all above mentioned countries have declined at least since 1990. Surface solar radiation for southern Sweden and the Baltic States started to increase in the late 1980s [*Ohmura*, 2006; *Gilgen et al.*, 2009], subsequently DTR in both regions levels-off or increases slightly as well. However, during the 1990s DTR stopped increasing which resulted in a significant decreasing linear trend for the whole period. The continuous decrease of DTR in Ukraine cannot be explained by a continued increase of emissions. Also, no radiation data is available for further interpretation. Support for the findings on an overall decreasing DTR can be found from soil moisture measurements. Robock and Li [2006] have shown that between 1958 until the mid 1990s soil moisture increased significantly for the Ukraine. They state that precipitation and temperature alone could not have caused this development. Using a land surface model they show that a reduction in downward shortwave radiation could have caused the observed increase in soil moisture, which is in line with the DTR decrease noted above.

2.4.4   Early increase in DTR and radiation

The final feature we want to discuss in detail is the early increase of DTR during the 1950s and 1960s, visible in different regions all over Europe but mainly in the northern, eastern and the periphery regions, namely Norway, Russia, the Baltic States, FCZS, FRY as well as Iceland, Algeria and Turkey. The early increase visible from the different DTR time series might be due to an 'earlier brightening' during this period. The hypothesis of an earlier brightening in Eastern Europe during the 1950s and 1960s is again supported by soil moisture measurement. Figure 3 of Robock and Li [2006] suggests that soil moisture in Russia decreased slightly between 1958 and 1970, indicating an increase in radiation.

No radiation data is available from the above mentioned regions prior to 1960. Still we can assume a similar technological development for Eastern Europe as for Western Europe but with a time shift of one to two decades as indicated by a later reversal in emissions and radiation during the period since 1960.

By investigating radiation and radiation related measurements for Western Europe prior to 1950 we can consequently find potential explanations for the observed early increase of the DTR. Evidence for an early brightening period (increase of incoming shortwave radiation) in Western Europe is presented in Ohmura [2006]. The surface solar radiation data in Figure 1 of Ohmura [2006] for Wageningen, Stockholm, Davos and Potsdam increases until the 1950s. For Wageningen this is supported from De Bruin et al. [1995]. In Sanchez-Lorenzo et al. [2008] sunshine duration for Western Europe increases from 1938 (earliest value of plot) until 1950.

2.5   Conclusions

We investigated annual mean DTR for the period 1950 until 2005 for 23 different countries and regions in and around Europe as well as Europe as a whole. A total of 16 out of these 23 regions as well as the European mean show a statistically significant period of decrease and a subsequent increase in DTR. Two additional regions (BeNeLux, Spain) show an increase, which however is not statistically significant in the multiple regression analysis. Of the remaining five regions, two (East Germany, Portugal) show no specific trend and three (Sweden, Baltic States, Ukraine) regions show a continuation of the decreasing trend. The trend analysis is limited by the lack of a standard homogeneity procedure and by the limited number of available measurement sites and their spatial distribution.

The connection between DTR, shortwave radiation and SO_2 emissions has been qualitatively discussed with respect to a common trend reversal. The period of reversal of DTR from decrease to increase is in most cases in line with social and economic development as indicated by SO_2-emissions or deposition, respectively. All reversals of DTR were shown to take place between 1965 and 1990. This is consistent with the change from decrease to increase of incoming shortwave radiation ("Global Dimming" to "Global Brightening"). Consequently, we conclude that the long-term trends in DTR are strongly

affected by changes in incoming shortwave radiation, presumably largely influenced by direct and indirect effects of aerosol from sulphurous emissions.

This may suggest that in more regions around the globe DTR will increase if the surface solar radiation continues to increase on a widespread basis.

2.6   Appendix A:

2.6.1   Illustrative example how to read Table 2.1

The example of Denmark, (Table 2.1, line 5) reads as follows: the first column contains the name of the region. The second column contains the R^2 between the time series and the best fitted trend of the form:

$$f(x) = f_1 * x + f_o \qquad (2.1)$$

Following the R^2 a small "o" indicates that the linear coefficient is statistically significant above the 90% level or in more common words: it is 90% likely that the linear coefficient cannot be zero if the time series should be represented by the given equation. Column three contains again the value for the R^2. However, now the comparison is performed between the time series of annual mean DTR of Denmark and the best fit of the type:

$$f(x) = f_2 * x^2 + f_1 * x + f_o \qquad (2.2)$$

Following this R^2 two lines of coding symbols contain the information that the linear coefficient (f_1) is now 99% significant (two "x") and the quadratic trend is different from zero at the 95% significance level (one "x"). For the third order polynomial, shown in the fourth column, the R^2 increases again to now 0.3. The three lines of symbols following the R^2 indicate that the cubic coefficient is now significant at the 99% level, the quadratic at the 95% level but the linear coefficient misses the 90% level and is marked consequently with a small "-". In the 5th column the R^2 increases to 0.33 thus explaining already 33% of the given annual mean time series. However the polynomial of the form,

$$f(x) = f_4 * x^4 + f_3 * x^3 + f_2 * x^2 + f_1 * x + f_o \qquad (2.3)$$

overestimates for the given time period.

2.6.2   Explanatory example Figure 4

The method underlying Figure 2.4 can be illustrated comparing Figure 2.2f (Denmark) and Figure 2.2o. The highest value for the seven year running mean during the given period for FRY appears in 1991 with 9.8°C, the lowest is 8.98°C in 1977. The absolute difference is 0.82°C; 10% of 0.82°C is 0.082°C. Consequently all years with a seven year running mean value of the time series of FRY within the range of 8.98°C and 9.06°C have been marked with a dash in Figure 2.4, line 6 (1975,1976,1978). These dashes consequently give a sort of error bar for the calculated year of reversal. For the reversal in the annual mean time series of Denmark, a much bigger uncertainty range is given, namely between 1981 and

1987. The highest value in the period 1965 to 1995 of the seven year running mean of the annual means from Denmark is 5.75°C (1970) the lowest is 5.21°C (1981). So the difference between the two extremes is 0.54°C which is only two thirds of FRY difference. This fact gives credit to the different overall variability of the investigated time series. After adding 10% of 0.54°C to the minimum of 5.21°C all years within the range of 5.21°C to 5.26°C (1982-1987) are marked with a dash (Figure 2.4, line 14).

2.7   Appendix B: Additional, detailed information on the regional annual means

2.7.1   Western Europe

Norway. The mean DTR, predominantly governed by stations around 60°N, shows an increase during the 1950s followed by a significant decrease until the late 1980s. Starting in 1987 DTR increases, but is then interrupted by a dip around 2000 (Figure 2.2a). This dip reduces the significance of the fitted polynomial, still the third and forth order polynomials are significant above 90%.

Sweden. The averaged time series for Sweden shows a highly significant negative linear trend (Figure 2.2b). The selected stations are all located south of 64°N, representing southern Sweden (Figure 2.3). The DTR appears to level off since the late 1980s. However, when reducing the Swedish data to cover only stations for the period until 2005, a tendency to an increase became apparent, this trend was not significant in any model. Also the selection would have given even more weight to the most southern part of Sweden.

Finland. The data for Finland consists of three stations, evenly divided from north to south, namely Helsinki, Jyvaskyla and Sodankyla. The national trend is best represented by a second order polynomial trend significant above the 99% level (Figure 2.2c).

Denmark. Though one of the smaller countries, Denmark contributes 5 equally distributed stations to the dataset (Figure 2.3). The best fitting trend model is the third order polynomial (Figure 2.2f). The second and third order coefficients are significant at 95% level, whereas the linear term shows only p-value of 0.18 corresponding to approximately 80% confidence level.

Great Britain. Only three stations met the demanded quality requirements of temporal coverage up to 2003, namely Oxford, Wick and Waddington. The former two are located in the industrialized southern area of the UK and show a distinct DTR reversal from decrease to increase. Wick is situated at the northern tip of the British mainland showing a general decrease. Despite this the fitted second order polynomial is significant at the 95% level, indicating a trend from decrease to increase (Figure 2.2e). An early reversal around 1965 is visible from the 7-year running-mean.

BeNeLux. Belgium and Luxembourg each contribute only one station to the selected dataset, hence they were analyzed together with the seven stations from the Netherlands. The analysis of the BeNeLux region showed no significant trend. The best fit however is a second order polynomial with p-values around 0.23 (Figure 2.2m). The seven year running mean trend shows an overall increase since 1980.

East Germany. No significant trend is apparent. Best fit is the second order polynomial (Figure 2.2j). P-values are in general above 0.7 (confidence level, below 30%) in all models and coefficients.

West Germany. For the mean of the 13 stations a distinct reversal from decrease to increase is visible in the national mean time series. Consequently the second order polynomial trend is significant at the 95% level in both coefficients (Figure 2.2i).

France. The 25 selected stations are distributed equally over France (Figure 2.3). Similar to West Germany the second order polynomial is significant at the 95% level emphasizing the DTR development form decrease to increase with the reversal period between 1965 and 1985.

Alpine Region. There are only two stations, one from Austria and one from Switzerland. Most Swiss stations had to be rejected due to homogeneity issues. Problems were caused by change of location and instrumentation. The only Swiss station that met the quality requirements is Basel-Binningen. For Austria only one station (Kremsmuenster) with complete data coverage from 1950 to 2005 is provided in ECA&D-P. The mean trend derived from the two stations is best described by a polynomial of the second order (Figure 2.2n). The main contribution to this shape is given by the Basel-Binningen station which shows a distinct decrease and increase.

Italy. The mean trend for Italy is calculated from four stations. The best fitting polynomial is second order (Figure 2.2t). Overall a strong decrease and subsequent increase is visible.

Spain. For Spain a slight decrease in the seven year running mean up to 1977 is visible. Thereafter an equally slightly visible increase in DTR can be seen (Figure 2.2r). However, the statistical analysis shows no significant trend on the 90% confidence level. The p-values for Spain are, 0.36 for the linear and 0.22 for the cubic coefficient.

Portugal. A total of three stations are sufficient according to the demanded quality requirements .Braganca shows an overall increase for the whole period while Lisboa (Lisbon) and Porto show a continuous decrease in DTR (Figure 2.2q).

2.7.2 Eastern Europe

Former Republic of Yugoslavia. The reliable period for the FRY region is from 1956 to 2004. The best fitting trend model for that time series is a fourth order polynomial trend with p-values below 0.05 for all coefficients. Consequently the development shows more than a single period of decrease and increase. From 1956 to about 1965 the DTR increases this is followed by a distinct decrease up to around 1980. From 1980 until 1990 a second

and more emphasized increase is dominant with a subsequent phase of more or less constant development until 2004 (Figure 2.2o). However, the most pronounced feature in this period is the decrease and then subsequent increase in DTR from 1965 to 1991.

Romania. The best fit is a third order polynomial with p-values of about 0.03 for the first and second coefficient, the p-value for the third coefficient is slightly higher with 0.051 and therefore misses the 95% confidence boundary. From the seven year running mean a period with a distinct decrease from 1961 to 1971 is visible, followed by a longer period of increasing DTR lasting until 1990, subsequently the running mean shows a constant development (Figure 2.2p).

Czechoslovakia. As for the area of the FRY, the former Czechoslovakian states are best fitted by a fourth order polynomial (Figure 2.2k). All tested coefficient of the fourth order polynomial are above the 95% significance level (p-values < 0.05). The decreasing period lasts until 1977 according to the seven year running mean, then the DTR increases until it stops around 1992. This is followed by a stable to slightly decreasing period until 2004.

Poland. Only two stations with data from 1966 to 2005 are available, Leba and Siedlce these both show very similar long-term trends. The best fit is a second order polynomial. p-values for the coefficients are 0.083 and 0.046. For Poland a decreasing period is visible from 1966 to 1980 and an increasing period from 1986 to 2005 (Figure 2.2g).

Baltic Region. A strong increase is visible in the seven year running mean up to 1966, followed by a decrease, leveling off in 1991. A short increase starting in 1990 come to an end by 1996 and then becomes a continued decrease (Figure 2.2h). The result of this is an overall linear decrease in the fitted trend model significant at 95% level.

Ukraine. The nearly monotonic drop of the Ukrainian mean DTR lasts over the whole period from 1951 to 2005 (Figure 2.2l). The linear trend is significant above 99%. The two most westerly located stations, L'Vov (Lwiw/Lemberg) and Uzhgorod show a dominant increase since the middle of the 1970s. For the two biggest cities of Ukraine, Khrakov and Kyiv (Kiev) a decrease in DTR until the mid-1990s is dominant follow by a leveling off or increase thereafter.

Russia. The largest region of the so called Eastern-European section is the European part of Russia with Brest (Brestzonalnaya) as only representative station for Belarus included. The mean DTR development for the overall 36 stations is best described by a third order polynomial. p-values are around 0.001 the R^2 is 0.22. Assuming that none of the high frequency is caught by the polynomial this is a quite high value. The seven year running mean describes an increase until 1966 followed by a continuous decrease until 1992 and thereafter an equally uninterrupted increase until 2003 (Figure 2.2d).

2.7.3   Surrounding regions

Iceland. The best fit for the DTR time series is the third order polynomial (Figure 2.2u). All coefficients are above 95% significant. Equal to Denmark and Finland, Iceland is considered to be a mixture of the Western and Eastern European trend type.

Turkey. The shape of the mean data series of the three stations is best described by a third order polynomial. The seven year running mean describes a distinct increase from 1950 until 1963, then a subsequent decrease is disturbed by a short period of increase between 1974 and 1984, thereafter the long-term decrease is continued until 1990. Finally an increase until 2004 is visible from the smoothed 7 year running-mean curve. The described interruption causes a reduction in the significance of the trend model, p-values are 0.150(1st), 0.053(2nd) and 0.027(3rd). When smoothing the described period the p-values are: 0.03(2nd) and 0.009(3rd). The linear coefficient never becomes statistically significant since there is no overall decrease or increase in the series.

Algeria. Three stations are available which are distributed roughly evenly along a north south transect (Figure 2.3). All stations, namely Alger-Dar el Beida, El Golea and Tamanrasset, present a similar trend best described with a third order polynomial. The significance of coefficient is above the 99% level. The seven year running mean is dominated by an increase from 1950 to 1963, followed by a decrease lasting until 1986. Finally, an increase can be noted up to 2004. The peek in 2001 is a prominent feature of the mean and can be equally found in each of the contributing stations.

2.8   Acknowledgements

3   DTR and radiation

On the relationship between diurnal temperature range and surface solar radiation in Europe

Knut Makowski, Eric B. Jaeger, Marc Chiacchio, Martin Wild, Tracy Ewen, Atsumu Ohmura

Institute for Atmospheric and Climate Science, ETH Zurich, Switzerland

Abstract

The surface solar radiation (SSR) is an important factor influencing the local and global energy budget. However, information on the spatial and temporal variation of SSR is limited. A more commonly available measure, which may provide such information, is the diurnal temperature range (DTR). In this study we analyze the relationship between DTR and SSR in Europe between 1970 and 2005 on seasonal and decadal scale. When comparing the mean anomalies time series composed of 31 pairs of sites with long-term SSR and DTR measurements we found a correlation coefficient of 0.87 in the annual mean and between 0.61 and 0.92 in the seasonal mean anomalies. When investigating the individual pairs of SSR and DTR individually we found that local correlations are mostly lower than the European mean and that they decrease rapidly in seasons and latitudes with low incident angles and at high alpine altitude. The highest correlation on local and seasonal scales seems to be connected with the variability of the large scale circulation in Europe. The output of 11 simulations of current generation regional climate models over Europe confirms the strong relationship between SSR and DTR. The seasonal dependence of the relationship is well reproduced but the absolute values of DTR and SSR are mostly too low. The pattern of decrease (dimming) and increase (brightening) in SSR and DTR was not reproduced in the modeled time series. There is still strong evidence from both models and observations that DTR is a reliable representative of SSR.

3.1   Introduction

Observing and anticipating changes of complex climate variables such as downwelling surface solar radiation (SSR hereinafter) in the past and the future is not always straight forward and, is yet, of utmost importance. Sunshine recorders, radiometers or pyrheliometers require high maintenance and a sufficient infrastructure and knowledge to produce reliable output. Much of the technology that is used today to measure radiative fluxes, which determine the energy balance and therewith the temperature, has been available with sufficient quality for only a few decades around the globe.

Measurements that can replace or approximate the lacking information are therefore highly desirable. A much more commonly available measure which may inherit a fingerprint of SSR is the diurnal temperature range (DTR) [*Makowski et al.*, 2008]. Until now only a few publications have highlighted the close connection between the diurnal temperature cycle and the SSR. In 1984 Bristow and Campbell already identified the need to obtain reliable SSR data. They reconstructed SSR using an empirical formula for three sites in the United States and emphasized that the relationship between DTR and SSR varies over the year, which should be taken into account [*Bristow and Campbell*, 1984].

Liu et al. [2004b] investigated a dataset of daily maximum and minimum temperature, cloud cover, and SSR which covers most of China for a period of 45 years. They found a correlation coefficient between DTR and SSR as high as 0.88 in the annual mean anomalies. Wild et al. [2007] suggested a close correlation between long-term changes in SSR and DTR on a global basis. Liu et al. [2004b] additionally show that changes in cloud cover were not the main cause for changes in the SSR and daily temperature range, whereas several studies that investigated various parts of North America found this to be the case [*Karl et al.*, 1984; *Plantico et al.*, 1990].

As stated above, only few studies compare DTR and SSR directly. For Europe, no work incorporating both measures has been published so far. Studies referring to one of the measures for e.g., Dai et al. [1997], show that correlations between DTR and precipitation are as high as 0.55, whereas the correlation between DTR and total cloud cover is only 0.35. Teuling et al. [2008] show a close correlation between SSR and evaporation in the northerly part of Europe whereas in Southern Europe SSR and precipitation are more closely correlated. This indicates that moisture availability is not a limiting factor for evaporation in Central and Northern Europe and therefore should have a minor influence on DTR in those areas. Since moisture can have a strong impact on DTR [*Zhou et al.*, 2008] this is an important finding for our study.

In the present work, we assess the relationship between SSR and the DTR in Europe on seasonal and decadal scales. The seasonal and decadal scale was used to reduce the strong short-term imprint of weather on the connection between SSR and DTR. We incorporate different types of data including measured station-based, measured gridded, and modeled.

Since this article is a contribution to the special issue on global dimming and brightening we will refer to this issue at several points.

3.2   Data

As stated above, the overall data can be divided into three groups: measured data on a station basis (DTR and SSR), gridded measured data (DTR) and gridded model data (DTR and SSR).

3.2.1   Station datasets

The most sparsely available data type that we use in this study is the measured station SSR data. Therefore, we started by identifying as many sites as possible, according to the criteria given below, for the period 1970 until 2005 which is the period best covered by data [*Chiacchio and Wild*, 2009]. In a second step, we identified stations that provided data for daily maximum and minimum for the same period. To provide a comparable dataset of SSR and DTR we used only stations separated by at most 200 kilometers. However, the mean distance between an SSR measurement site and the next DTR measurement site which we identified is only 59 km (Table 3.1).

Surface solar radiation

The SSR data used in this study is obtained from the GEBA database which contains monthly values of energy balance components on a station basis [*Gilgen and Ohmura*, 1999]. After updating the GEBA database with information provided by the World Radiation Data Center, we identified, on an annual basis, all stations in Europe that met the following demands despite the standard quality procedures in GEBA. Each station with not more than five years of missing data between 1970 and 2005 was accepted. An annual value was accepted if not more than one month was missing. If one month was missing, it was filled by using a station climatology derived from the previous, complete years within the 1970 to 2005 period. For the calculation of seasonal data, the same stations were used for easier comparison between the annual and the seasonal time series. Seasons of SSR, as for all other data, were calculated as mean values of March, April, May – spring; June, July, August – summer; September, October, November – autumn and December, January, February – winter. For the winter mean of 1970, for e.g., December 1970, January and February 1971 were used. Consequently, no winter for 2005 was calculated. No missing month was accepted for the calculation of the seasonal values. Following this analysis, 31 sites were identified which were suitable for the analysis (open circles, Figure 3.1). Although we have selected the sites used for this analysis most carefully, we cannot exclude the possibility that there remain some errors in the data. However, we believe that they do not have a substantial influence on the major outcomes of this study.
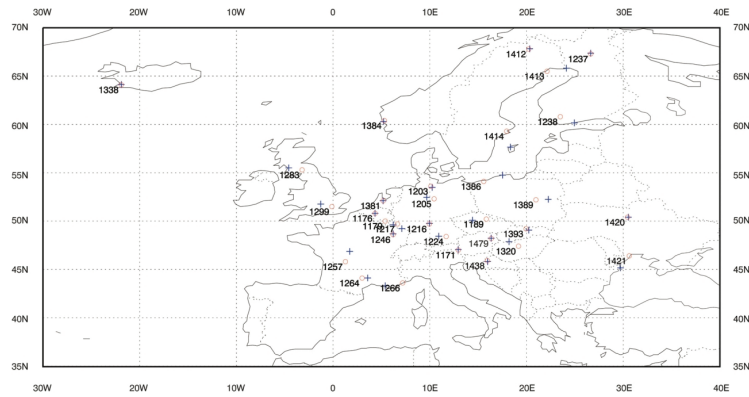
Figure 3.1 *Map of all sites used in this study. Circles (red) show locations of the surface solar radiation (SSR) measurement site, crosses (blue) those of the sites measuring diurnal temperature range (DTR). The numbers represent the IDs of each pair of stations (one DTR one SSR) as defined in Table 3.1.*

DTR station data

Most of the DTR data used here originates from an earlier study; the retrieval procedure and qualitative criteria can be found in Makowski et al. [2008]. The original source of the majority of the station DTR data used is the dataset of the European Climate Assessment and Dataset (ECAD) project [*Tank et al.*, 2002]. In addition to the data from Makowski et al. [2008], we included the following stations: Haparanda (also from the ECAD project), Sonnblick, Wien Hohe Warte, Bergen Flesland, Visby and Kiruna [from *Makowski*, 2006]. Finally, we obtained data from airport authorities at Prestwick via the commercial provider AWIS – Weather Services (crosses, Figure 3.1).

For the calculation of the monthly means, no more than 10 missing days were accepted. For the annual means no missing months are accepted; if one month was missing it was filled by the mean of the previous and the consecutive year. If one of those was not available then the complete year was rejected. The absolute maximum of accepted filled months for a given year was three. In total, no more than three years missing for the selection of a station was accepted. However, only Prestwick has three missing years and Kiruna two missing years, whereas all other sites provide complete data or miss only one year in the annual time series.

Table 3.1 *Latitudes [Eckhardt et al.], longitudes (Lon), names, identification number (IDs), country codes (CTRY) and distances between all pairs of sites of diurnal temperature range (DTR) and surface solar radiation (SSR).*

IDs	SSR sites	CTRY	Lat	Lon	DTR sites	CTRY	Lat	Lon	Dist
1171	Sonnblick	AT	47.00	12.95	Sonnblick	AT	47.05	12.95	6
1176	Uccle	BE	50.80	4.35	Uccle	BE	50.80	4.35	0
1179	St.Hubert	BE	50.00	5.40	Luxembourg Airport	LU	49.62	6.22	73
1189	Hradec Kralove	CZ	50.20	15.85	Praha-Klementinum	CZ	50.08	14.42	103
1203	Hamburg	DE	53.60	10.11	Hamburg Bergdorf	DE	53.48	10.25	16
1205	Braunschweig	DE	52.30	10.45	Hannover	DE	52.47	9.68	56
1216	Wuerzburg	DE	49.70	9.96	Würzburg	DE	49.77	9.97	8
1217	Trier	DE	49.70	6.66	Saarbrücken-Ensheim	DE	49.22	7.12	63
1224	Weihenstephan	DE	48.40	11.70	Augsburg	DE	48.43	10.93	57
1237	Sodankyla	FI	67.30	26.65	Sodankyla	FI	67.37	26.65	8
1238	Jokioinen	FI	60.80	23.50	Helsinki	FI	60.17	24.95	106
1246	Nancy-Essey	FR	48.60	6.21	Nancy	FR	48.67	6.20	8
1257	Limoges	FR	45.80	1.28	Déols-Chateauroux	FR	46.85	1.72	122
1264	Millau	FR	44.10	3.01	Mont-Aigoual	FR	44.12	3.58	46
1266	Nice	FR	43.60	7.20	Marseille	FR	43.30	5.38	151
1283	Eskdalemuir	GB	55.30	-3.20	Prestwick	GB	55.50	-4.58	90
1299	London, Weather C.	GB	51.50	-0.12	Oxford	GB	51.77	-1.27	85
1320	Budapest	HU	47.40	19.18	Hurbanovo	SK	47.87	18.20	90
1338	Reykjavik	IS	64.10	-21.90	Reykjavik	IS	64.13	-21.90	3
1381	De Bilt	NL	52.10	5.18	De Bilt	NL	52.10	5.18	0
1384	Bergen	NO	60.40	5.31	Flesland	NO	60.28	5.22	14
1386	Kolobrzeg	PL	54.10	15.58	Leba	PL	54.75	17.53	146
1389	Warszawa	PL	52.20	20.98	Siedlce	PL	52.25	22.25	87
1393	Zakopane	PL	49.20	19.96	Poprad-Tatry	SK	49.07	20.25	26
1412	Kiruna	SE	67.80	20.23	Kiruna	SE	67.82	20.32	4
1413	Lulea	SE	65.50	22.13	Haparanda	SE	65.82	24.12	98
1414	Stockholm	SE	59.30	17.95	Visby	SE	57.65	18.33	185
1420	Kyiv	UA	50.40	30.45	Kyiv	UA	50.40	30.53	6
1421	Odessa	UA	46.40	30.63	Sulina	RO	45.17	29.73	154
1438	Sljeme-Puntijarka	HR	45.90	15.96	Zagreb-Gric	HR	45.82	15.97	9
1479	Wien, Hohe Warte	AT	48.20	16.36	Wien, Hohe Warte	AT	48.23	16.35	3

3.2.2 DTR gridded datases

We use two different gridded datasets to compare our results to. The CRU TS2.10 and the gridded dataset from the European Union (EU) FP6 project ENSEMBLES. For both datasets we calculate the area weighted mean for the land area within 25°W to 35°E and 43°N to 68°N which is the same area cover by our DTR and SSR station dataset (Figure 3.1).

CRU

The dataset CRU TS2.10 from the Climate Research Unit (CRU) of the University of East Anglia [*Mitchell and Jones*, 2005] provides monthly mean values for various measures for the global land area, including diurnal temperature range. The temporal coverage is 1901 to 2002 on a 0.5° x 0.5° grid. Periods with missing data in the CRU dataset are completed using climatology data from the 1961 to 1990 period. We removed, as far as possible, the

data filled by climatology values according to the station information dataset provided by CRU. From Figure 7 of Mitchell and Jones [2005] we found that since about 1990 the number of stations used to create the dataset in the area of Europe and the former Union of Soviet Socialist Republics (USSR) varied considerably. For the area of Europe more than 550 stations were available from 1965 until 1985. Subsequently, the overall amount broke down to about 100 until the late 1990s when the number increases again up to 350 and declines again thereafter towards the end of the dataset in 2002. For the area of the former USSR the development of station availability is comparable. For the years between 1960 and the late 1980s the amount of available data in total stays rather constant and includes about 250 sites. During the early 1990s nearly no data are available. The number of available sites also increases thereafter but only up to 150 stations.

We have described the development of data availability in the CRU dataset in detail to illustrate that we had to be careful during our comparison with the measured data, which does vary only slightly in the amount of available data over time. We will refer back to this in the results sections.

ECAD

The gridded dataset from the EU-FP6 project ENSEMBLES is based on the data gathered in the European Climate Assessment and Dataset Project. Subsequently, we will refer to this dataset as the ECAD dataset. This should not be confused with the DTR station data we used partly originating from the ECAD project. The ECAD dataset [*Haylock et al.*, 2008] contains daily data between 1950 and 2006. We use the data with a spatial resolution of 0.5° x 0.5° on the same regular grid as the CRU dataset. The variables contained in the ECAD dataset are daily mean temperature and daily precipitation as well as daily maximum and daily minimum temperature from which we calculated monthly means of DTR. Approximately 1000 stations were used in total for this dataset. Prior to 1960 and after 2000 the number of stations is markedly lower (for e.g., year 2000 about 1000 sites; year 2002 about 800 sites; year 2006 about 550 sites, see Figures 2 and 3 in [*Haylock et al.*, 2008]). Based on this, we restricted our analysis of this dataset to the period 1970 until 2000.

3.2.3   Model data

We use monthly mean DTR and SSR fields from the RCMs included in the EU-FP6 project ENSEMBLES (www.ensembles-eu.org). Most RCMs have three experiments available: a control simulation (CTL) for contemporary climate at 50km and 25km resolution (both for 1958-2001) and a transient simulation (1951-2050 or -2100) at 25km resolution conducted for the European continent. The control simulations were all driven at the lateral boundaries using the ERA40 re-analysis [*Uppala et al.*, 2005], whereas the transient simulations use different GCM boundary conditions. Here, we focus only on the CTL simulations at 25km resolution. Additionally, for two RCMs the 50km simulations were used. We assess only those simulations that have been interpolated onto the regular

CRU grid covering the European continent and parts of the North Atlantic. All analyses have been performed for Europe, excluding the Mediterranean, using land-points only.

Table 3.2 *Abbreviations of hosting institutions together with the analyzed resolutions and models, and the corresponding references including the model descriptions.*

Institute	Model	Resolution	Reference
C4I22	RCA	25km	[*Jones et al.*, 2004; *Kjellström et al.*, 2005]
CNRM22	Aladin	25km	[*ALADIN International Team*, 1997]
DMI22	HIRHAM	25km	[*Christensen et al.*, 1996]
ETHZ22/ETHZ44	CLM	25km/50km	[*Steppeler et al.*, 2003]
ICTP22	RegCM	25km	[*Giorgi and Mearns*, 1999; *Pal et al.*, 2007]
KNMI22/KNMI44	RACMO	25km/50km	[*Lenderink et al.*, 2003]
MPI22	REMO	25km	[*Jacob et al.*, 2001]
SMHI22	RCA	25km	[*Jones et al.*, 2004; *Kjellström et al.*, 2005]
OURANOS22	CRCM	25km	[*Plummer et al.*, 2006]

The 11 RCM simulations analyzed in this study are detailed in **Table 3.2**. Since two simulations were performed with the same model, we use the institution name to unambiguously refer to a model version. Details on the model dynamics and physics or the simulation setups can be found on the ENSEMBLES homepage (www.ensembles-eu.org) or in the references given in **Table 3.2**.

3.3   Correlations and trends in annual and seasonal mean anomalies

In the following section and in section 3.4, we use observational data from stations and gridded data where measurements of daily maximum and minimum surface air temperature are available. With these measurements, the diurnal temperature range or amplitude is obtained and a comparison to the corresponding SSR data from the Global Energy Balance Archive (GEBA) [*Gilgen and Ohmura*, 1999] is made.

We investigated the anomalies of DTR and SSR averaged (unweighted) over the European region. Anomalies were used to avoid potential biases caused by few missing measurements which occur especially in SSR.

3.3.1   Correlations of mean series of DTR and SSR

In a first step of correlation calculations, we used the non-detrended anomalies time series of DTR and SSR as they are comparable to other studies, such as Dai et al. [1997] who showed a close correlation between DTR, precipitation, and clouds on a regional to continental scale. In addition, Liu et al. [2004b] investigated the correlation of DTR and SSR in China. Upon comparing the two time series, strong correlations were found for the period 1970 to 2005 in the annual means (0.87), and also for the different seasons: spring (MAM): 0.88, summer (JJA): 0.92, autumn (SON): 0.88 and winter (DJF): 0.61 (Figure 3.2a-e). All correlations are significant at the 99% level. It is clear that the higher the

correlations, the bigger the influence of SSR on DTR; indeed the highest values can be found in summer, followed by spring and autumn. The annual mean correlation coefficient of 0.87 agrees well with the findings from Liu et al. [2004b] in China and is substantially higher than the correlations between DTR and precipitation or cloud cover as found in Dai et al. [1997]. The quality of the correlation is described by the correlation coefficient while the strength is described by the slope of the regression line. We found that with an increasing amount of SSR in the seasonal mean the slope changes (decrease). The change of the slope in the different seasons points to a not completely linear relationship between DTR and SSR (Figure 3.2b-e). Potential causes for this non-linearity may be changing hydrological conditions during the different seasons and the non-linear relationship between radiation and temperature (i.e., the Stefan-Boltzmann law).
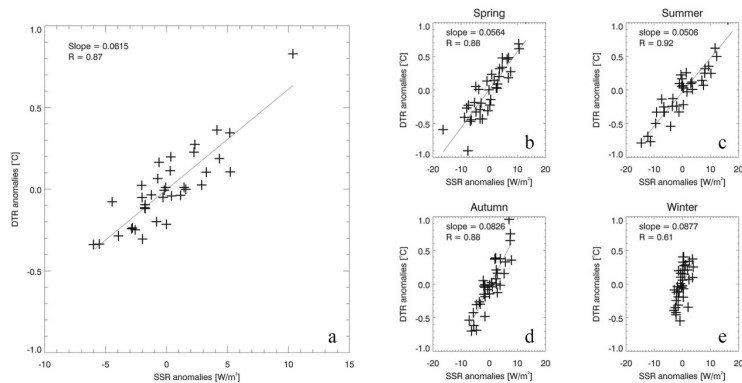

Figure 3.2 *Scatter plots of anomaly means of the station dataset of diurnal temperature range (DTR) and surface solar radiation (SSR). Plots include a best fit regression line and their slopes as well as the corresponding correlation coefficient, (R). These plots are shown for annual mean (a) and the different seasons (b - e). Note the different scales on the x-axis.*

In order to distinguish between the decadal and interannual agreement of the two measures, we detrended the mean time series and recalculated the correlations between the high (interannual variability) and the low (multi-annual to decadal variability) frequency part of each series. To detrend the time series, a fit was determined by the robust locally weighted regression algorithm 'Lowess' [*Cleveland*, 1979] and subtracted from the time series. The correlation coefficients for the detrended residuals or high-frequency changes in DTR and SSR are of the same magnitude as the raw time series, namely spring: 0.86, summer: 0.94, autumn: 0.88, winter: 0.61 and 0.89 for the annual mean. In contrast, the correlations of the low frequency (smoothed) time series are substantially different. The best agreement in the low frequency, long-term behavior could be found in spring (0.98), while all other seasons show correlation coefficients around 0.76. The correlation of the annual means is 0.49. All

correlation coefficients are significant at 95%. This indicates that multidecadal changes have a substantial influence on DTR and SSR causing a close relationship between both measures.

3.3.2   Statistical trend analysis of European mean anomalies

To assess the temporal development of each of the two measures more thoroughly in a statistical way a multi regression analysis was carried out using polynomial trend models from first to fourth order polynomials. Each coefficient was tested using a two sided t-test. We refrained from testing the axis-intersect since we are using anomalies which are distributed near zero by definition. We call a trend significant (at the 95% level) if all coefficients are significant at the certain level and the residuals show white noise (no autocorrelations in the residuals).

The annual mean time series of SSR shows a significant trend of second order, decreasing from 1970 to 1985 and increasing thereafter (Figure 3.3a). This confirms the well known phenomenon of global dimming and global brightening [*Stanhill and Cohen*, 2001; *Liepert*, 2002; *Pinker et al.*, 2005; *Wild et al.*, 2005] in Europe. Though DTR is closely correlated to SSR it does not show a significant trend in any of the tested trend models. We consider the damping influence of factors like soil moisture, evaporation and clouds as most likely reasons which have led to the weakened, long-term trend development.

On a seasonal scale the DTR time series of spring shows a significant increasing linear trend. The trend is mirrored in the SSR time series but is only significant at the 90% level (Figure 3.3b). In summer and autumn SSR development again can be approximated by a second order polynomial, in both cases DTR trends show similar behavior but miss the required significance level of 95% (Figure 3.3c and Figure 3.3d). The trends for SSR are in-line with Chiacchio and Wild [2009]. Since we used a smaller subset of the GEBA dataset, we are able to extend the analysis of our time series up to 2005. It confirms an ongoing of the brightening trend in the annual mean of SSR, as is also the case, and most pronounced, in the summer season. For further discussion of the possible mechanisms which may have led to the observed development of SSR we refer to Chiacchio and Wild [2009]. Concerning DTR trends, we found no continuous decrease in any of the seasons or the annual mean, unlike many DTR observations around the globe which show a decrease between 1950 and the 1980s [*Karl et al.*, 1984; *Karl et al.*, 1991; *Karl et al.*, 1993; *Jones*, 1995; *Easterling et al.*, 1997]. In contrast, we found evidence for an ongoing increase of DTR, most dominant in spring, summer and autumn, which confirms our earlier findings on the annual mean trends in different regions in Europe [*Makowski et al.*, 2008].
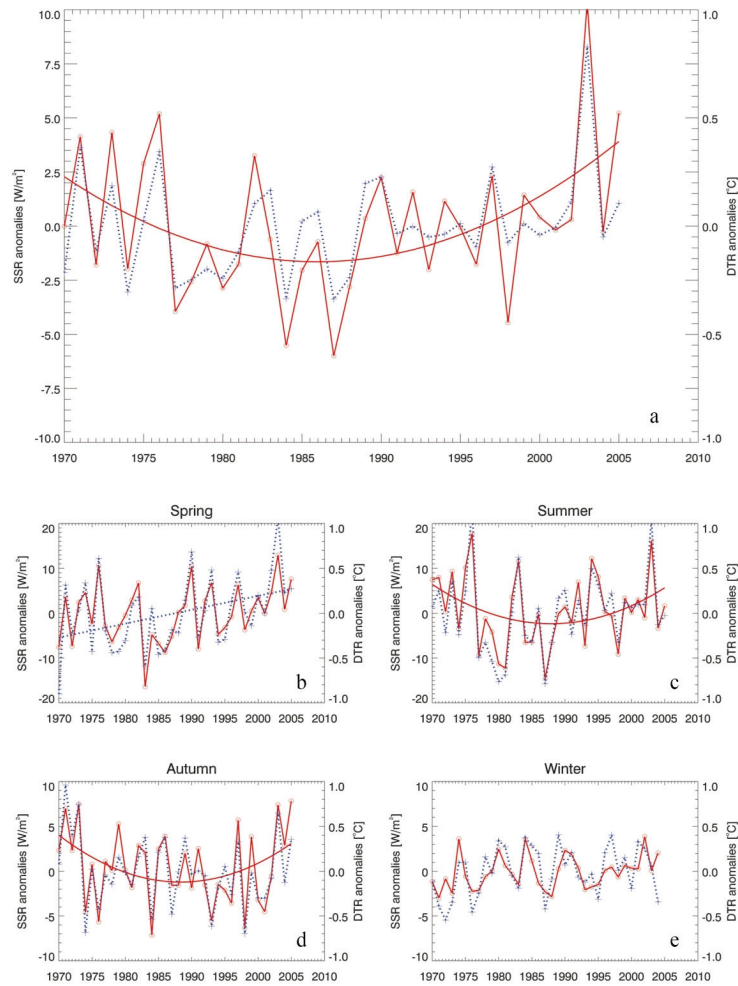
Figure 3.3a-e *Times series plots of anomalies averaged over the station dataset of diurnal temperature range (DTR, dashed blue with crosses) and surface solar radiation (SSR, solid red with circles). Plots include the best fit trend model between first and fourth order polynomial if the trend is significant at the 95% level.*

3.3.3   Representativeness of the station datasets for Europe

In this section we investigate the representativeness of our 31 point sources of information by comparing them to gridded observational datasets of the Climate Research Unit of the University of East Anglia [*Mitchell and Jones*, 2005] and the recently published ENSEMBLES dataset [*Haylock et al.*, 2008]. The purpose of this section is to assess the generality of our findings from the means of 31 point measurements for the general area of Northern and Central Europe.

We calculated the area weighted mean series for ECAD and CRU for the domain within 25°W to 35°E and 43°N to 68°N, which is equivalent to the area which includes all 31 measurements. In general we found good agreement between the mean anomalies on an annual basis (Table 3.3, Figure 3.4). Besides the calculation of the correlation coefficient for the "raw", measured anomaly data we have again split the time series into their high- and low-frequency parts by applying a Lowess algorithm [*Cleveland*, 1979] as described above. In Table 3.3, we compiled the correlation coefficients between the anomaly series of the DTR station dataset (annual and seasonal), the ECAD dataset (1970-2000) and the CRU dataset (1970-2002 and 1970-1990) respectively. For the comparison with the CRU dataset we used different periods to show the strong difference which occurs due to the change in data availability of CRU (for details see section 3.2.2). For the comparison between ECAD DTR and station dataset DTR we used the period 1970-2000 (see section 3.2).
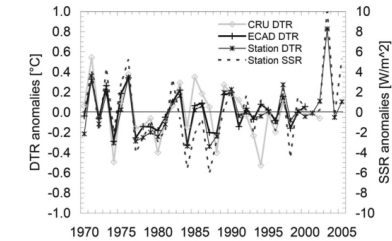
Figure 3.4 *Anomaly time series from 1970 to 2005 of the ECAD (bold solid black with crosses) and CRU (bold, solid grey with diamonds) gridded dataset (area weighted mean of: 25°W/35°E and 43°N/68°N) and station dataset anomaly series of diurnal temperature range (DTR, thin black with asterisk) and surface solar radiation (SSR, dashed line).*

In all cases the correlations between the DTR station dataset mean and ECAD were higher than if compared to CRU. This is equally true for the comparison of the unfiltered anomaly time series and also for the detrended high frequency variations. The mean difference between the correlation coefficients of the original time series and the detrended high frequency variations is about 0.03. The differences are consequently negligible, which shows that the interannual variations are strongly correlated and neither disturbed nor dependant on any low frequency agreement in the compared time series. To reduce the overall information we focus on the detrended (high frequency; Table 3.3, line 4-6) and long-term (low frequency; Table 3.3, line 7-9) variability correlations for the rest of this section.

Agreement of the high frequency, detrended mean series

The correlation coefficient between annual mean DTR of CRU and the station dataset DTR is only 0.77. However, when comparing only the 1970-1990 period it increases to 0.87. The difference originates from an inhomogeneity in the time series due to an abrupt change in data availability in the CRU dataset since 1990 (Figure 3.4) as described in Mitchell and Jones [2005]. The ECAD dataset series shows a higher correlation with the annual mean anomaly series of the station dataset of 0.94 (Table 3.3, Column 1, Line 4-6).

Table 3.3 *The Correlation coefficients as derived from the comparison between ECAD and CRU gridded dataset time series of diurnal temperature range (DTR) with station dataset DTR and surface solar radiation (SSR). The first three lines give coefficients for the original anomalies time series, the second three contain the remaining high frequency, interannual variations after detrending with the Lowess algorithm. The last three lines give the correlations of the low frequency part of the original time series as derived from Lowess. Coefficients given in bold are significant at the 95% level.*

		annual		spring		summer		autumn		winter	
		DTR	SSR	DTR	SSR	DTR	SSR	DTR	SSR	DTR	SSR
	ECAD 1970-2000	**0.94**	**0.87**	**0.65**	**0.72**	**0.82**	**0.84**	**0.75**	**0.58**	**0.83**	**0.48**
original	CRU 1970-2002	**0.71**	**0.50**	**0.55**	**0.51**	**0.65**	**0.62**	**0.6**	**0.45**	**0.69**	0.33
	CRU 1970-1990	**0.83**	**0.62**	**0.62**	**0.53**	**0.81**	**0.78**	**0.67**	**0.56**	**0.75**	0.32
	ECAD 1970-2000	**0.94**	**0.89**	**0.62**	**0.72**	**0.79**	**0.85**	**0.74**	**0.55**	**0.89**	**0.49**
short-term	CRU 1970-2002	**0.77**	**0.57**	**0.56**	**0.53**	**0.63**	**0.61**	**0.60**	**0.43**	**0.68**	0.27
	CRU 1970-1990	**0.87**	**0.72**	**0.57**	**0.50**	**0.78**	**0.80**	**0.61**	**0.61**	**0.75**	0.32
	ECAD 1970-2000	**0.67**	**0.87**	**0.97**	**0.78**	**0.97**	**0.88**	**0.92**	**0.95**	**0.71**	**0.57**
long-term	CRU 1970-2002	-0.14	0.31	**0.62**	**0.61**	**0.59**	**0.81**	**0.88**	**0.94**	**0.79**	**0.80**
	CRU 1970-1990	**0.83**	0.41	**0.90**	**0.81**	**0.95**	**0.79**	0.20	0.05	**0.89**	**0.83**

We also compared the DTR time series from CRU and ECAD against the time series of the station dataset SSR on annual and seasonal scales. In general we found lower agreement in all seasons between the station dataset SSR and DTR from CRU and ECAD compared to the results from station dataset DTR and SSR. However, the highest correlations were found in summer, 0.85 (SSR vs. ECAD), 0.61 (SSR vs. CRU 1970-2002) and 0.80 (SSR vs. CRU 1970-1990).

In comparing the annual mean anomalies of SSR against the two time series of the gridded datasets, we found differing results. The annual coefficients of the two CRU periods investigated were lower than those of corresponding summer season, namely 0.57 for SSR vs. CRU, 1970-2002, and 0.72 for SSR vs. CRU, 1970-1990. For the comparison of ECAD DTR against the station dataset SSR we found a correlation coefficient of 0.89, which is exactly the same result as from the comparison of the two station datasets (Table 3.4, Line 1).

Agreement in the low frequency component of annual and seasonal means

The correlations in the long-term variability of the average time series of the station dataset DTR and SSR and the means derived from ECAD and CRU are in general high and significant. This shows that not only the high frequency characteristics can be captured with as few as 31 sites, but also the lower frequency variability (Table 3.3, line 7-9).

The most remarkable feature of the investigation on the low frequency is the strong disagreement between annual mean DTR of CRU 1970-2002 and the station datasets of DTR and SSR. However, when looking at the shorter period of CRU (1970-1990) it is obvious that it is not a disagreement due to a lack of a physical connection, but rather a data homogeneity issue as described above (section 3.2.2).

It is noteworthy that the values of the mean time series of DTR derived from ECAD and CRU differ by only 0.1°C, whereas the station dataset DTR series is on average 0.5°C lower than CRU and consequently 0.6°C lower than the ECAD time series. This bias is potentially due to the low station density in our station dataset in south-east Europe where annual mean DTR values as high as 10°C occur.

In summary, we found better agreement between our station dataset DTR and SSR with the recently published ECAD dataset than with the CRU dataset. Since the ECAD dataset is focused especially on Europe and has been developed with at least 20% more station data, we are confident that it is more reliable for the investigated area. The high correlations between ECAD and the station time series which we use in this study underline that the results we obtained from our station series are representative of not only 31 locations, but of the overall domain which we investigated.

3.4   Local comparison of long- and short-term variability

In addition to looking at the correlations in the different seasons, we also compared each individual pair of stations (Table 3.1, Figure 3.1) to gain information on spatial patterns. To distinguish between long- and short-term (interannual) agreements, we divided the original time series again into the high and low frequency components by detrending them with a Lowess filter. In the following sections we first take a look at the high frequency variations before discussing the long-term variability.

3.4.1   Correlations of local, detrended time series of DTR and SSR

The results are compiled in the left hand side (columns 2-6) of Table 3.4. The comparison shows that, in general, the correlations of the detrended European mean time series (non-detrended show in Figure 3.2 and Figure 3.3) are higher than those of individual sites correlated with each other. This is a reasonable result since the averaging over the whole region smoothes out any locally disturbing influences such as advection of cold or warm air masses. Nevertheless, only few seasons for some sites miss the level of significant

correlation as shown in Table 3.4 (all correlations significant above the 95% level are marked in bold font). More than one missing significant season can be found only at the stations 1171 – Sonnblick/Sonnblick (AT) and 1412 – Kiruna/Kiruna (SE).

Table 3.4 Correlation coefficients (Pearson) of diurnal temperature range (DTR) and surface solar radiation (SSR). The first column contains the IDs giving information on the correlated pair of DTR and SSR sites as defined in Table 3.1. Columns 2-6 contain coefficients of detrended time series residuals. Columns 7-11 contain coefficients of the low frequency, long-term variability of the time series (determined with the Lowess algorithm). Bold numbers are significant at 95% level.

IDs	Spring	Summer	Autumn	Winter	Annual	Spring	Summer	Autumn	Winter	Annual
All mean	0.86	0.94	0.88	0.61	0.89	0.98	0.75	0.77	0.77	0.49
1171	0.21	0.33	0.33	-0.40	0.35	0.86	0.86	-0.80	0.95	0.73
1176	0.83	0.75	0.78	0.48	0.69	0.39	0.77	-0.47	-0.88	-0.36
1179	0.74	0.76	0.82	0.23	0.71	0.14	0.58	0.09	-0.79	-0.25
1189	0.75	0.74	0.77	0.37	0.75	0.63	0.86	0.36	0.85	0.45
1203	0.67	0.95	0.71	0.07	0.69	0.90	0.95	0.86	0.23	0.85
1205	0.74	0.94	0.73	0.50	0.83	-0.83	-0.14	0.22	0.12	-0.92
1216	0.83	0.87	0.90	0.79	0.89	0.37	0.96	0.90	0.78	0.88
1217	0.83	0.67	0.89	0.58	0.68	0.94	0.82	0.86	0.10	0.92
1224	0.65	0.63	0.80	0.63	0.65	0.79	0.60	0.28	0.50	0.43
1237	0.62	0.90	0.71	-0.01	0.64	-0.31	0.96	0.63	0.36	0.26
1238	0.70	0.65	0.39	0.36	0.61	0.71	0.74	0.87	0.91	0.70
1246	0.82	0.83	0.90	0.49	0.80	0.82	0.63	0.96	0.32	0.53
1257	0.86	0.83	0.83	0.55	0.70	0.77	0.17	0.88	-0.17	0.62
1264	0.80	0.66	0.71	0.77	0.69	0.70	0.23	0.46	-0.03	-0.04
1266	0.53	0.43	0.43	0.70	0.56	0.75	0.53	0.80	0.52	0.69
1283	0.70	0.74	0.51	0.43	0.53	0.79	0.83	0.02	0.72	0.53
1299	0.86	0.94	0.79	0.50	0.90	0.71	0.83	0.89	0.81	0.71
1320	0.72	0.58	0.75	0.56	0.70	0.87	-0.93	0.94	0.53	-0.77
1338	0.74	0.68	0.39	0.18	0.48	0.04	-0.95	-0.31	-0.05	-0.78
1381	0.80	0.87	0.77	0.75	0.73	0.83	0.78	0.90	0.27	0.81
1384	0.76	0.74	0.43	0.63	0.55	0.11	0.83	-0.32	0.41	0.34
1386	0.50	0.85	0.62	0.62	0.64	0.09	-0.04	0.64	0.69	-0.78
1389	0.61	0.76	0.79	0.67	0.58	0.62	0.73	0.78	0.73	0.66
1393	0.61	0.90	0.54	0.71	0.70	0.02	0.68	0.13	0.86	0.16
1412	0.34	0.90	0.51	0.08	0.50	-0.73	0.94	0.53	0.78	0.75
1413	0.72	0.66	0.52	0.07	0.62	0.38	0.91	-0.26	0.73	0.54
1414	0.65	0.70	0.48	0.48	0.49	0.95	0.97	0.56	0.66	0.96
1420	0.49	0.32	0.51	0.70	0.20	-0.39	0.15	0.88	0.77	0.69
1421	0.50	0.25	0.42	0.54	0.37	0.81	0.39	0.54	0.96	0.59
1438	0.67	0.59	0.44	0.60	0.65	-0.67	-0.89	0.01	-0.85	-0.95
1479	0.65	0.72	0.79	0.61	0.65	0.87	0.84	0.37	0.87	0.88

The pair 1171 is measured at the Austrian Observatory Sonnblick at an altitude of 3106m (a.s.l.). All seasonal correlation coefficients show low values; during winter it is even significantly negative at the 95% level. At this altitude several reasons lead to a much lower correlation of DTR and SSR throughout the year. The absence of a stable boundary layer leads to a strong influence of well mixed, advected air masses. The height leads to

much reduced cloud coverage and the snow cover, almost annual, leads to a high albedo. The lack of horizontal land area at this high altitude station, which could receive the energy from the sun, changes the energetic behavior of the surrounding area. All factors are most intense during the period of low insolation, leading to the non-significant low or even negative correlation coefficients.

Kiruna, where the station pair 1412 is measured is not located at high altitude yet at high latitude. The low correlation coefficients in the short-term variations are occurring during winter and spring. Since both sites receive rather small amounts of sunlight the variability is also rather low leading to lower correlations.

The consequence of low insolation combined with sites located at high altitudes on the relationship between DTR and SSR can also be seen in the pairs 1237 (Sodankyla-FI), 1338 (Reykjavik-IS) and 1413 (Haparanda-SE), all of which are located north of 65°N, and show a non significant correlation coefficient in the winter season.

3.4.2 Correlations of local, long-term characteristics

In this section we will assess the correlations between the low frequency or long term variability of the individual station pairs as defined in Table 3.1. Looking at the right hand side of Table 3.4 (columns 7-11) it is obvious that time series agree less in their lower frequency fraction. This behavior is partly explainable by the different nature of the high and low frequency part of the time series. The individual points of the high frequency component of a seasonal series are determined with a gap of 9 months in between (the seasonal mean consists of 3 months), which leads to the absence of autocorrelations between the various data points. The low frequency part is by definition derived from more than one consecutive point. Consequently each point contains information from the surrounding points. This leads to a much more persistent, disturbing influence of a potential erroneous outlier on the correlation of the long term changes between the DTR and SSR series. Taking this into account we will subsequently only discuss the substantial results and discrepancies.

The results of the long-term correlations are more heterogeneous compared to those of the high frequency analysis. Two thirds of all correlated averaging periods show significant positive correlation. The correlation coefficients of the overall mean series are not generally the highest, still all are significantly positive. It is noteworthy that amongst the overall means the long-term variations of the seasons have higher correlations than the annual mean. Summarizing the individual averaging periods of the station pairs, only 8 out of the 31 pairs are not significant or negatively correlated during the summer season, which underpins the close relationship between DTR and SSR in the season with the highest amount of radiation.

The station pairs with the largest discrepancies (3 or 4 of the seasonal means not significant or negatively correlated) in the correlation of long-term variability are 1179 –

St. Hubert/Luxemburg Airport, 1205 – Braunschweig/Hannover, 1338 – Reykjavik/Reykjavik (IS) and 1438 – Sljeme-Puntijarka/Zagreb-Gric (HR) (Table 3.4).

Sljeme-Puntijarka (SSR of 1438) and Zagreb-Gric (DTR of 1438) are separated by a horizontal distance of only 9km. The difference in height is also negligible. Still this pair shows no significant correlation in any of the investigated seasons or the annual mean is instead significantly negative. When comparing the series of DTR and SSR of the station pair 1438 to the closest located pairs we found that prior to 1985 the series of SSR at 1438 shows an extraordinary behavior (increase followed by a steep decrease – series not shown) compared to those of 1479 and 1320 (although not the case for 1171, for the reasons stated below). This is evident in all seasons and subsequently in the annual mean series. As a further check, we recalculated all correlations beginning from 1985 which resulted in a significant increase of the long term correlation coefficients; spring: 0.80/-0.67 (now/before), summer: 0.75/-0.89, autumn: 0.42/0.01, winter: 0.91/-0.85 and in the annual mean: 0.55/-0.95. These results refer to only 20 years of data but still they indicate that more of an inhomogeneity issue rather than a physical process might explain the low and non-significant correlation between DTR and SSR at 1438.

The pair 1338 (Reykjavik/Reykjavik), which is the second station pair with 4 non-significant or negative correlated seasons in the long term analysis (Table 3.4), is located close to the Arctic Circle and at the coast of an island. On the one hand, this leads to an intense maritime and advective influence, and on the other hand, to a low imprint of SSR due to low insolation angles in all seasons, most intensely during the winter period in the Northern Hemisphere.

The last two pairs with at least three non-significant or negatively correlated seasons are; 1179 – St. Hubert/Luxemburg Airport and 1205 – Braunschweig/Hannover. All four measurement series (of DTR and SSR) show no extraordinary long term trend behavior and no indication of data inhomogeneities. Also their geographical location is not at a high altitude or latitude or very close to the sea. The only potential influencing factor is the distance between the DTR an SSR sites which is in both cases more than 50 km. Since there are many other station pairs with an equal or higher horizontal distance which are strongly correlated, this is not necessarily the explanation from the strong disagreement. Consequently further investigations are needed.

3.4.3 Influence of the large scale circulation on the long- and short-term agreement between DTR and SSR

The geographical overviews given in Figure 3.5 show the values of the highest correlation coefficients of all seasons and the season in which they occurred (indicated with colored symbols). Figure 3.5a gives the distribution of the highest correlation coefficients of the detrended short-term variations, while Figure 3.5b shows those for the low frequency parts of the DTR and SSR time series. The symbols are smaller if the correlation is not significant at 99% level (we used a higher level of significance compared to Table 3.4 because we are dealing with the best regression of each station amongst the different

seasons). The colors denote during which season the maximum correlation between DTR and SSR was reached (green – spring, red – summer, orange – autumn, blue - winter). Along a transect (see arrow in Figure 3.5a) from north to south-southwest the colored symbols build belt like patterns, beginning with the highest correlation coefficients occurring in the summer season in the most northern belt, which consists of the British Isles, Benelux, northern Germany and Scandinavia (red circles). Highest correlation coefficients in autumn occur in the area of western France, southern Germany, the Czech Republic and eastern Poland (orange triangles).
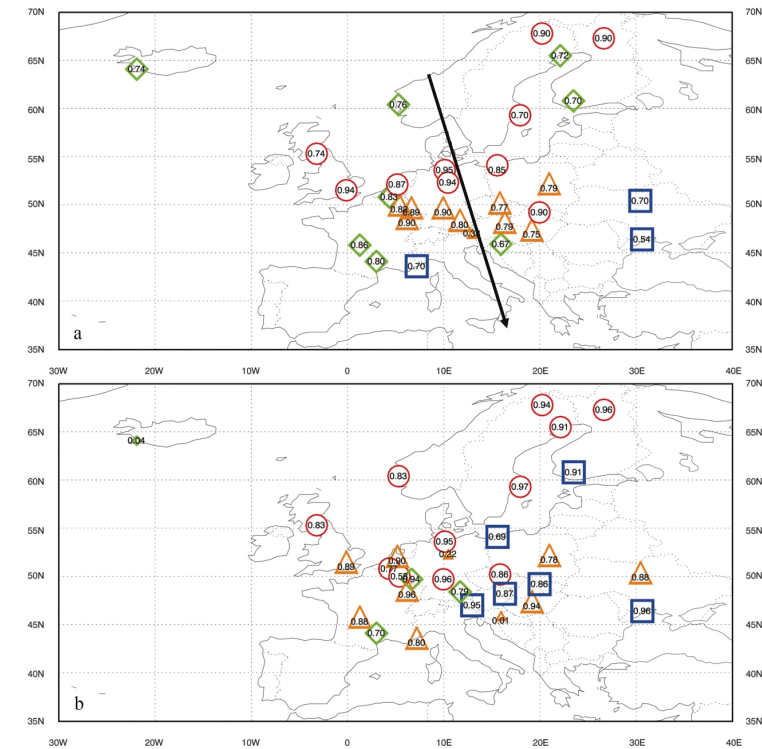
Figure 3.5 *Map of the seasons with highest correlation in the detrended, short-term (a) and long-term (b) variations for each pair of stations. Symbols contain the corresponding correlation coefficient. Smaller symbols denote correlations not significant at the 99% level. Red circles denote highest correlation of all seasons between diurnal temperature range (DTR) and surface solar radiation (SSR) in summer, orange triangles in autumn, green diamonds in spring and blue squares in winter. Arrow indicates pattern transect as defined in the text.*

This second belt is followed by the most southern belt which is a mixture of springtime (green diamonds) and winter (blue squares) seasons with maximum correlation coefficients occurring around the Mediterranean and spanning the Balkan States from Hungary to the Ukraine in the east.

High correlation coefficients between DTR and SSR in each pair as well as in the overall mean series for Europe are dependent on the agreement in the long-term trend behavior and the interannual variability. The interannual variability of both SSR and DTR is determined by the large scale circulation causing high variability in cloud cover and precipitation. One of the most important features of climate in the European area is the influence of synoptic scale pressure systems. The trajectory along which they are moving and their region of origin are related to the position of the polar front, which again is dependant on the annual orbit of the earth around the sun. Figure 3.5a shows that the correlation between DTR and SSR is highly dependent on the interannual variability in cloud coverage or absence due to large scale circulation, because it mirrors the position of the polar front in the different seasons. During summer it is located northward, and with decreasing zenith angle towards autumn it moves southward together with the main trajectories of the low pressure systems. During the winter season, the dynamic low-pressure systems can reach as far south as the Mediterranean and as far east as the Black Sea, while causing interannual variability in SSR via alteration of cloud coverage. With the increasing zenith angle the polar front moves northward again causing the highest correlation coefficients of all seasons in the Balkan States, Hungary and south-western France. If still we claim the interannual variability of synoptic scale pressure systems to be of utmost importance for the highest correlation between DTR and SSR on a seasonal and interannual scale, long-term behavior of SSR and DTR are not only dependent on clouds or cloud absence but also on transmissivity of the atmosphere which is determined by the aerosol burden of the atmosphere. Norris and Wild [2007] show that removing the cloud effect from SSR emphasizes the dimming and brightening trend which we also identified in the European mean series of DTR and SSR (Figure 3.3).

From the correlations of the long-term variations no distinct pattern is apparent. Most prominent, however, is the cluster of the highest winter maximum correlations east of 10°E and summer maxima north of 55°N (Figure 3.5b). This pattern might be due to the Siberian High, which causes persistent clear sky situations. Long-term, changes in SSR consequently may have left their finger print here most prominently. The fact that the strongest correlations between DTR and SSR in Northern Europe appear during the summer season (in the long-term as well as in the short-term variations) is rather little surprising, since during this period SSR is largest and can drive DTR effectively.

3.5   Modeling DTR and SSR

In this section we assess the representation of SSR and DTR and most importantly their relationship to each other and the measurements in different Regional Climate Model (RCM) simulations from the ENSEMBLES project. The purpose of this section is to assess

the usefulness of RCMs to better understand the various physical mechanisms governing to relationship between DTR and SSR by analyzing how realistic the model output is.

For the comparison of our station datasets against model output we use nine different models which all performed simulations for the same region and for the same boundary conditions, using ERA40 re-analysis data, with 0.22° (25km) resolution. For two of the nine different model versions we analyzed additional simulations at coarser resolution (0.44°/50km). More detailed information on the selected simulations can be found in section 3.2.3. As previously mentioned, we use the institution name combined with "22" or "44", representing the resolution of 0.22°/25km or 0.44°/50km respectively, to unambiguously refer to a model version (**Table 3.2**).

3.5.1   Modeled DTR and SSR in the ENSEMBLES RCMs

From the monthly mean output of the models we derived annual and seasonal mean values for each year between 1970 and 2000 using the same definitions of seasons as for the station data. In Table 3.5 we summarized the results from the correlation calculation between detrended modeled DTR and SSR. For comparison we added the correlation coefficients as derived from the station datasets in Table 3.5. To ensure an appropriate comparison we recalculated all correlation coefficients between measured DTR and SSR for the period 1970-2000.

Table 3.5 *Correlation coefficients of diurnal temperature range (DTR) and surface solar radiation (SSR) in each simulation and in the first two lines for comparison of the measurements for the periods 1970-2005 (05) and 1970-2000 (00). Bold numbers are significant at the 99% level.*

	SPR	SUM	AUT	WIN	ANN
station data 05	**0.88**	**0.92**	**0.88**	**0.61**	**0.87**
station data 00	**0.86**	**0.92**	**0.89**	**0.68**	**0.82**
C4I22	**0.90**	**0.84**	**0.83**	**0.61**	**0.89**
CNRM22	**0.92**	**0.87**	**0.85**	**0.71**	**0.81**
DMI22	**0.93**	**0.94**	**0.83**	**0.66**	**0.72**
ETHZ22	**0.87**	**0.96**	**0.92**	**0.68**	**0.90**
ETHZ44	**0.87**	**0.91**	**0.90**	**0.72**	**0.89**
ICTP22	**0.94**	**0.93**	**0.88**	**0.57**	**0.86**
KNMI22	**0.87**	**0.95**	**0.89**	**0.68**	**0.85**
KNMI44	**0.87**	**0.93**	**0.89**	**0.74**	**0.82**
MPI22	**0.92**	**0.87**	**0.85**	0.16	**0.74**
OURANOS22	**0.94**	**0.92**	**0.92**	**0.70**	**0.84**
SMHI22	**0.91**	**0.88**	**0.87**	**0.67**	**0.90**
MODEL MEAN	0.90	0.91	0.88	0.63	0.84

In general we found the highest correlation coefficients between DTR and SSR in spring and summer in the models. The mean of all correlation coefficients in spring and summer is 0.90 and 0.91, respectively (Table 3.5, line: "model mean"). These values are very

similar to the measurement correlation coefficients, namely 0.86 for spring and 0.93 for the summer season (Table 3.5, line 2). The coefficients of the winter season are generally lowest, analogous to the measurement data analysis. They range from 0.50 to 0.75 (measurement data analysis: 0.67) except for one outlier with 0.41 (MPI22). The mean of the annual mean correlation coefficients of all models is 0.87, which falls in between the measurement correlation coefficients, namely 0.86 (1970-2000) and 0.89 (1970-2005).

The low frequency variability (not shown) of DTR and SSR agrees well in all models and seasons with positive significant correlations values ranging from 0.54 to 1.00 except for two outliners which were identified in the winter mean of MPI22 (-0.40) and the annual mean of DMI22 (0.32).

To summarize, we can state that the internal correlations between modeled DTR and SSR are very similar to the correlations of measured DTR and SSR in both seasonal and annual averages. When comparing the course of the seasons, most simulations reproduced internally realistic correlation coefficients, from mid to high correlation coefficients in spring and summer to mid and low correlation coefficients in autumn and winter.

3.5.2   Verification of modeled time series of European DTR and SSR

We use all simulations forced by ERA40 boundary conditions and analyzed for the period 1970-2000. To analyze their temporal performance the measured DTR is compared to the modeled DTR (Table 3.6) and the measured SSR to the modeled SSR (Table 3.7). Once again we have split the time series into their low and high frequency part by applying a Lowess algorithm [*Cleveland*, 1979].

The highest correlation coefficients (Table 3.6 and Table 3.7, indicated with an asterisk) in spring, summer and autumn in both DTR and SSR high frequency variability are found in both the ETHZ22 or the ETHZ44. For the winter period the best performance for the high variability part of SSR time series is found in KNMI44. Also with respect to DTR, KNMI44 performs well. However, the best representation of model DTR (detrended) could be found in the DMI22 and C4I22. The lowest correlation coefficients between modeled and measured high frequency variability (Table 3.6 and Table 3.7, indicated with an apostrophe) for nearly all seasons in DTR and SSR are found in CNRM22.

The low frequency variations of DTR and SSR are compiled in the right hand side (columns 7-11) of Table 3.6 and Table 3.7. It is most striking that all models reproduce the long term variation during winter and especially autumn quite well. The finding that all models perform equally well indicates that the prescribed ERA40 boundary conditions are likely causing this agreement. This suggests that not only the high frequency changes during autumn and winter are influenced by large scale circulation but also the long term fluctuations.

Table 3.6 *As Table 3.5 but for measured compared with modeled diurnal temperature range. Columns 2-6 contain coefficients of detrended time series residuals. Columns 7-11 contain coefficients of the low frequency, long-term variability of the time series (determined with Lowess algorithm). Bold coefficients are significant at the 99% level. Numbers with an asterisk give the highest correlation coefficients of all simulations in each period, while the lowest are marked with an apostrophe.*

	SPR	SUM	AUT	WIN	ANN	SPR	SUM	AUT	WIN	ANN
C4I22	**0.67**	0.42	**0.69**	**0.65***	**0.55**	-0.34	0.19	**0.77**	**0.89**	-0.41'
CNRM22	0.41'	**0.48**	**0.66'**	0.37'	**0.57**	**-0.54'**	0.24	**0.65'**	0.18	0.17
DMI22	**0.78**	**0.64**	**0.79**	**0.65***	**0.53**	0.24	**0.64**	**0.78**	**0.85**	-0.36
ETHZ22	**0.83***	**0.78**	**0.84***	**0.58**	**0.87***	**0.51**	**0.60**	**0.91**	**0.96**	0.36
ETHZ44	**0.82**	**0.80***	**0.80**	**0.60**	**0.83**	**0.65***	**0.75***	**0.83**	**0.98***	0.44*
ICTP22	**0.64**	0.41	**0.76**	**0.59**	**0.51**	**0.62**	**0.54**	**0.92***	**0.98***	0.12
KNMI22	**0.80**	0.30'	**0.73**	**0.63**	**0.64**	0.09	-0.12	**0.87**	**0.98**	-0.32
KNMI44	**0.73**	**0.47**	**0.74**	**0.64**	**0.65**	0.15	-0.16'	**0.84**	**0.97**	-0.27
MPI22	**0.76**	**0.65**	**0.69**	**0.64**	**0.67**	**0.54**	0.40	**0.88**	**0.86**	-0.11
OURANOS22	**0.63**	0.34	**0.68**	0.39	0.43'	0.10	-0.02	**0.90**	0.17'	-0.26
SMHI22	**0.67**	**0.50**	**0.75**	**0.55**	**0.54**	-0.38	0.18	**0.76**	**0.93**	-0.17
model mean	0.70	0.53	0.74	0.57	0.62	0.15	0.30	0.83	0.80	-0.07

It is further noteworthy that in the mean of all simulations the summer season series of both DTR and SSR were reproduced worst of all seasons in the low and high frequency part. Jacob et al. [2007] and Jaeger et al. [2008] discuss the weak RCM performance in summer and attributed it to the increased importance of small-scale processes such as convection or land-atmosphere interactions for the regional European summer climate, in contrast to the predominance of the large-scale circulation for the winter climate.

Table 3.7 *As Table 3.6 but for surface solar radiation.*

	SPR	SUM	AUT	WIN	ANN	SPR	SUM	AUT	WIN	ANN
C4I22	**0.72**	**0.52**	**0.64**	**0.60**	**0.61**	**-0.62**	0.26	**0.86**	**0.81**	**-0.76**
CNRM22	0.40'	0.34'	**0.60'**	0.39'	**0.49**	-0.43	0.17	**0.79**	-0.05'	0.13
DMI22	**0.77**	**0.78**	**0.76**	**0.67**	**0.77**	0.04	0.31	**0.56**	**0.84**	-0.35
ETHZ22	**0.78**	**0.83***	**0.82**	**0.67**	**0.79**	-0.28	**0.75***	**0.95**	0.49	-0.08
ETHZ44	**0.79***	**0.83***	**0.83***	**0.68**	**0.83***	-0.18	0.40	**0.82**	**0.90***	-0.37
ICTP22	**0.74**	**0.61**	**0.68**	**0.56**	**0.47**	0.37*	**0.50**	**0.98***	0.75	-0.23
KNMI22	**0.75**	0.35	**0.72**	**0.78***	0.44'	-0.27	-0.16'	**0.68**	0.75	**-0.85'**
KNMI44	**0.74**	0.45	**0.76**	**0.78***	**0.55**	-0.17	-0.09	**0.59**	0.79	**-0.77**
MPI22	**0.76**	**0.61**	**0.63**	**0.59**	**0.61**	0.35	0.39	**0.95**	0.08	-0.08
OURANOS22	**0.68**	**0.56**	**0.72**	**0.58**	**0.48**	0.35	0.41	**0.90**	0.27	0.23*
SMHI22	**0.74**	**0.64**	**0.75**	**0.67**	**0.61**	**-0.69'**	-0.06	**0.86**	**0.88**	**-0.72**
model mean	0.72	0.59	0.72	0.63	0.60	-0.14	0.26	0.81	0.59	-0.35

Since aerosols were included as climatology only, the missing agreement between modeled and measured time series of DTR and SSR during the higher insolation seasons of the year might also be an indication of the importance of the influence of scattering and absorbing

aerosols which changed substantially during the second half of the 20th century [*Mylona*, 1996; *Lefohn et al.*, 1999; *Vestreng et al.*, 2007] thus altering the SSR [*Marmer et al.*, 2007] and consequently the DTR [*Makowski et al.*, 2008].

3.5.3   Modeled relationship versus measured relationship of DTR and SSR

In addition to assessing the reliability of the model-internal correlations and the long- and short-term time series behavior of DTR and SSR, we also investigated the absolute values compared to the different seasons in the measurement datasets. In Figure 3.6 we compiled all scatter plots of all model versions and compared them to the station measurement data, which are as we have shown in section 3.3.3 representative for the entire European domain. Each panel contains all scatter plots for the four seasons and the annual mean of measured DTR against measured SSR (grey) and modeled DTR against modeled SSR (black). The measured and modeled seasons are connected with one line each. The dotted line connects winter (lower left), autumn, spring and summer (upper right) of the station datasets, and the solid line connects those of the simulations. The anchor points for the connecting lines are the arithmetic means of both measures for each season. The dashed lines connect each plotted season of the measurements with the corresponding season of the model simulation. The scatter plot of the annual mean (grey and black, 'x') is always located in the middle of the five different black or grey scatter plots.

From the dotted line, which connects the measured data, one can see a homogeneous picture of increasing DTR and SSR. Highest values occur during the season with the highest zenith angle, and lowest values with the lowest zenith angle. This is not reproduced in each of the 11 model simulations however. The most striking feature while comparing the modeled data against the measured data is the fact that 8 out of 11 model simulations underestimate either DTR or SSR or both. The dashed lines (black) in each scatter plot connect the means of the corresponding season and indicate the type of overall error. If they are more or less vertical (C4I22, DMI22), then DTR is either under or overestimated, if they are more horizontally oriented they point towards an under or overestimation of SSR. If the dashed lines are "parallel" to the potential regression lines (ETHZ22/44, KNMI22/44, MPI22) of each season's scatter plot then they indicate a systematic low or high bias in both DTR and SSR. In general, panels with parallel dashed lines for the different seasons show the simulations with a systematic bias, whereas panels with dashed lines which point in completely different directions identify potentially more complex and seasonally different errors.
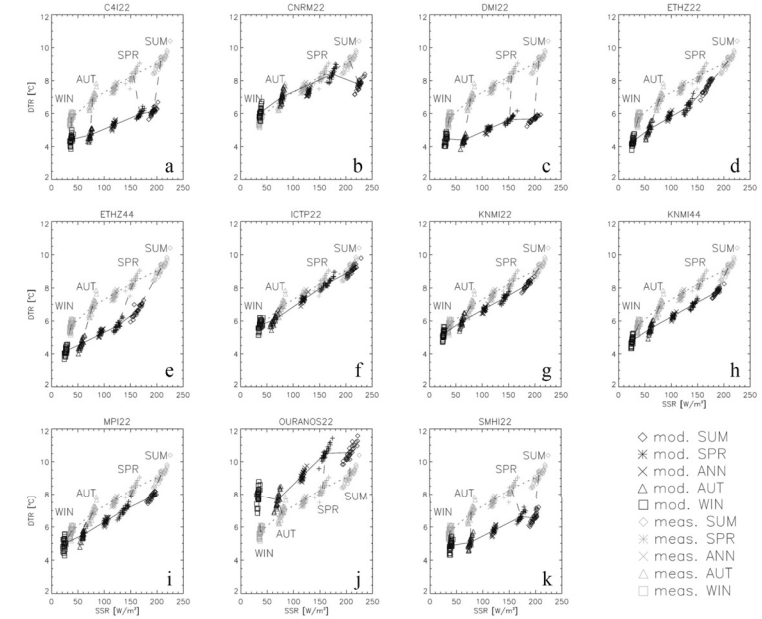
Figure 3.6 *Scatter plots of diurnal temperature range (DTR) and surface solar radiation (SSR) anomalies. Scatter plots of measured station dataset are the same in each panel and given as a reference (grey). The seasons are connected with a dotted line and labeled with WIN for winter, AUT for autumn, SPR for spring and SUM for summer, respectively. Fifth unlabeled scatter cloud in each color (black or grey) represents the annual mean. The symbols representing each season and the annual mean are given in the legend. Dashed lines connect the corresponding seasons of measured (meas.) and modeled (mods.) data. Modeled data is given in black. The solid line connects the different seasons.*

A further two weaknesses are obvious from the comparison of the 9 model versions with the measured data. First, the simulations C4I22, DMI22, OURANOS22 and SMHI22 all show that, either winter and summer are too low or spring and autumn are too high in the internal comparison (Figure 3.6 a, c, j, k). Second, when looking additionally at CNRM22 and ETHZ22/44 (Figure 3.6 b, d, e) it is clear that the summer period seems to be the most difficult to reproduce correctly for the models.

ETHZ22/44 and KNMI22/44 (Figure 3.6 d, e and Figure 3.6 g, h) represent two pairs of simulations that have been run with the same model setup but different horizontal resolutions. We found the same systematic deficiencies compared to the measured data, but a stronger low bias in the coarse resolution simulations.

3.6   Summary and Conclusions

This study provides evidence for a strong connection between SSR and DTR on annual scale and in different seasons in both observations and Regional Climate Model simulations. In the annual mean anomalies the correlation is 0.86 for the period 1970-2005. On the seasonal scale the detrended summer season shows the highest correlations in the measurements (0.92) and the models (0.91) followed by spring (0.88/0.90 measurements/models), autumn (0.88/0.88) and winter (0.61/0.63). We also show that the DTR anomaly series which we derived from a set of 31 carefully selected sites represents the major characteristics of the entire European domain as seen in ECAD and CRU gridded datasets; this applies for the high and low frequency component of the time series.

The multidecadal evolution of the annual mean DTR time series over the complete period from 1970-2005, if still not significant at the 95% level, follows that of the SSR series, which once more shows the well known behavior of decrease and increase, also termed global dimming and brightening,. The dimming and brightening is most evident in the annual mean and the summer and autumn season, with trends significant at the 95% level.

An assessment of the highest correlated season for each pair of a DTR and an SSR site showed that synoptic scale pressure systems likely have a strong influence on the interannual variability, contributing to the reported high correlation between DTR and SSR.

The comparison of the observed relationships with their counterparts in the current generation Regional Climate Models revealed several major issues. In most models the seasonal correlation coefficients and their changing behavior in the annual cycle (highest summer, lowest winter) are correctly reproduced and of comparable magnitude as in the measurements.

By comparing absolute values of DTR and SSR from measurements and models we found that more than 50% of the simulations analyzed produced, in general, too low values in DTR and SSR. The seasons often do not have the right relationship compared with each other; we found, for example, summer seasons with lower mean SSR than the mean of the spring season of the same model.

When comparing the measured time series of DTR and SSR against the model DTR and SSR we found that the interannual variation of DTR and SSR is reproduced fairly well with correlation coefficients mostly between 0.5 and 0.8. It is noteworthy that on average the short- and long-term variability of the summer season were reproduced worst, despite the fact that the simulations were all driven by ERA40 reanalysis boundary conditions. This may be a result of small scale processes being poorly resolved in the models, particularly since these processes play an important role in summer. Aerosol influence may also be responsible since their concentrations are determined from a climatology rather than from actual values. The lacking time dependence of atmospheric aerosol burden might explain the missing long-term temporal change of SSR and DTR, especially in the summer season. In contrast, the autumn period reproduced realistic results in the short and even

more in the long-term development. This may be interpreted as an indication for the strong influence of the large scale circulation on the long-term behavior of DTR and SSR during the period of the year when incident angles are low.

From these results we conclude that DTR and SSR in Europe are strongly interconnected and influenced by the same factors. The connection is stronger on seasonal scales than on the annual scale. The agreement on the level of interannual variability is high and robust which shows the strong influence of large scale circulation and cloud coverage. We consider it possible to estimate seasonal and interannual variability of SSR from DTR data in Europe. Concerning the long-term development of SSR, the presented findings encourage us that we may be able to estimate SSR from DTR, however longer and carefully homogenized time series are needed for this purpose and other factors, such as the role of humidity and soil moisture, need to be better quantified.

3.7   Acknowledgements

4 Alternative measures for the daily temperature amplitude

Diurnal temperature range, periodic amplitude and surface solar radiation

Knut Makowski, Atsumu Ohmura

Institute for Atmospheric and Climate Science, ETH Zurich, Switzerland

Abstract

We analyze the connection between surface solar radiation (SSR) and two different measures of daily temperature amplitude for twenty sites around the globe. One is the commonly used diurnal temperature range (DTR) the other is the periodic amplitude (PerAmp). The latter is defined as the monthly averaged warmest hour minus the on average coldest hour of the day. The averaging causes a reduction of the influences of advected air masses in the PerAmp. Consequently PerAmp should be more closely connected to SSR than DTR. Comparing the mean annual cycles, the total difference between the PerAmp and SSR curves is about 10% less than between SSR and DTR. At Arctic sites PerAmp reflects in the best case 84% of the SSR variability while DTR shows a maximum of 50%. In the mid-latitudes, annual cycles of both temperature amplitude measures and SSR are closely connected. Differences between SSR and the amplitudes are usually in the range of 10% to 15% or 400-600MJ/m^2. The perennial variability of the individual site of DTR and PerAmp is in most cases significant and positively correlated with SSR. Correlations between SSR and PerAmp are in more than 60% of the cases higher than between SSR and DTR. In the long term development we found the highest agreement between SSR and the daily amplitudes in the Asian Subtropics and in the Arctic. When focusing on the long term development of different seasons PerAmp shows a superior performance at 80% of the stations during spring and 75% of the stations during winter. Both seasons are strongly influenced by advection. We conclude that PerAmp is

indeed more strongly related to SSR than DTR. The substantially large amount of data which has to be processed to derive PerAmp is, however, a major drawback and needs to be considered.

4.1   Introduction

The diurnal temperature range (DTR) is defined as the difference between daily maximum and daily minimum temperature. The monthly or annual mean is used to detect climate change due to its sensitivity to variations in the radiative energy balance [*Karl et al.*, 1991; *Karl et al.*, 1993; *Kukla and Karl*, 1993; *Jones*, 1995; *Dai et al.*, 1999]. DTR contains very useful information on the greenhouse effect and solar radiation [*Wild et al.*, 2007; *Makowski et al.*, 2008; *Makowski et al.*, 2009].

However, using only the measurement of daily maximum and minimum temperature of the daily temperature cycle limits the possibility to attribute the long-term changes to a specific component in the balance. The limitation is due to the strong and partly coincidental influence of advection. This influence cannot easily be tracked and thus not accounted for because it is not documented at what time of the day the daily maximum or minimum occurs by the usage of an extreme thermometer where most of the historical measurement originate from.

A potential alternative to cope with these problems is the periodic amplitude (PerAmp), which was introduced as early as 1883 by Julius von Hann [1883]. He suggested a distinction between the DTR, or as he called it the aperiodic amplitude, and the periodic amplitude. The expressions aperiodic and periodic represent the key point of the distinction. The PerAmp is supposedly only caused by periodic factors, such as the solar insolation and convection and further locally induced elements as, e.g., fog, cold air aggregation or local wind systems like land and sea breeze. All of the foresaid influences occur in a regular 24-hour periodicity. The DTR or aperiodic amplitude is, on the other hand, more or less strongly influenced by factors like, for e.g., wind speed and direction, precipitation and advection of cold or warm air masses, which are not bound to the 24 hour cycle of a day and not dependent on the local energy fluxes.

In the presented work we present climatologies of the PerAmp and DTR for different latitudes and altitudes. We show that the PerAmp, which can also be interpreted as the non-advective part of the DTR, is strongly connected to incoming SSR and other locally induced characteristics of the mean daily temperature cycle, such as atmospheric longwave radiation.

4.2   Data and methods

4.2.1   Deriving DTR and periodic amplitude

As stated in the introduction, the development of the daily temperature amplitude or DTR over time is a useful measure to identify changes in the energy balance. However, it has one major weakness, which is the appearance of the daily temperature extreme values due to the influence of advected air masses and not as a result of the local energy balance. The consequence of the advective component within the DTR is that it is hard to attribute the changes in DTR to a specific forcing, particularly when looking at local or regional scales. A solution was introduced by von Hann [1883] who suggested to use two different definitions of the daily temperature amplitude: one is due to a change within a 24-hour periodicity determined by discrete temperature measurements, and the other is the total daily amplitude determined by an extreme thermometer. He called the former the periodic (24-hour periodicity) and the latter the aperiodic amplitude. The aperiodic amplitude is nowadays known as DTR. It represents the overall difference between daily maximum and minimum temperature. The monthly mean or more general, the temporal mean DTR is given by,

$$\text{DTR} = \frac{1}{N_{days}} \sum_{d=1}^{N_{days}} (\max T_d - \min T_d) \qquad (4.1)$$

where $\max T_d$ and $\min T_d$ are the maximum and minimum temperature respectively, on day d of the month under consideration with N_{days} in total.

Von Hann [1883] defined the periodic amplitude (PerAmp) as the temperature difference between monthly mean warmest and coldest hours of the day. Consequently, PerAmp is caused directly and indirectly by the diurnal and seasonal variation in the solar elevation angle which is also influenced by long term changes in incoming surface solar radiation (SSR).

The striking point of von Hann's approach is the assumption that averaging the hourly temperature measurements ($\overline{T}_h$) to a month-long climatology of the daily temperature development should result in the removal of the mostly coincidental occurring advective influences that affect the diurnal cycle.

After the mean temperature, $\overline{T}_h = \frac{1}{N_{days}} \sum_{d=1}^{N_{days}} T_{d,h}$ of each hour (N_{days} representing the number of days of the month under consideration) has been calculated. PerAmp can be derived as follows,

$$\text{PerAmp} = \max_h \overline{T}_h - \min_h \overline{T}_h \qquad (4.2)$$

In Figure 4.1 a weather chart of a given month, containing hourly temperature records is indicated. The filled orange and green fields mark the occurrence of the minimum or

maximum temperature of each day. The difference of the mean of all daily maxima and minima gives the DTR. The PerAmp in contrast is derived from the mean warmest and mean coldest hour of the day so it represents the maximum and minimum of a month-long mean 24-hour temperature curve.

Figure 4.1 *Sketch of a temperature chart showing the values which are used to derive the diurnal temperature range (DTR) and the periodic amplitude (PerAmp). DTR is derived from the mean of all daily maxima (orange) minus the mean of all daily minima (orange). PerAmp is the difference of the monthly mean warmest (red frame) and the monthly mean coldest (blue frame) hour of the day.*

To further illustrate the overall idea, two extreme station examples shall be considered, the geographical South Pole and a station in the middle of the Sahara Desert. During the polar night no element of the local energy balance exists that could cause a 24-hour change in temperature. Therefore, all of the measured DTR is caused by advected air masses and thus the occurrence of the daily extremes is completely coincidental – at least from a daytime point of view. Also during the polar day the incident angle of the sun does not change considerably during 24 hours (here we are excluding the fact that the area at the South Pole is tilt against the horizon) so the measured temperature amplitude within 24 hours is again caused by advection.

A completely opposing example would be an imaginary place in the middle of the Sahara Desert where all of the measured DTR is purely due to the periodic influence of the solar zenith angle and heat retaining processes of the ground and lower troposphere. Consequently, the measured difference between mean daily maximum and mean daily minimum is periodic.

4.2.2   Data

The site selection was chosen to cover major climatic regions at various latitudes and altitudes and was influenced by the availability of hourly temperature observations for
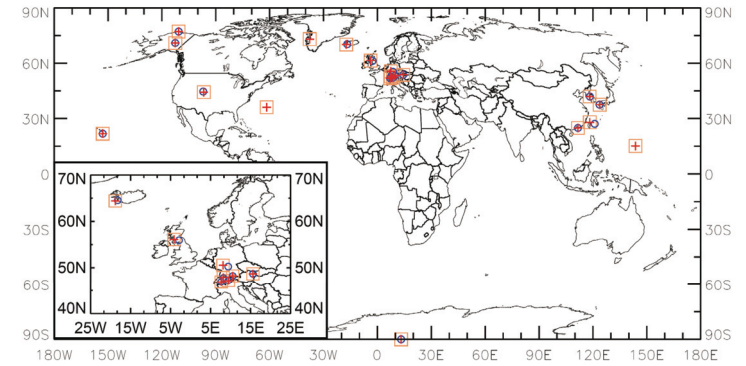
Figure 4.2 *Maps of the data used in the analyses. Red crosses indicate sites with hourly temperature and daily maximum and minimum temperature measurements. Blue circles give the location of the referring surface solar radiation measurement sites. The orange squares indicate the usage of ERA40 measurement data.*

calculating PerAmp. We consider changes in incoming SSR as the most important factor for changes in DTR and PerAmp since at most sites it is a dominant variable in the energy balance. Therefore, we tried to identify colocated long-term measurements of DTR, hourly air temperature and SSR (crosses and circles in Figure 4.2, Table 4.1).

Hourly, daily minimum and maximum air temperature
Probably the best sources for hourly and daily maximum and minimum air temperature data are the observations at airports. Due to the necessity of wide areas at and around the runways, the required ventilation in the measurement area is assured even if the airport is located close to or within urban areas. In order to obtain precise data we used hourly airport data of the US and allied forces, provided by AWIS Weather Services Inc., which gathered and formatted the data and performed extensive quality checks. To investigate the applicability in different altitudes we used data from the Swiss Federal Office of Meteorology and Climatology (MeteoSwiss). According to the availability of SSR data we obtained further high precision temperature measurements from meteorological observatories around the globe, amongst those Hohenpeissenberg (Germany), Wien - Hohe Warte (Austria), Hong Kong (China), Taipei (Taiwan) and the NOAA/ESRL Global Monitoring Division sites Barrow (Alaska, US), Mauna Loa (Hawaii, US) and South Pole. Since measurement data usually contains gaps, we interpolated hourly and daily values when values of the previous and following hour or day were available. In total we used about 7.5 million hourly values of which 0.8% are interpolated. The DTR data consists of more than 300 000 daily maximum and minimum values of which 0.11% (max) and 0.09%

Table 4.1 *Background information on the used sites and data. Identification codes (ID), latitudes (N (deg.)), longitudes (E (deg.)), altitude in meters above sea level (alt (masl)), years of available measurement data (Years), years of overlapping measurement (overlap) and distances between the temperature and next SSR site (Dist (km)) and the names of diurnal temperature range (Station name (DTR)) and surface solar radiation (Station name (SSR)) sites. If the SSR site is named ERA40 then no measured data is available and modeled (ERA40) data has been used instead.*

ID	Station name (Temp.)	N (deg.)	E (deg.)	alt (masl)	Years	Station name (SSR)	N (deg.)	E (deg.)	alt (masl)	Years	Dist (km)	overlap
BARW	Barrow	71.32	-156.6	11	77-03	Barrow	71.32	-156.6		51-74;77-04		26
BGSF	Kangerlussuag	67.02	-50.7	53	42-06	ERA40	67.02	-50.7		58-01		41
BIKF	Keflavik	63.97	-22.6	50	44-06	Reykjavik	64.13	-21.9	52	57-04	40	43
DAVS	Davos	46.8	9.83	1590	81-05	Davos	46.8	9.82	1592	78-05	3	25
EDDF	Frankfurt Main Intl.	50.05	8.6	112	47-06	Wuerzburg	49.77	9.97	275	59-05	100	29
EGPK	Prestwick	55.5	-4.58	20	49-61;73-06	Eskdalemuir	55.32	-3.2	242	56-05	92	36
HHPG	Hohenpeissenberg	47.8	11.02	977	70-04	Hohenpeissenberg	47.8	11.02	990	53-05		34
HOKO	Hong Kong	22.33	114.18	24	70-04	Hong Kong Obs.	22.32	114.17	65	69-78;84-05	10	25
JFJO	Jungfraujoch	46.55	7.97	3580	81-05	Jungfraujoch	46.55	7.97	3576	81-05		22
KBKF	Aurora Buckley Field	39.72	-104.75	1726	61-70;73-05	Boulder	40	-105.25	1609	77-05	57	29
MLOA	Mauna Loa	19.54	-155.58	3397	77-03	Mauna Loa	19.54	-155.58		77-04		23
PAFA	Fairbanks	64.82	-147.85	132.9	46-06	Fairbanks	64.82	-147.87	138	50-76		16
PGUA	Anderson AFB	13.57	144.93	185	49-06	ERA40	13.57	144.93		58-01		42
RJFF	Fukuoka Intl.	33.58	130.45	12	48-06	Fukuoka Intl.	33.58	130.38	3	60-05		43
RKSS	Gimpo Intl.	37.57	126.8	17	46-06	Seoul	37.57	126.98	86	86-05	15	18
SPOL	South Pole	-89.98	24.8	2810	77-03	South Pole	-89.98	24.8		77-04		23
TAIP	Taipei	25.07	121.55	6	71-04	Ishigkijima	24.33	124.17	6	64-05	280	32
TXKF	Bermuda	32.37	-64.68	6.1	42-06	ERA40	32.37	-64.68		58-01		39
VIEN	Vienna Hohe-Warte	48.25	16.37	203	70-04	Vienna Hohe-Warte	48.25	16.37	202	64-05		34
ZUER	Zurich	47.38	8.57	432	81-05	Zurich	47.38	8.57	556	81-05		25

were filled with interpolated values. While calculating monthly means of each hour of the day only days with at least 18 hours of available data were accepted. For the calculation of monthly mean values only months with at least 15 valid days were used for PerAmp and DTR data.

We further calculated seasonal and annual means to investigate the temporal connection between SSR and the two amplitudes. For the seasonal means no missing months were accepted. For the annual means we accepted three missing months of data that we subsequently filled with climatological values. This allowed us to retain at least 66% of the measured information. The climatologies of DTR and PerAmp were calculated for the period 1971-2000.

Surface solar radiation data

As stated above we consider changes in incoming SSR in the mean as the most important factor influencing the long-term characteristic of DTR and PerAmp. Therefore, we compared the obtained temperature amplitude data to surface solar radiation station data from the Global Energy Balance Archive (GEBA) [*Gilgen and Ohmura*, 1999] including additional stations (Mauna Loa Observatory, Barrow, South Pole, Boulder) from the NOAA/ESRL/GMD Solar and Thermal Radiation (STAR) group [*Dutton et al.*, 2006] (circles in Figure 4.2). Observations of temperature and SSR are mostly taken at the same town or even place. In some cases we accepted distances larger than a few kilometers, namely Keflavik/Reykjavik (40 km), Aurora Buckley Field/Boulder (57km), Prestwick/Eskdalemuir (92 km), Frankfurt/Wuerzburg (100 km) and Taipei/Ishigakijima

(280 km). At three sites (Kangerlussuag, Bermuda, Anderson AFB) no sufficient radiation data were available in a reasonable distance from the temperature measurement site. To provide data for these stations and additional information to all other sites, we derive SSR data from the corresponding grid cell (squares in Figure 4.2) of the ERA40 re-analysis data from the European Center for Medium-Range Weather Forecasts, ECMWF [*Uppala et al.*, 2005].

The measured SSR data mostly consists of monthly means from the GEBA database. The sites maintained by the STAR group provide hourly data from which we calculated monthly means if at least 50% measurements of each hour during the period of a month were available. At all sites the annual means were calculated when at least 50% of the originally measured monthly data were available. Missing monthly data were filled with climatological values of the 1971-2000 period. In total, we filled 131 months of the 9060 months from 20 sites. Consequently, 1.4% of the used data consist of filled values.

Comparing ERA40 and measured SSR

Before taking a closer look at the temporal development of SSR and the daily amplitudes, it seems worthwhile to comment on the climatologies of ERA40 and measured SSR as shown in Figure 4.3.

In Europe, SSR climatologies of the ERA40 reanalysis are in general underestimating measured annual SSR amplitudes. The underestimation increases with the seasonal insolation and the altitude, meaning the highest absolute underestimation could be found at the Jungfraujoch during the summer months. This result most likely reflects the influence of averaging various elements, such as altitude and cloud cover, over the area of a grid cell. The measurements at Frankfurt, Zurich and Vienna are in good agreement with the modeled SSR data. These stations are, in terms of altitude and surrounding landscape, representative for wider areas of central Europe. Besides Aurora – Buckley Field, Prestwick is the only mid latitudinal site where SSR was overestimated by ERA40 (note here that SSR is measured at Eskdalemuir). The largest disagreement found at Prestwick is as high as 50W/m^2 in June. In general the error is higher during the summer than during the winter months.

At the high latitudinal sites of the Northern Hemisphere the agreement between measured and modeled SSR in the climatologies is rather good. Largest under- and overestimations (+/- 20W/m^2 to +/- 25W/m^2) occur during the months with the highest amount of SSR. At the South Pole the measured and modeled SSR climatologies are in excellent agreement.

SSR at the rather exceptional site at Mauna Loa is clearly underestimated during each month of the year. Mauna Loa as a single peak in the middle of the Pacific destabilizes the surrounding atmosphere and causes regular condensation and precipitation. Because the measurement site is at a high altitude of 3397m a.s.l. it is mostly above clouds and fog. This effect, which increases SSR compared to the surrounding area, cannot be represented in the referring ERA40 grid cell.

At the Asian sites heterogeneous results are apparent. For example Taipei is fairly well represented by the ERA40 climatology. In contrast, at Seoul and Fukuoka, the SSR is massively overestimated, again most pronounced during the summer months. Since both sites are not at an unusual geographical location, it is likely that the model produces systematic errors, most probable are amounts of cloud cover which are too low.

The last station left to discuss is Hong Kong at which the comparison with the ERA40 climatology reveals severe deficiencies not only in total amount of SSR during one or the other months but also in the overall characteristic of the annual cycle. Unlike the other examples the months of June, July and August are reproduced best. All other months prior to and after that period are overestimated. The largest discrepancies occur in March and April and are as large as 60W/m^2.

Summarizing the comparison of measured and modeled SSR we conclude that in most cases the annual cycle is reproduced fairly well. The greatest under- or overestimations occur mostly during the season with the highest absolute amount of SSR. For the three stations of the dataset used in this article, which provide no SSR data, we are confident that the ERA40 estimates are a qualitatively good replacement for the measurement.

4.2.3   Methodology to compare DTR and PerAmp against SSR

We compare PerAmp and DTR to SSR to identify on the one hand which of the two amplitudes are more closely connected to SSR, and on the other hand, we aim to assess the possibility of deriving SSR from the temporal and spatially more commonly available temperature measurements.

The comparison between the mean daily temperature amplitudes DTR and PerAmp and SSR is done in a twofold way. First, we will investigate the climatologies of DTR and PerAmp and their comparability with the mean annual cycle of SSR (measurement data from GEBA where available, otherwise from ERA40). We aim to overlay the climatology data of SSR and DTR and PerAmp, respectively. For this purpose we minimized the total difference between the SSR and the investigated amplitude by shifting the amplitudes values in the y-direction, while stretching or compressing iteratively. Given in a simple formula, we minimized:

$$\sum_{i=1}^{12} | \text{SSR}_i - (\text{Amp}_i * \lambda + \bar{\mu}) |. \qquad (4.3)$$

Where λ is an iteratively changing factor and the variable $\bar{\mu}$ a stepwise changed constant, shifting the values in the y-direction (all amplitude values are multiplied and shifted with the same values during one step of iteration). The results are expressed in W/m^2 or MJ/m^2 indicating the lowest possible total difference between the investigated amplitude and the SSR. When trying to estimate SSR from DTR or PerAmp this difference could be best understood as error.

The second step of comparison though with less emphasis than the previously described analysis will be the correlation of station based time series on the scale of annual and seasonal means. We would like to point out that most likely some of the amplitude or SSR time series contain inhomogeneities which we did not account for. The homogenization of the data is in most cases not possible due to lack of information and parallel measurement. Therefore, we want to emphasize that the comparison of the time series needs to be interpreted most carefully. However, we still consider these conclusions too valuable to simply omit them.

4.3   Climatologies of daily amplitudes and radiation

We classified and arranged the different sites under investigation according to their climatological characteristics, thereafter latitude, longitude and altitude (Figure 4.2). The subgroups which we will hereinafter refer to can be summarized as follows:

1. subpolar and polar sites (Barrow, Fairbanks, Kangerlussuag, Keflavik, South Pole)

2. mid-latitudinal sites (Aurora Buckley Field, Prestwick, Frankfurt, Vienna,

Hohenpeissenberg, Zurich, Davos, Jungfraujoch)

3. subtropical sites (Hong Kong, Taipei, Seoul, Fukuoka)

4. tropical and subtropical island sites (Anderson AFB - Guam, Mauna Loa, Bermuda)

The mid-latitudinal sites include additionally a vertical profile of sites (Zurich 432m a.s.l., Davos 1590m a.s.l., Jungfraujoch 3580m a.s.l.) which are all within a horizontal distance of about 150km at most. Also one of the island sites, Mauna Loa 3397m a.s.l., provides information on high altitudinal behavior of the daily amplitudes and SSR.

4.3.1   Polar and subpolar sites of the Northern Hemisphere and the South Pole

Since we arranged the investigated sites according to their northward location in Figure 4.2 the arctic polar and subpolar sites can be found in the top row while the South Pole is located at the lower edge. A common characteristic of all sites is that at least one month has no or almost no measurable incoming SSR if still Fairbanks and Keflavik are located slightly south of the Polar Circle (Table 4.1). From this it follows that during this period the DTR can only be caused by advection, thus the PerAmp should be close to zero. The final form of the PerAmp at Barrow, Fairbanks and Keflavik is in close relationship to the "Fram"-type annual DTR cycle as described by Ohmura [1984]. In this article a description of the various influences of the different energy balance components of local origin that generate a double peak of the annual cycle which is a key feature of the "Fram"-type can be found.
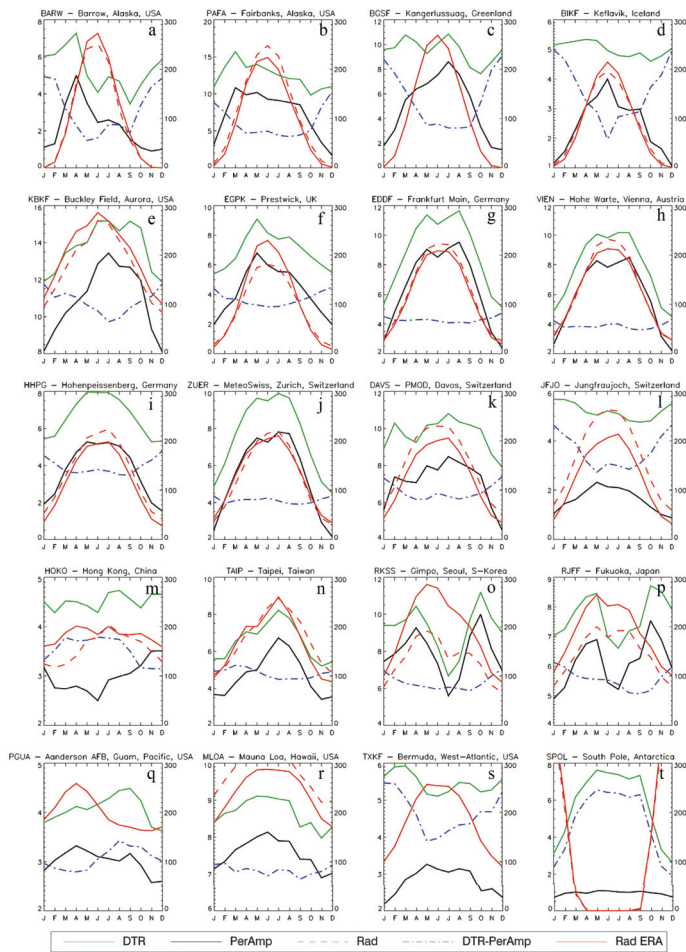
Figure 4.3 The annual mean cycles (climatologies) of diurnal temperature range (DTR) in solid green, the periodic amplitude (PerAmp) in solid black, the measured surface solar radiation (SSR) in dashed red, the modeled SSR (ERA40) in solid red and the difference between DTR and PerAmp, which can be interpreted as the advective influence on the daily temperature cycle (dashed, dotted blue).

Table 4.2 Sum of annual surface solar radiation (SSR) at the investigated sites and sums of total and relative minimum differences between annual cycles of SSR and periodic amplitude (PerAmp) or diurnal temperature range (DTR) respectively. Column 1 groups the sites according to their geographical character. Column 2 identification codes as defined in Table 4.1, column 3 the annual SSR as measured or modeled by ERA40, column 4 total error/difference when estimating SSR from PerAmp, column 5 relative difference given in %, column 6 and 7 as 4 and 5 but between SSR and DTR. Column 8, difference of relative errors (column 7-5).

		ann. SSR	tot. diff SSR vs. PerAmp		tot. diff SSR vs. DTR		SSR/PerAmp
	ID	MJ/m^2	MJ/m^2	%	MJ/m^2	%	-SSR/DTR
Arctic	BARW	3051.23	1527.32	50%	2559.42	84%	34%
	PAFA	3556.94	1254.84	35%	1962.80	55%	20%
	BGSF	3554.02	876.99	25%	2386.60	67%	42%
	BIKF	2774.10	470.97	17%	1966.77	71%	54%
Mid-latitudes	KBKF	5592.73	691.64	12%	690.90	12%	0%
	EGPK	2960.34	386.53	13%	473.72	16%	3%
	EDDF	3934.71	551.81	14%	490.58	12%	-2%
	VIEN	4079.29	555.47	14%	428.56	11%	-3%
	HHPG	4264.14	266.90	6%	211.18	5%	-1%
	ZUER	3914.59	412.85	11%	323.27	8%	-2%
	DAVS	4785.89	898.77	19%	1070.87	22%	4%
	JFJO	5262.26	379.55	7%	2100.70	40%	33%
Subtropics	HOKO	4929.30	803.67	16%	803.67	16%	0%
	TAIP	5525.03	353.94	6%	463.76	8%	2%
	RKSS	4161.79	1009.84	24%	1018.94	24%	0%
	RJFF	4585.69	1183.88	26%	1183.88	26%	0%
Islands	PGUA	6263.13	548.42	9%	854.92	14%	5%
	MLOA	8883.15	178.12	2%	327.19	4%	2%
	TXKF	5727.60	429.13	7%	1742.93	30%	23%
	SPOL	4069.59	4054.33	100%	4054.33	100%	0%

Indeed we found that in contrast to DTR the values of PerAmp dropped to values between 1°C and 2°C during the months without insolation (Figure 4.3a-d). At the South Pole there should be no daily cycle at all from a solar point of view since the change in incident angle

is negligible during 24 hours. Consistent with this consideration the PerAmp shows values around 1°C during the whole year in contrast to DTR, which increases with the daily mean temperature during the polar day (Figure 4.3t) indicating the increasing advective influence.

From the comparison of amplitude climatologies of the Northern Hemispheric polar and subpolar sites with the measured SSR climatologies, we found that we can reduce the error for estimates of SSR derived from PerAmp on average to a total of 1033MJ/m^2 (32%). This is about 37% less than the error of estimating SSR climatologies from DTR, which becomes as high as 2219MJ/m^2 or a total of 69% (Table 4.2). According to the statements above it is impossible to estimate SSR at the South Pole from either DTR or PerAmp, respectively. The minimized difference between the annual cycles of the amplitudes and the South Pole SSR is consequently 100% or 5405MJ/m^2.

4.3.2   The mid-latitudes including a vertical profile

In the mid-latitudes the relationship between DTR and SSR is rather close as presented for sites in the United States [*Bristow and Campbell*, 1984], Europe [*Makowski et al.*, 2009], Russia [*Roderick and Farquhar*, 2002] and China [*Liu et al.*, 2004b]. In the annual cycles of DTR and PerAmp at Prestwick, Frankfurt, Vienna, Zurich and Buckley Field a distinct warm season dip is apparent. This phenomenon has been described by Durre and Wallace [2001] for several sites in the eastern United States. The dip is caused by the summer depression in the maximum temperature due to evapotranspirative cooling (the lack of a coinciding depression in SSR evidences that it is not due to clouds). This is a purely locally caused phenomenon and is therefore also apparent in the PerAmp. In the mid- and high-altitudinal stations, such as Hohenpeissenberg, Davos and Jungfraujoch the warm season dip is pronounced in PerAmp compared with the DTR climatologies (see May, June, July minima in Figure 4.3i, k, l). The emphasis of the warm season dip at Frankfurt, Vienna, Hohenpeissenberg and Zurich (if is still nicely reproduced in PerAmp as locally influential factor on diurnal temperature cycle) causes a larger difference between PerAmp and SSR compared to DTR and SSR. However, the differences when trying to overlay daily amplitudes and SSR is extremely low. It is noteworthy that while approximating PerAmp and DTR to SSR of Zurich, Vienna and Frankfurt similar numbers that shifted, stretched or compressed the amplitude towards the SSR climatology, yielded the best fit. This points to a constant relationship between SSR and the daily amplitudes. The comparison of DTR and PerAmp with SSR differ within 4% at the max apart from one exception (JFJO). The largest difference when comparing the two amplitudes with SSR occurred at Jungfraujoch. Already from looking at the site's panel in Figure 4.3, it is obvious that the annual cycle of the PerAmp is much more closely connected to SSR than the DTR climatology. The difference between the two approximations is 33%. It results from as much as 40% or 2101MJ/m^2 difference between DTR and SSR but only 7% (380MJ/m^2) error between SSR and PerAmp in the best estimate.

4.3.3   Subtropical sites in South-East Asia

We aggregate four different Asian sites in this group all within a distance of 2000km of each other. Still the largest dissimilarities seem to be connected to the latitudinal location. Fukuoka and Gimpo/Seoul show amplitudes in the range of 7-10°C comparable to Taipei where DTR and PerAmp agree well with SSR. The most characteristic factor of the two more northerly located sites within this subset is the huge warm seasonal dip between May and September. In contrast to the European mid-latitudinal sites this decrease is also indicated in SSR showing the annual maximum already in May. This fact leads to the conclusion that it is not likely due to the influence of vegetation but rather by an increase in cloud cover due to the onset of the rainy season in June caused by the South-East Asian monsoon [*Arakawa*, 1969].

At Seoul and Fukuoka the temperature amplitudes could only be fitted with a minimum total error as large as 25% of the 4374MJ/m^2 (averaged, total radiation of Fukuoka and Seoul). The more southerly located sites Hong Kong and Taipei were much better reproducible by fitting the daily amplitudes to the annual SSR curve, 9% difference between PerAmp and SSR at Hong Kong and only 2% at Taipei. Looking at Figure 4.3l this result seems rather surprising for Hong Kong. The reason for the rather small difference is the fact that the SSR curve is very flat due to the relatively small changes in solar zenith angle throughout the year. At Taipei in contrast both DTR and PerAmp are closely connected to SSR (note here that the measured radiation data for Taipei was obtained from the Japanese island Isihigakijima) which shows a strong amplitude. The missing summer depression of the amplitudes is caused by the central and eastern ranges which exceed 3500m a.s.l. in the vicinity of Taipei. This high ridge causes a lee situation and reduces monsoonal summer rain [*Arakawa*, 1969] which would otherwise reduce DTR and PerAmp more intensively by cloud cover and evaporation.

4.3.4   Tropical and subtropical islands

The final subset consists of three island sites located between 32° N and 14° N. The most northerly located island, Bermuda shows a distinct annual cycle of SSR (Figure 4.3s). This annual cycle is, however, completely lacking in the DTR climatology, the PerAmp in contrast gives a much more realistic impression on the annual forcing of SSR. The total difference between SSR and PerAmp can consequently be reduced to 7% in contrast to the smallest error when fitting DTR against SSR. In the latter case the difference is 1743MJ/m^2 or as much as 30% of the radiation received during the complete year.

Looking at Figure 4.3q, which shows the annual cycles at Anderson Air Force Base (Guam), reveals that PerAmp is again more closely connected to the shortwave radiative forcing than DTR. The total errors sum up to 9% (PerAmp vs. SSR) and as much as 14% (DTR vs. SSR). The difference in errors is 307MJ/m^2, which is about 5% of the total annual SSR at Guam.

Rather unusual for an islands measurement site, the Mauna Loa Observatory is located at a height of 3397m a.s.l.. At the mid-latitudinal high mountain site, Jungfraujoch, the PerAmp showed a much better agreement with SSR than with DTR. At Mauna Loa the characteristic of the annual cycle of both daily temperature amplitudes is comparable. The minimized difference between SSR (highest one of all presented stations) and the two different temperature amplitudes sums up to only 2% between PerAmp and SSR and 4% between DTR and SSR. The influence of the height obviously outweighs the maritime influence, since absolute DTR and PerAmp values are more comparable to the size of values measured in Zurich or Prestwick than for example at Bermuda.

4.4 Time series of daily amplitudes and radiation

The following section focuses on the temporal correlation between SSR and the two investigated daily temperature amplitudes. As already mentioned in the data section we would like to emphasize that some of the investigated sites contain inhomogeneities in the daily temperature amplitudes. Obvious deficiencies can be seen in the temperature DTR time series of Fairbanks (PAFA) (not shown). Little pronounced but potentially erroneous shifts in the daily amplitudes were found at Taipei (TAIP) and Bermuda (TXKF).

When comparing both DTR and PerAmp to SSR, the inhomogeneities are less influential for the resulting correlation coefficients as long as they are just compared against each other. When interpreting the absolute values we want to point out that at least for the sites mentioned above, any interpretation should be judged most carefully. Furthermore, the number of compared data points is in general rather low and varies between the different station pairs. Information on the number of investigated data points can be found in Table 4.1. The number in the column 'overlap' gives the amount of years where both SSR and the referring amplitude value exist. We determined this measure only for the annual means since the data availability varies only slightly between the annual mean and the seasons.

In order to distinguish between the perennial to decadal and interannual agreement of the SSR with the two amplitudes, we detrended the time series and calculated the correlations between the high (interannual variability) and the low (perennial to decadal variability) frequency part of each series. To detrend the time series, a fit was determined by the robust locally weighted regression algorithm 'Lowess' [*Cleveland*, 1979].

In Tables 3 and 4 we summarized the correlation coefficients for annual mean and the seasons between SSR and PerAmp or DTR, respectively. To show if SSR correlates better with DTR or PerAmp we added the difference between the corresponding correlation coefficients. Bold numbers are giving 95% significant, italics emphasize negative correlation coefficients.

4.4.1 Short-term agreement between SSR and the daily amplitudes

In the perennial development during winter the SSR and the daily amplitudes, DTR and PerAmp correlate well (Table 4.3). This is especially evident in the mid latitudes

[*Makowski et al.*, 2009], the subtropics and partly at the islands and subpolar and polar sites. SSR agrees substantially better with PerAmp in spring and summer at almost all sites. In the annual mean the correlations between SSR and PerAmp are higher in all polar and subpolar sites as well as at the island sites. In autumn and winter SSR agrees better with DTR than with PerAmp, however as mentioned above, correlations in winter are in general low and not significant.

Table 4.3 *Correlation coefficients (R) between high frequency part of surface solar radiation (SSR) and periodic amplitude (PerAmp) and SSR and diurnal temperature range (DTR) time series. Column 1 station IDs. Columns 2-6 give correlation coefficients between SSR and PerAmp for the annual mean and each season. Columns 7-11 as columns 2-6 but for R between SSR and DTR. Bold numbers are significant at 95% level. Negative values are in italics. Columns 12-16 give the differences between columns 2-6 and 7-11.*

	R_SSR/PerAmp					R_SSR/DTR					R_SSR/PerAmp − R_SSR/DTR				
	ann	spr	sum	aut	win	ann	spr	sum	aut	win	ann	spr	sum	aut	win
BARW	.35	.29	**.50**	.13	.31	*-.22*	.07	*-.03*	.26	.13	.57	.22	.52	*-.13*	.19
PAFA	.23	*-.04*	.54	.00	*-.40*	*-.03*	*-.04*	.46	.15	*-.17*	.26	*-.01*	.08	*-.14*	*-.23*
BGSF	**.37**	**.47**	**.62**	.17	*-.03*	.16	**.44**	**.52**	**.42**	.09	.21	.03	.10	*-.25*	*-.12*
BIKF	**.50**	**.53**	**.64**	.29	*-.22*	.26	**.44**	**.59**	.20	.10	.24	.09	.06	.09	*-.32*
KBKF	.28	.31	**.54**	.27	.13	.27	.31	**.51**	**.38**	.10	*.01*	.00	.02	*-.11*	.03
EGPK	**.59**	**.54**	**.76**	.21	.19	**.40**	**.55**	**.67**	**.40**	.17	.20	*-.01*	.09	*-.19*	.02
EDDF	**.70**	**.69**	**.74**	**.61**	.05	**.76**	**.76**	**.68**	**.75**	.02	*-.06*	*-.06*	.06	*-.15*	.03
VIEN	**.66**	**.65**	**.71**	**.46**	*-.08*	**.60**	**.63**	**.67**	**.76**	*-.05*	.06	.03	.05	*-.30*	*-.03*
HHPG	**.63**	**.76**	**.68**	**.57**	.33	.33	.46	.56	.39	.31	.30	.30	.12	.18	.02
ZUER	**.74**	**.91**	**.76**	**.59**	*-.04*	**.77**	**.88**	**.72**	**.69**	*-.00*	*-.03*	.04	.03	*-.10*	*-.04*
DAVS	**.46**	**.50**	**.71**	**.54**	.27	**.53**	**.46**	**.66**	**.85**	.26	*-.08*	.04	.05	*-.31*	.01
JFJO	.17	.31	*-.19*	*-.21*	.04	*-.23*	.27	*-.24*	***-.56***	*-.20*	.40	.03	.05	.35	.24
HOKO	**.74**	**.89**	**.72**	**.49**	.08	**.69**	**.87**	.29	**.42**	.22	.06	.02	.43	.07	*-.14*
TAIP	**.57**	**.66**	**.61**	**.52**	.29	**.64**	**.69**	**.60**	**.62**	**.48**	*-.08*	*-.02*	.00	*-.10*	*-.19*
RKSS	**.66**	**.73**	**.56**	**.43**	*-.13*	**.65**	**.64**	**.56**	**.53**	*-.07*	.01	.10	.00	*-.10*	*-.05*
RJFF	.11	**.42**	**.51**	.10	*-.15*	.18	**.42**	**.45**	.27	*-.06*	*-.07*	.00	.06	*-.18*	*-.09*
PGUA	.01	**.31**	*-.06*	*-.23*	*-.13*	*-.08*	.14	*-.19*	*-.28*	*-.11*	.09	.17	.13	.05	*-.02*
MLOA	**.63**	**.73**	**.59**	**.66**	*-.12*	**.60**	**.68**	**.49**	**.78**	*-.07*	.04	.05	.09	*-.12*	*-.05*
TXKF	*-.20*	*-.13*	.01	**.32**	*-.21*	*-.28*	*-.25*	*-.27*	*-.14*	.04	.09	.13	.28	.46	*-.25*
SPOL	*-.10*	.11		*-.23*	***-.44***	*-.22*	***-.41***		*-.14*	*-.30*	.12	.52		*-.09*	*-.14*

4.4.2 Long-term agreement between SSR and the daily amplitudes

We also compared the filtered low frequency time series. The results are compiled in Table 4.4. In contrast to the short term fluctuation, SSR agrees well (correlates positively) with both DTR and PerAmp during winter. However, the correlations between SSR and PerAmp are higher than between SSR and DTR at most sites. Most subtropical sites show

Table 4.4 *as Table 4.3 but for low frequency part of the time series.*

	$R_{SSR/PerAmp}$					$R_{SSR/DTR}$					$R_{SSR/PerAmp} - R_{SSR/DTR}$				
	ann	spr	sum	aut	win	ann	spr	sum	aut	win	ann	spr	sum	aut	win
BARW	.86	.93	.84	.30	.78	.76	.76	-.38	.41	.76	.10	.17	1.22	-.11	.02
PAFA	.37	.12	.22	-.59	.71	.76	-.07	.31	.71	.22	-.39	.19	-.09	-1.30	.48
BGSF	.17	.38	.38	.65	.88	-.23	-.15	-.26	-.63	.88	.40	.53	.65	1.29	.00
BIKF	-.16	-.38	.28	-.67	.04	-.72	-.58	-.45	-.83	-.46	.56	.20	.73	.16	.50
KBKF	.77	.69	-.49	.60	.19	.71	.59	-.60	.71	-.33	.19	.09	.11	-.11	.52
EGPK	-.79	-.39	-.79	.07	.51	-.28	-.37	-.21	-.92	-.04	-.51	-.01	-.58	.99	.55
EDDF	-.13	-.59	-.59	.13	.30	-.55	-.60	-.05	-.18	.22	.42	.01	-.54	.31	.08
VIEN	.63	.74	.83	-.69	.81	.90	.95	.91	-.18	.72	-.27	-.21	-.07	-.51	.09
HHPG	.86	.64	.65	.74	.73	.50	-.17	.34	.81	.69	.37	.81	.32	-.07	.05
ZUER	-.35	.95	-.09	.78	-.08	-.58	.99	-.17	.61	.32	.23	-.04	.08	.17	-.40
DAVS	-.64	.53	.43	.87	.01	-.48	.50	-.43	.92	-.59	-.16	.03	.86	-.05	.60
JFJO	.14	.81	-.36	-.41	.71	.10	.54	-.33	-.42	.55	.04	.26	-.03	.00	.16
HOKO	.95	.87	.93	.60	.93	.95	.76	.84	.63	.93	-.01	.11	.09	-.03	-.00
TAIP	.69	.56	.25	.63	.91	.80	.65	.42	.91	.93	-.11	-.09	-.17	-.28	-.02
RKSS	.50	.55	.68	.57	.82	.43	.48	.64	.38	.69	.07	.07	.04	.19	.13
RJFF	-.04	.06	-.08	.04	-.69	-.07	-.07	.15	-.01	-.51	.03	.13	-.23	.05	-.18
PGUA	-.30	-.27	.18	-.29	-.73	-.29	-.32	-.15	-.19	-.66	-.01	.05	.33	-.10	-.07
MLOA	-.58	.22	-.30	-.32	.17	-.55	.20	-.29	-.09	.12	-.03	.01	-.02	-.22	.05
TXKF	-.66	-.46	-.46	-.87	-.58	-.87	-.90	-.82	-.93	-.74	.21	.43	.36	.06	.16
SPOL	-.75	-.00		-.94	-.82	-.54	-.64		.45	-.83	-.21	.64		-1.39	.01

significant, positive correlations in all seasons. In general, neither DTR nor PerAmp is more clearly closer connected to SSR. It is noticeable that at the island sites PerAmp and DTR correlate significantly negative with SSR in almost all seasons and in the annual mean.

4.5   Summary, Conclusions and Outlook

In this article we introduced and defined an alternative daily temperature amplitude measure other than DTR, named the PerAmp as suggested by Julius von Hann [1883]. PerAmp is designed to be more closely connected to the periodic solar forcing than DTR. Therefore we compared both DTR and PerAmp to SSR measurements. We found in general a close connection between radiation and both temperature amplitude measures.

When focusing on the annual mean cycle, PerAmp is substantially more closely related to SSR than DTR. We attribute this to the lower advective influence in the PerAmp compared to DTR. The largest improvements when estimating the SSR annual cycle from PerAmp could be found in the Arctic region where SSR could be estimated from PerAmp with

about 40% less error (total error 17-50%) than from DTR (total error 55-84%). In the mid-latitudes and subtropics both measures agree well with the SSR annual cycle. Typical estimation errors in the mid-latitudes are around 10-15% or 400-600MJ.

When comparing the temporal evolution of PerAmp and SSR we found that in the high frequency (interannual to perennial) variability DTR and PerAmp are mostly significantly correlated with SSR. Positive correlations between SSR and PerAmp are in more than 60% of the cases higher than between SSR and DTR. Regionally this is most evident in the Northern Hemisphere at the polar and subpolar sites. Looking at the high frequency variability from an annual and seasonal mean point of view, it is apparent that for 80% of the stations in spring and 100% of the stations in summer, the PerAmp correlates substantially higher with SSR than DTR.

In the low frequency, long term development we found highest agreement between SSR and the daily amplitudes in the Asian subtropical sites and partially in the Arctic where PerAmp is more highly correlated with SSR than DTR. Concerning the annual and seasonal mean focus of the low frequency (multi-annual to decadal) variability, higher agreement between PerAmp and SSR (than between DTR and SSR) is apparent in more than 60%. The superior performance of PerAmp is most pronounced in the strongly advective influenced seasons of spring (80% of the stations) and winter (75% of the stations). It is remarkable that SSR and both daily temperature amplitudes seem to be anti-correlated in the long-term variability at the investigated tropical and subtropical islands sites and at the South Pole. So far we did not find any reasonable explanation for this finding.

In summary, we state that PerAmp is more closely connected to SSR than to DTR. If a reconstruction of the annual cycle of radiation is necessary PerAmp is in most cases the best option to use. On a perennial to multidecadal scale PerAmp is more strongly related to SSR than to DTR. Overall the benefits when using PerAmp to reconstruct SSR will be potentially larger than deteriorations in cases where PerAmp agrees worse with SSR.

However, the amount of data which has to be obtained is an important issue to consider. In a next step we will try to advance Bristow and Campbell's [1984] relationship between SSR and homogenized data of DTR or PerAmp respectively, which will bring us closer to a reconstruction of SSR on spatial and temporal scales.

4.6   Acknowledgements

5 Conclusions and Outlook

5.1 Conclusions

This thesis has focused on the connections between surface solar radiation (SSR) and the daily temperature amplitudes: DTR and PerAmp, in Europe and on a global scale. However, more effort was put into the elaboration of changes of DTR since it is better known and well established in the scientific community. Most of the investigated data was measured or modeled for the second half of the 20th century and the early years of the 21st century. The changes of DTR, PerAmp and SSR and their interactions presented in this work are discussed under consideration of potentially influential factors, such as change in cloudiness or aerosol producing, anthropogenic emissions where possible.

In section 2 the trends of DTR in Europe were assessed under the assumption that SSR has changed substantially from decrease to increase. The trend analysis was confined to national boundaries; this accommodates the fact that anthropogenic emissions are bound to state law. The outcome shows that indeed different trend types occur for different regions within Europe, economically alike countries show alike DTR trends. Consequently a clear separation between Eastern and Western Europe became apparent. When focusing on the larger European nations with a substantial amount of industrial production and consequently emissions, the development of the annual mean DTR mirrors the increase and decrease of aerosol precursor emissions. Regarding the smaller nations it is apparent that transboundary transport is of considerable importance for the long-term trend behavior. From these findings it can be in general concluded that industrial emissions are a major factor influencing radiation and diurnal temperature range in Europe. A second major finding of the first section is that the DTR is not decreasing much but rather significantly increasing since the early 1980s in Europe. This contradicts the general opinion on decreasing DTR trends and questions the present argumentation on a global DTR decrease due to greenhouse gas and cloud forcing.

The subsequent logical step which has led to more insight on the subject of the thesis was to connect DTR and SSR quantitatively much rather than qualitatively as in section 2. The results are presented in detail in section 3. In this chapter of the thesis modeled and measured data in Europe were considered. We found exceptionally high correlation (correlation coefficients around 0.9) between SSR and DTR for the annual mean and seasonal mean European mean time series between 1970 and 2005. To identify the changes on perennial and multidecadal timescales a separation of the modeled and measured time series into high and low frequency components was performed. Thereafter, they were internally and crosswise compared. The results emphasize the strong connection between

DTR and SSR on interannual timescales. The seasonal agreement of the perennial fluctuations is connected to large scale circulative influence. This can be concluded from the finding, that the highest correlations at the individual investigated pairs of DTR and SSR sites unfold under the influence of the seasonally dependent storm-tracks. The correlations between DTR and SSR in measured and modeled data agree well, while in general the models produce incorrect absolute values and trend behavior. Both errors can be traced back to erroneous reproduction of absolute cloud cover and trends and the lack of temporal developing aerosol loads. The overall conclusions of section 3 are that DTR and SSR are indeed quantitatively closely connected and that models are capable of reproducing both measures and their relationship to one another realistically, given the preconditions that the forcings are introduced correctly.

The final chapter (section 4) is dedicated to the consideration that, at a given point on the globe, the close connection between the daily temperature amplitude and the incoming radiation is mainly disturbed by the influenced of advected air masses. An alternative daily temperature amplitude measure, the periodic amplitude (PerAmp) is introduced in section 4. PerAmp is designed to be less influence by advection than DTR. To elaborate this hypothesis it is thoroughly compared with SSR and DTR concerning its potential to be used aside DTR as an approximation measure for SSR. Discussed are the annual mean cycle and the behavior of the high and low frequency components of the time series measured at about 20 sites around the globe. We found that in the high frequency part of the data the SSR and PerAmp are mostly more closely correlated than SSR and DTR. This applies most prominent to Arctic sites. In the subtropics the agreement between SSR and both amplitudes in the low frequency part is remarkable. Concerning the mean annual cycles we can state that those determined by PerAmp are in most cases more closely connected to SSR than those from DTR, again this is most clearly in the Arctic. We conclude from the final section of the thesis that in regions with low incident angels throughout the year, advection plays an important role in the long term development of the daily temperature amplitude and therefore hinders DTR to be closely connected to SSR. If information about SSR is desired in those regions then the PerAmp can be of great value. Also, in other parts of the world PerAmp performed reasonably well compared with DTR. However, because PerAmp is derived from hourly measurement, the amount of data which needs to be obtained and processed is substantially higher than for DTR.

The findings in this thesis confirm in all sections the strong connection between radiation and the daily temperature amplitude as stated in the initial hypothesis. The final conclusions which can be derived from the above statement are:

Changes in SSR either caused by clouds or aerosols have altered and will in the future alter the daily temperature amplitude and therewith the mean temperature.

The daily temperature amplitude is connected close enough to SSR to enable rough estimates on the development of SSR in the past century.

5.2   Outlook

Following the above stated conclusions a major task will be to derive homogeneous DTR time series which can then help to separate the shortwave solar forcing from the longwave greenhouse gas warming. The fact that the air pollution agents, which alter SSR have changed over time from mixed carbonaceous and sulfurous to more sulfurous or from absorbing to more scattering, will be an issue to consider. Global datasets such as the Global historical climate network dataset (GHCN-D) of NCDC/NOAA or regionally restrained data sets such as the European Climate Assessment Dataset are available. However, a careful homogenization with methods as represented for example by Della-Marta [2006] are necessary.

Appendix A

Impact of surface solar dimming and brightening on global warming

Martin Wild, Atsumu Ohmura, Knut Makowski

Institute for Atmospheric and Climate Science, ETH Zürich, Universitätsstr. 16, CH-8092 Zürich, Switzerland

Abstract

Speculations on the impact of variations in surface solar radiation on global warming range from concerns that solar dimming has largely masked the full magnitude of greenhouse warming, to claims that the recent reversal from solar dimming to brightening rather than the greenhouse effect was responsible for the observed warming. To disentangle surface solar and greenhouse influences on global warming, trends in diurnal temperature range are analyzed. They suggest that solar dimming was effective in masking greenhouse warming, but only up to the 1980s, when dimming gradually transformed into brightening. Since then, the uncovered greenhouse effect has revealed its full dimension, as manifested in a rapid temperature rise (+0.38°C/decade over land since mid-1980s). Recent solar brightening cannot supersede the greenhouse effect as main cause of global warming, since land temperatures increased by 0.8°C from 1960 to 2000, even though solar brightening did not fully outweigh prior dimming over this period.

A.1   Introduction

Solar radiation reaching the ground is a key determinant of surface temperature. Various studies suggest that solar energy at the surface has not been stable over time but showed significant changes on decadal timescales [*Ohmura and Lang*, 1989; *Dutton et al.*, 1991; *Gilgen et al.*, 1998; *Stanhill and Cohen*, 2001; *Liepert*, 2002; *Wild et al.*, 2004; *Pinker et al.*, 2005; *Wild et al.*, 2005]. Such changes are likely to have an effect on surface

temperature [*Ramanathan et al.*, 2001; *Wild et al.*, 2005]. In addition, increased levels of atmospheric greenhouse gases are expected to result in an increased flux of thermal (longwave/terrestrial) radiation from the atmosphere to the surface, thereby reducing thermal cooling of the Earth surface and enhancing surface temperature according to greenhouse theory. Concerns have been raised that increases in aerosol from air pollution and associated dimming of surface solar radiation could have masked to a large extent the temperature rise induced by increasing greenhouse gases, so that the observed temperature records would not reflect the entire dimension of greenhouse warming [*Andreae et al.*, 2005]. This would imply that we underestimate the sensitivity of the climate system to increased levels of greenhouse gases, which has potentially major implications for predictions of future climate. On the other hand, the emerging evidence fore a widespread decline of solar dimming during the 1980s and reversal to a brightening thereafter [*Pinker et al.*, 2005; *Wild et al.*, 2005] may give raise to speculations that recent global warming could be due to surface solar brightening rather than the greenhouse effect. We intend to disentangle the effects of changes in surface solar and thermal (greenhouse) radiation on global warming in the following.

A.2   Observational data

We investigate this issue by using, in addition to the surface radiation data at the authors' institute from the Global Energy Balance Archive (GEBA) [*Gilgen and Ohmura*, 1999] and the Baseline Surface Radiation Network (BSRN) [*Ohmura et al.*, 1998], a gridded surface temperature dataset. This dataset is provided by the Climate Research Unit (CRU), University of East Anglia   and contains information on observed surface air temperatures over land on a 0.5° grid [*Mitchell and Jones*, 2005]. It includes mean, daily maximum and daily minimum temperatures on a monthly basis from 1900 to 2002. Annual values of global and hemispheric temperature estimates are approximately accurate to +/- 0.05°C (two standard errors) for the period since 1951 [*Brohan et al.*, 2006]. Surface radiation measurements from BSRN reach an absolute accuracy of 5 W/m2 in both surface downward solar and thermal radiation, with a 2 W/m2 relative accuracy (changing sensor sensitivity) [*Ohmura et al.*, 1998]. Historic radiation data from GEBA are of variable accuracy depending on the individual station [*Wild et al.*, 1995; *Gilgen et al.*, 1998]. We focus on land surfaces, where our knowledge of the common variation in surface radiation and temperature is best. We confine our analysis to the period from 1958, when widespread measurements of surface radiation were initiated during the International Geophysical Year (IGY), up to 2002, where data are available.

A.3   Effects of solar dimming and brightening on temperature changes 1958-2002

A.3.1   Change in land mean temperature

Annual mean temperature changes averaged over land surfaces from 1958 to 2002 as deviations from 1960 are determined in Figure A.1 from the CRU dataset. It is evident that the temperature rise was small in the first half of the period, but became significant during the second half. Since we estimated that trends in surface solar radiation showed a widespread reversal from dimming to brightening in the mid-1980s [*Wild et al.*, 2005], we subdivide the temperature records in two sections, before and after 1985.
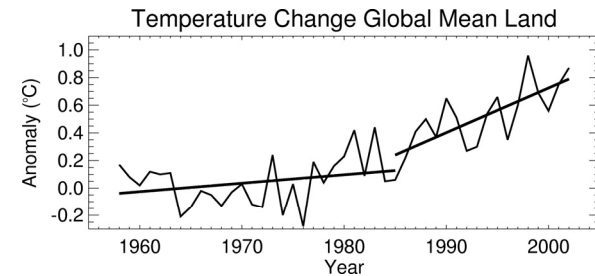

Figure A.1 Temperature change over the global land surfaces from 1958 to 2002 with respect to 1960. While the temperature rise during the period of solar dimming from the 1960s to the 1980s is moderate, temperature rise is more rapid in the last two decades where dimming was no more present. The time series is derived from CRU temperature dataset (Mitchell and Jones 2005).

Linear trends over the two periods 1958–1985 and 1985–2002 are given in Table A.1 In the timeframe 1958-1985, representing the period of solar dimming, only a marginal temperature increase is found (0.0036°C/year or 0.036°C/decade). The temperature increase during the period 1985-2002, where solar dimming was no longer effective, is an order of magnitude larger (0.038°C/year or 0.38°C/decade). This gives an indication that changes in surface solar radiation may have influenced the temperature evolution over the past decades and provides motivation to further investigate the relation between surface radiation and temperature.

A.3.2   Change in daily maximum and minimum temperature

To disentangle the influence of surface solar and thermal radiation on global warming, we need to focus not only on changes in mean temperature, but also on the daily temperature cycle. Thereby we use the fact that solar and thermal radiation, have different effects on the daily temperature cycle. Since the solar flux is only in effect during daylight, it affects the daily maximum temperature (TMAX) more than daily minimum temperature (TMIN).

The nighttime minimum temperature, on the other hand, is mainly affected by the thermal radiative exchanges. Nighttime surface radiative cooling depends on the capacity of the atmosphere to absorb and re-emit thermal radiation towards the surface. An analysis of TMIN and TMAX therefore holds the potential to separate the influence of solar and thermal radiation on surface temperature. Note that daytime temperatures are less sensitive to radiative changes than nighttime temperatures, since the radiative energy at the surface can be distributed more effectively by the turbulent fluxes of sensible and latent heat within the predominately convective daytime boundary layer, than during the predominantly stable nighttime conditions [*Ohmura*, 1984; *Dai et al.*, 1999].

Trends in TMIN and TMAX determined from the CRU dataset and averaged over land surface for the above two periods are given in Table A.1. It is remarkable that during the period with prevailing solar dimming 1958-1985, TMAX is declining. This decline is consistent with the decreasing availability of solar energy at the surface and supports the assumption that solar dimming had a discernible influence on surface temperature in this period. TMIN on the other hand, less affected by solar dimming, shows an increase, indicative of an increasing greenhouse forcing.

If we assume in a thought experiment that no solar dimming had occurred, one could assume that the mean temperature rise would not have been substantially different from the rise in TMIN (0.11°C/decade, a conservative estimate considering that dimming might also had a cooling effect on nighttime temperatures), Compared to the actually observed mean temperature increase of 0.036°C/decade, this would imply that solar dimming would have dampened the mean temperature rise on the order of 60 –70% between 1958 and 1985.

Table A.1 *Changes in mean, daily minimum and daily maximum temperature as well as diurnal temperature range over global land surfaces on an annual mean basis, for two periods: 1958 - 1985 and 1985-2002ₐ. Units are °C/decade.*

	1958-1985[b]	1985-2002[c]	relative changes
T mean	0.036 (0.04)	0.38 (0.08)	+0.34
T min	0.11 (0.04)	0.40 (0.08)	+0.29
T max	-0.04 (0.04)	0.37 (0.08)	+0.41
DTR	-0.15 (0.01)	-0.03 (0.02)	+0.12

[a]*Determined by linear regression, 1-sigma uncertainty estimates given in parentheses. Derived from CRU temperature dataset [Mitchell and Jones, 2005].* [b]*The period, where significant dimming of surface solar radiation has been observed.* [c]*The period where the dimming was no longer present [Wild et al., 2005].*

On the other hand, the period 1985-2002, during which solar dimming reversed into brightening, exhibits a significant increase in both TMAX and TMIN (Table A.1). The increase in TMAX and TMIN is in this period very similar, with the increase in TMAX being only slightly lower than in TMIN. The change in the linear slope from the 1958–

1985 to the 1985-2002 period, given in the last column of Table A.1, is thus larger in TMAX than TMIN. This implies that the increase in TMAX has caught up to the increase in TMIN, and is in line with the hypothesis that solar dimming was not present anymore to prevent TMAX from keeping pace with TMIN. Since temperature changes during daytime are less sensitive to radiative changes than during nighttime as outlined above, the similar rise in TMAX and TMIN suggests that during daytime the (solar and thermal) surface radiative forcing was at least as large as, or even larger than during nighttime. This is in line with the findings that solar dimming leveled off or transitioned to brightening noted in Wild et al. [2005].

A.3.3   Change in Diurnal temperature range

These tendencies are also evident in changes in the diurnal temperature range (DTR), defined as difference between TMAX and TMIN. In Figure A.2, we determined the change in annual land mean DTR for the same period 1958-2002 from the CRU dataset, with respect to the 1960-1990 mean. Several studies reported a decrease in this quantity over much of the 20th Century [*Karl et al.*, 1993; *Easterling et al.*, 1997; *Dai et al.*, 1999]. As a major factor an increasing cloud cover has been suggested, in line with the notion of a dimming of solar radiation. From Figure A.2 it becomes evident that the decrease of DTR over the global land surfaces only lasted into the mid-1980s, but then leveled off (cf. also DTR trends in Table A.1). This has also been noted in the recent study by Vose et al. [2005] with no further interpretation. Here we want to point to the striking similarity between the distinct change in the DTR regime during the 1980s in Figure A.2, and the simultaneous change in the surface solar radiation regime from dimming to brightening noted in Wild et al. [2005]. Thus, the evolution of DTR provides independent evidence for a large scale change in the surface radiative forcing regime during the 1980s.
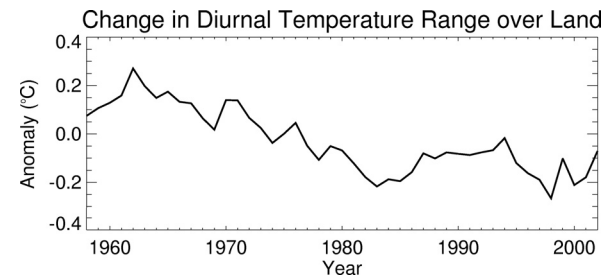

Figure A.2 *Change in diurnal temperature range averaged over the global land surfaces from 1958 to 2002, shown as deviations from the 1961-1990 mean. Diurnal temperature range decreases until the mid-1980 and levels off afterwards. The time series is derived from CRU temperature dataset (Mitchell and Jones 2005).*

To study the DTR evolution and its relation to surface radiative forcing on a more regional basis, we are in the process of collecting temperature records from a large number of meteorological stations in North America, Europe and Asia [*Makowski*, 2006]. At a majority of these widespread locations, the tendency for a recovery in the DTR is also seen on a station level, in line with the recovery of surface solar radiation [*Makowski*, 2006].

A.4   Discussion

Surface temperature may only effectively respond to changes in surface solar radiation, if these changes are caused by processes which change the total amount of solar energy absorbed in the climate system (such as through scattering aerosol, clouds reflectance or variations in the solar flux incident at the top of atmosphere) [*Ramanathan et al.*, 2001; *Wong et al.*, 2006]. However, if the surface radiation changes are merely caused by a redistribution of solar absorption between atmosphere and surface with little effect on the total amount absorbed in the climate system (such as through absorbing aerosol), the temperature change at the surface would be largely suppressed by an opposed temperature change in the energetically tightly coupled troposphere, thereby limiting changes in surface temperature despite changes in surface solar radiation. Latest emission inventories suggest that both scattering sulfur and absorbing black carbon aerosol showed large changes in line with surface solar radiation, with decreasing tendencies since the 1980s after decades of increase [*Stern*, 2006; *Streets et al.*, 2006]. This suggests that the variations in surface solar radiation are at least partly caused by scattering processes which change the total amount of solar energy absorbed in the climate system, and are therefore particularly effective in modifying surface temperature as outlined above.

Potential additional energy from solar brightening noted during the 1990s may not only have gone into heating of the surface, but also into additional evaporation. This is supported by pan evaporation measurements in energy-limited environments which partially indicate, after decades of decrease [*Ohmura and Wild*, 2002; *Roderick and Farquhar*, 2002], a recent recovery, in line with changes in surface solar radiation [e.g., *Liu et al.*, 2004a]. The rapid increase in land surface temperature despite evidence for a concurrent increase in evaporative surface cooling also implies a strong increase in surface radiative forcing in the 1990s.

Surface radiative forcing and temperature during the 1990s is not only determined by surface solar variations, but also strongly governed by the reduced thermal surface cooling with enhanced greenhouse capacity of the atmosphere, manifest in increased downward thermal radiation from the atmosphere to the surface. Evidence for increasing downward thermal radiation is obtained from the surface measurements of the BSRN [*Ohmura et al.*, 1998], a project of the World Climate Research Program (WCRP) with its data centre at the authors' institute, aimed at detecting important changes in the Earth's radiation fields. Downward thermal radiation measured at 12 worldwide distributed sites from BSRN shows on average an increase of 0.26 W/m^2 per year since the beginning of the measurements in 1992, in line with our expectations from greenhouse theory and models.

The increase in downward thermal radiation was found despite some indications for decreasing cloud amount during the 1990s [*Rossow and Duenas*, 2004].

To estimate the integrated (overall) effect of variations in surface solar radiation over the past 40 years, we analyzed the latest update of GEBA. In the majority of the surface solar radiation records from GEBA we find that, despite the widespread trend reversal from dimming to brightening, the amount of solar radiation at the surface has not reached the 1960 level. On average, the brightening has compensated for roughly 50% of the dimming since 1960. Despite the fact that surface insolation at the turn of the millennium is rather lower than in the 1960s, land surface temperatures have increased by 0.8°C over this period (Figure A.1). This suggests that the net effect of surface solar forcing over the past decades cannot be the principal driver behind the overall temperature increase, since over the past 40 years, cooling from solar dimming still outweighs warming from solar brightening. Rather, the overall temperature increase since the 1960s can be attributed to greenhouse forcing as also evident in the BSRN data outlined above. Thus, speculations that solar brightening rather than the greenhouse effect could have been the main cause of the overall global warming over the past decades appear unfounded.

A.5   Summary

In the present study we investigated the role of solar dimming and brightening in the context of recent global warming. Our analysis showed that the decadal changes of land mean surface temperature as well as TMAX, TMIN, and DTR are in line with the proposed transition in surface solar radiation from dimming to brightening during the 1980s and the increasing greenhouse forcing. This suggests that solar dimming was effective in masking greenhouse warming up to the mid 1980s, but not thereafter, when the dimming disappeared. The temperature response since the mid-1980s may therefore be a more genuine reflection of the greenhouse effect than during the decades before, which were subject to solar dimming. Unlike to the decades prior to the 1980s, the recent rapid temperature rise therefore no longer underrates the response of the climate system to greenhouse forcing and reflects the full magnitude of the greenhouse effect. This is also supported by observational records of increasing downward thermal radiation at the surface during the 1990s. The observed temperature increase of 0.38°C/decade over land surfaces since the mid-1980s may be in the upper range of sensitivity of the climate system to the recently imposed greenhouse forcing, since surface solar forcing enhanced rather than dampened the greenhouse-induced temperature increase in this period. On the other hand, the overall temperature increase of 0.8°C at land surfaces since the 1960s (corresponding to 0.2°C/decade) may pose a lower bound on the sensitivity of the climate system to greenhouse forcing over the past decades, since surface solar forcing over the entire past 40 years still decreased rather than increased, despite the recent recovery. This implies a substantial increase in thermal (greenhouse) surface radiative forcing since the 1960s, in order to enhance land surface temperatures by 0.8°C despite indications for a reduced heating due to surface solar changes over the past 40 years. We estimate therefore,

that the greenhouse forcing over the past decades has enhanced land surface temperatures by certainly more than 0.20°C per decade, but unlikely more than 0.38°C per decade. This may help to reduce the uncertainties in our knowledge on the sensitivity of the climate system to increasing levels of greenhouse gases, since it allows to disentangle the influence of surface solar radiation variations on global warming.

A.6   Acknowledgements

References

Abakumova, G. M., E. M. Feigelson, V. Russak, and V. V. Stadnik (1996), Evaluation of long-term changes in radiation, cloudiness, and surface temperature on the territory of the former soviet union, *Journal of Climate*, *9*(6), 1319-1327.

ALADIN International Team (1997), The ALADIN Project: Mesoscale modelling seen as a basic tool for weather forecasting and atmospheric research, *WMO Bulletin*, *46*(4), 317–324.

Alpert, P., P. Kishcha, Y. J. Kaufman, and R. Schwarzbard (2005), Global dimming or local dimming?: Effect of urbanization on sunlight availability, *Geophysical Research Letters*, *32*(17), Artn L17802, Doi 10.1029/2005gl023320.

Andreae, M. O., C. D. Jones, and P. M. Cox (2005), Strong present-day aerosol cooling implies a hot future, *Nature*, *435*(7046), 1187-1190, Doi 10.1038/Nature03671.

Arakawa, H. (Ed.) (1969), *Climates of Northern and Eastern Asia*, 248 pp., Elsevier, Amsterdam [etc.].

Beer, J., W. Mende, and R. Stellmacher (2000), The role of the sun in climate forcing, *Quaternary Science Reviews*, *19*(1-5), 403-415.

Berge, E., J. Bartnicki, K. Olendrzynski, and S. G. Tsyro (1999), Long-term trends in emissions and transboundary transport of acidifying air pollution in Europe, *Journal of Environmental Management*, *57*(1), 31-50.

Braganza, K., D. J. Karoly, and J. M. Arblaster (2004), Diurnal temperature range as an index of global climate change during the twentieth century, *Geophysical Research Letters*, *31*(13), Artn L13217, Doi 10.1029/2004gl019998.

Bristow, K. L., and G. S. Campbell (1984), On the Relationship between Incoming Solar-Radiation and Daily Maximum and Minimum Temperature, *Agricultural and Forest Meteorology*, *31*(2), 159-166.

Brohan, P., J. J. Kennedy, I. Harris, S. F. B. Tett, and P. D. Jones (2006), Uncertainty estimates in regional and global observed temperature changes: A new data set from 1850, *Journal of Geophysical Research-Atmospheres*, *111*(D12), Artn D12106, Doi 10.1029/2005jd006548.

Chiacchio, M., and M. Wild (2009), Long-term Seasonal Variations of Surface Solar Radiation in Europe, *Journal of Geophysical Research-Atmospheres*, in prep.

Christensen, J. H., O. Bossing Christensen, P. Lopez, E. Van Meijgaard, and M. Botzet (1996), The HIRHAM4 Regional Atmospheric Climate Model, *DMI - Scientific Report*, *96-4*.

Cleveland, W. S. (1979), Robust Locally Weighted Regression and Smoothing Scatterplots, *Journal of the American Statistical Association*, *74*(368), 829-836.

Dai, A., A. D. DelGenio, and I. Y. Fung (1997), Clouds, precipitation and temperature range, *Nature*, *386*(6626), 665-666.

Dai, A., K. E. Trenberth, and T. R. Karl (1999), Effects of clouds, soil moisture, precipitation, and water vapor on diurnal temperature range, *Journal of Climate*, *12*(8), 2451-2473.

Debruin, H. A. R., B. J. J. M. Vandenhurk, and D. Welgraven (1995), A Series of Global Radiation at Wageningen for 1928-1992, *International Journal of Climatology*, *15*(11), 1253-1272.

Della-Marta, P. M. (2006), A method of homogenizing the extremes and mean of daily temperature measurements, *Journal of Climate*, *19*(17), 4179-4197.

Durre, I., and J. M. Wallace (2001), The warm season dip in diurnal temperature range over the eastern United States, *Journal of Climate*, *14*(3), 354-360.

Dutton, E. G., R. S. Stone, D. W. Nelson, and B. G. Mendonca (1991), Recent Interannual Variations in Solar-Radiation, Cloudiness, and Surface-Temperature at the South-Pole, *Journal of Climate*, *4*(8), 848-858.

Dutton, E. G., D. W. Nelson, R. S. Stone, D. Longenecker, G. Carbaugh, J. M. Harris, and J. Wendell (2006), Decadal variations in surface solar irradiance as observed in a globally remote network, *Journal of Geophysical Research-Atmospheres*, *111*(D19), Artn D19101, Doi 10.1029/2005jd006901.

Easterling, D. R., B. Horton, P. D. Jones, T. C. Peterson, T. R. Karl, D. E. Parker, M. J. Salinger, V. Razuvayev, N. Plummer, P. Jamason, and C. K. Folland (1997), Maximum and minimum temperature trends for the globe, *Science*, *277*(5324), 364-367.

Eckhardt, S., A. Stohl, S. Beirle, N. Spichtinger, P. James, C. Forster, C. Junker, T. Wagner, U. Platt, and S. G. Jennings (2003), The North Atlantic Oscillation controls air pollution transport to the Arctic, *Atmospheric Chemistry and Physics*, *3*, 1769-1778.

Englehart, P. J., and A. V. Douglas (2005), Changing behavior in the diurnal range of surface air temperatures over Mexico, *Geophysical Research Letters*, *32*(1), Artn L01701, Doi 10.1029/2004gl021139.

Gilgen, H., M. Wild, and A. Ohmura (1998), Means and trends of shortwave irradiance at the surface estimated from global energy balance archive data, *Journal of Climate*, *11*(8), 2042-2061.

Gilgen, H., and A. Ohmura (1999), The Global Energy Balance Archive, *Bulletin of the American Meteorological Society*, *80*(5), 831-850.

Gilgen, H., A. Roesch, M. Wild, and A. Ohmura (2009), Decadal Changes in Shortwave Irradiance at the Surface in the Period from 1960 to 2000 Estimated from Global Energy Balance Archive Data, *Journal of Geophysical Research-Atmospheres*, *in press*, doi:10.1029/2008JD011383.

Giorgi, F., and L. O. Mearns (1999), Introduction to special section: Regional climate modeling revisited, *Journal of Geophysical Research-Atmospheres*, *104*(D6), 6335-6352.

Haylock, M. R., N. Hofstra, A. M. G. Klein Tank, E. J. Klok, P. D. Jones, and M. New (2008), A European daily high-resolution gridded dataset of surface temperature and precipitation for 1950-2006, *Journal of Geophysical Research-Atmospheres*, *113*, D20119, doi:10.1029/2008JD010201.

Jacob, D., B. J. J. M. Van den Hurk, U. Andrae, G. Elgered, C. Fortelius, L. P. Graham, S. D. Jackson, U. Karstens, C. Kopken, R. Lindau, R. Podzun, B. Rockel, F. Rubel, B. H. Sass, R. N. B. Smith, and X. Yang (2001), A comprehensive model inter-comparison study

investigating the water budget during the BALTEX-PIDCAP period, *Meteorology and Atmospheric Physics*, *77*(1-4), 19-43.

Jacob, D., L. Barring, O. B. Christensen, J. H. Christensen, M. de Castro, M. Deque, F. Giorgi, S. Hagemann, G. Lenderink, B. Rockel, E. Sanchez, C. Schar, S. I. Seneviratne, S. Somot, A. van Ulden, and B. van den Hurk (2007), An inter-comparison of regional climate models for Europe: model performance in present-day climate, *Climatic Change*, *81*, 31-52, DOI 10.1007/s10584-006-9213-4.

Jaeger, E., I. Anders, D. Lüthi, B. Rockel, C. Schär, and S. I. Seneviratne (2008), Analysis of ERA40-driven CLM simulations for Europe, *Meteorologische Zeitschrift*, *17*(4), 369-367.

Jones, C. G., U. Willen, A. Ullerstig, and U. Hansson (2004), The Rossby Centre Regional Atmospheric Climate Model part 1: Model climatology and performance for the present climate over Europe, *Ambio*, *33*(4-5), 199-210.

Jones, P. D. (1995), Maximum and Minimum Temperature Trends in Ireland, Italy, Thailand, Turkey and Bangladesh, *Atmospheric Research*, *37*(1-3), 67-78.

Karl, T. R., G. Kukla, and J. Gavin (1984), Decreasing Diurnal Temperature-Range in the United-States and Canada from 1941 through 1980, *Journal of Climate and Applied Meteorology*, *23*(11), 1489-1504.

Karl, T. R., G. Kukla, V. N. Razuvayev, M. J. Changery, R. G. Quayle, R. R. Heim, D. R. Easterling, and C. B. Fu (1991), Global Warming - Evidence for Asymmetric Diurnal Temperature-Change, *Geophysical Research Letters*, *18*(12), 2253-2256.

Karl, T. R., P. D. Jones, R. W. Knight, G. Kukla, N. Plummer, V. Razuvayev, K. P. Gallo, J. Lindseay, R. J. Charlson, and T. C. Peterson (1993), A New Perspective on Recent Global Warming - Asymmetric Trends of Daily Maximum and Minimum Temperature, *Bulletin of the American Meteorological Society*, *74*(6), 1007-1023.

Kjellström, E., L. Bärring, S. Gollvik, U. Hansson, C. Jones, P. Samuelsson, M. Rummukainen, A. Ullerstig, U. Willén, and K. Wyser (2005), A 140-year simulation of European climate with the new version of the Rossby Centre regional atmospheric climate model (RCA3), *SMHI Reports Meteorology and Climatology*, *108*, 54 pp.

Klein, H., and A. Benedictow (2006), EMEP MSC-W (Meteorological Synthesizing Centre-West) Data Note 1/2006: Transboundary data by main pollutants (S, N, O3) and PM.

Kukla, G., and T. R. Karl (1993), Nighttime Warming and the Greenhouse-Effect, *Environmental Science & Technology*, *27*(8), 1468-1474.

Lefohn, A. S., J. D. Husar, and R. B. Husar (1999), Estimating historical anthropogenic global sulfur emission patterns for the period 1850-1990, *Atmospheric Environment*, *33*(21), 3435-3444.

Lenderink, G., B. J. J. M. van den Hurk, E. van Meijgaard, A. van Ulden, and J. Cuijpers (2003), Simulation of present-day climate in RACMO2: first results and model developments, *KNMI Technical Report*, *252*, 24 pp.

Liepert, B. G., and G. J. Kukla (1997), Decline in global solar radiation with increased horizontal visibility in Germany between 1964 and 1990, *Journal of Climate*, *10*(9), 2391-2401.

Liepert, B. G. (2002), Observed reductions of surface solar radiation at sites in the United States and worldwide from 1961 to 1990, *Geophysical Research Letters*, *29*(10), Artn 1421, Doi 10.1029/2002gl014910.

Liu, B. H., M. Xu, M. Henderson, and W. G. Gong (2004a), A spatial analysis of pan evaporation trends in China, 1955-2000, *Journal of Geophysical Research-Atmospheres*, *109*(D15), Artn D15102, Doi 10.1029/2004jd004511.

Liu, B. H., M. Xu, M. Henderson, Y. Qi, and Y. Q. Li (2004b), Taking China's temperature: Daily range, warming trends, and regional variations, 1955-2000, *Journal of Climate*, *17*(22), 4453-4462.

Makowski, K. (2006), Veränderung der maximalen und minimalen Tagestempertauren im Bereich der nördlichen Hemisphäre, MSc thesis, 108 pp, University Zurich, Zurich.

Makowski, K., M. Wild, and A. Ohmura (2008), Diurnal temperature range over Europe between 1950 and 2005, *Atmospheric Chemistry and Physics*, *8*(21), 6483-6498.

Makowski, K., E. Jaeger, M. Chiacchio, M. Wild, T. Ewen, and A. Ohmura (2009), On the relationship between diurnal temperature range and surface solar radiation in Europe, *Journal of Geophysical Research-Atmospheres*, *in press*, 10.1029/2008JD011104.

Makowski, K., and A. Ohmura (2009), Diurnal temperature range, periodic amplitude and surface solar radiaton, *International Journal of Climatology*, *submitted*.

Marmer, E., B. Langmann, H. Fagerli, and V. Vestreng (2007), Direct shortwave radiative forcing of sulfate aerosol over Europe from 1900 to 2000, *Journal of Geophysical Research-Atmospheres*, *112*(D23), Artn D008037, Doi 10.1029/2006jd008037.

Mishchenko, M. I., I. V. Geogdzhayev, W. B. Rossow, B. Cairns, B. E. Carlson, A. A. Lacis, L. Liu, and L. D. Travis (2007), Long-term satellite record reveals likely recent aerosol trend, *Science*, *315*(5818), 1543-1543, DOI 10.1126/science.1136709.

Mitchell, T. D., and P. D. Jones (2005), An improved method of constructing a database of monthly climate observations and associated high-resolution grids, *International Journal of Climatology*, *25*(6), 693-712, Doi 10.1002/Joc.1181.

Mylona, S. (1996), Sulphur dioxide emissions in Europe 1880-1991 and their effect on sulphur concentrations and depositions, *Tellus Series B-Chemical and Physical Meteorology*, *48*(5), 662-689.

Norris, J. R., and M. Wild (2007), Trends in aerosol radiative effects over Europe inferred from observed cloud cover, solar "dimming" and solar "brightening", *Journal of Geophysical Research-Atmospheres*, *112*(D8), Artn D08214, Doi 10.1029/2006jd007794.

Ohmura, A. (1984), On the Cause of Fram Type Seasonal Change in Diurnal Amplitude of Air-Temperature in Polar-Regions, *Journal of Climatology*, *4*(3), 325-338.

Ohmura, A., and H. Lang (1989), Secular variations of global radiation in Europe, in *IRS '88: Current Problems in Atmospheric Radiation*, edited by J. Leonoble and J. F. Geleyn, pp. 298-301, A. Deepak Publ., Lille, France.

Ohmura, A., E. G. Dutton, B. Forgan, C. Frohlich, H. Gilgen, H. Hegner, A. Heimo, G. Konig-Langlo, B. McArthur, G. Muller, R. Philipona, R. Pinker, C. H. Whitlock, K. Dehne, and M. Wild (1998), Baseline Surface Radiation Network (BSRN/WCRP): New precision radiometry for climate research, *Bulletin of the American Meteorological Society*, *79*(10), 2115-2136.

Ohmura, A., and M. Wild (2002), Is the hydrological cycle accelerating?, *Science*, *298*(5597), 1345-1346.

Ohmura, A. (2006), Observed long-term variations of solar irradiance at the earth's surface, *Space Science Reviews*, *125*(1-4), 111-128, DOI 10.1007/s11214-006-9050-9.

Pal, J. S., F. Giorgi, X. Q. Bi, N. Elguindi, F. Solmon, X. J. Gao, S. A. Rauscher, R. Francisco, A. Zakey, J. Winter, M. Ashfaq, F. S. Syed, J. L. Bell, N. S. Diffenbaugh, J. Karmacharya, A. Konare, D. Martinez, R. P. da Rocha, L. C. Sloan, and A. L. Steiner (2007), Regional climate modeling for the developing world - The ICTP RegCM3 and RegCNET, *Bulletin of the American Meteorological Society*, *88*(9), 1395-1409, Doi 10.1175/Bams-88-9-1395.

Pinker, R. T., B. Zhang, and E. G. Dutton (2005), Do satellites detect trends in surface solar radiation?, *Science*, *308*(5723), 850-854, DOI 10.1126/science.1103159.

Plantico, M. S., T. R. Karl, G. Kukla, and J. Gavin (1990), Is Recent Climate Change across the United-States Related to Rising Levels of Anthropogenic Greenhouse Gases, *Journal of Geophysical Research-Atmospheres*, *95*(D10), 16617-16637.

Plummer, D. A., D. Caya, A. Frigon, H. Cote, M. Giguere, D. Paquin, S. Biner, R. Harvey, and R. De Elia (2006), Climate and climate change over North America as simulated by the Canadian RCM, *Journal of Climate*, *19*(13), 3112-3132.

Ramanathan, V., P. J. Crutzen, J. T. Kiehl, and D. Rosenfeld (2001), Atmosphere - Aerosols, climate, and the hydrological cycle, *Science*, *294*(5549), 2119-2124.

Robock, A., and H. B. Li (2006), Solar dimming and CO_2 effects on soil moisture trends, *Geophysical Research Letters*, *33*(20), Artn L20708, Doi 10.1029/2006gl027585.

Roderick, M. L., and G. D. Farquhar (2002), The cause of decreased pan evaporation over the past 50 years, *Science*, *298*(5597), 1410-1411.

Rossow, W. B., and E. N. Duenas (2004), The International Satellite Cloud Climatology Project (ISCCP) Web site - An online resource for research, *Bulletin of the American Meteorological Society*, *85*(2), 167-172, Doi 10.1175/Bams-85-2-167.

Sanchez-Lorenzo, A., M. Brunetti, J. Calbo, and J. Martin-Vide (2007), Recent spatial and temporal variability and trends of sunshine duration over the Iberian Peninsula from a homogenized data set, *Journal of Geophysical Research-Atmospheres*, *112*(D20), Artn D20115, Doi 10.1029/2007jd008677.

Sanchez-Lorenzo, A., J. Calbo, and J. Martin-Vide (2008), Spatial and Temporal Trends in Sunshine Duration over Western Europe (1938-2004), *Journal of Climate*, *21*(22), 6089-6098, Doi 10.1175/2008jcli2442.1.

Smith, S. J., H. Pitcher, and T. M. L. Wigley (2005), Future sulfur dioxide emissions, *Climatic Change*, *73*(3), 267-318, DOI 10.1007/s10584-005-6887-y.

Stanhill, G., and S. Cohen (2001), Global dimming: a review of the evidence for a widespread and significant reduction in global radiation with discussion of its probable causes and possible agricultural consequences, *Agricultural and Forest Meteorology*, *107*(4), 255-278.

Stanhill, G., and S. Cohen (2005), Solar radiation changes in the United States during the Twentieth Century: Evidence from sunshine measurements, *Journal of Climate*, *18*(10), 1503-1512.

Stenchikov, G. L., and A. Robock (1995), Diurnal asymmetry of climatic response to increased CO_2 and aerosols: Forcings and feedbacks, *Journal of Geophysical Research-Atmospheres*, *100*(D12), 26211-26227.

Steppeler, J., G. Doms, U. Schattler, H. W. Bitzer, A. Gassmann, U. Damrath, and G. Gregoric (2003), Meso-gamma scale forecasts using the nonhydrostatic model LM, *Meteorology and Atmospheric Physics*, *82*(1-4), 75-96, DOI 10.1007/s00703-001-0592-9.

Stern, D. I. (2006), Reversal of the trend in global anthropogenic sulfur emissions, *Global Environmental Change-Human and Policy Dimensions*, *16*(2), 207-220, DOI 10.1016/j.gloenvcha.2006.01.001.

Stone, D. A., and A. J. Weaver (2003), Factors contributing to diurnal temperature range trends in twentieth and twenty-first century simulations of the CCCma coupled model, *Climate Dynamics*, *20*(5), 435-445, DOI 10.1007/s00382-002-0288-y.

Streets, D. G., Y. Wu, and M. Chin (2006), Two-decadal aerosol trends as a likely explanation of the global dimming/brightening transition, *Geophysical Research Letters*, *33*(15), Artn L15806, Doi 10.1029/2006gl026471.

Tank, A. M. G. K., J. B. Wijngaard, G. P. Konnen, R. Bohm, G. Demaree, A. Gocheva, M. Mileta, S. Pashiardis, L. Hejkrlik, C. Kern-Hansen, R. Heino, P. Bessemoulin, G. Muller-Westermeier, M. Tzanakou, S. Szalai, T. Palsdottir, D. Fitzgerald, S. Rubin, M. Capaldo, M. Maugeri, A. Leitass, A. Bukantis, R. Aberfeld, A. F. V. Van Engelen, E. Forland, M. Mietus, F. Coelho, C. Mares, V. Razuvaev, E. Nieplova, T. Cegnar, J. A. Lopez, B. Dahlstrom, A. Moberg, W. Kirchhofer, A. Ceylan, O. Pachaliuk, L. V. Alexander, and P. Petrovic (2002), Daily dataset of 20th-century surface air temperature and precipitation series for the European Climate Assessment, *International Journal of Climatology*, *22*(12), 1441-1453, Doi 10.1002/Joc.773.

Teuling, A. J., M. Hirschi, A. Ohmura, M. Wild, M. Reichstein, P. Ciais, N. Buchmann, C. Ammann, L. Montagnani, A. D. Richardson, G. Wohlfahrt, and S. I. Seneviratne (2008), A regional perspective on trends in continental evaporation, *Geophysical Research Letters*, in press, Doi 10.1029/2008GL036584.

Trenberth, K. E., P. D. Jones, P. Ambenje, R. Bojariu, D. Easterling, A. Klein Tank, D. Parker, F. Rahimzadeh, J. A. Renwick, M. Rusticucci, B. Soden, and P. Zhai (2007), Observations: Surface and Atmospheric Climate Change., 987 pp.

Uppala, S. M., P. W. Kallberg, A. J. Simmons, U. Andrae, V. D. Bechtold, M. Fiorino, J. K. Gibson, J. Haseler, A. Hernandez, G. A. Kelly, X. Li, K. Onogi, S. Saarinen, N. Sokka, R. P. Allan, E. Andersson, K. Arpe, M. A. Balmaseda, A. C. M. Beljaars, L. Van De Berg, J. Bidlot, N. Bormann, S. Caires, F. Chevallier, A. Dethof, M. Dragosavac, M. Fisher, M. Fuentes, S. Hagemann, E. Holm, B. J. Hoskins, L. Isaksen, P. A. E. M. Janssen, R. Jenne, A. P. McNally, J. F. Mahfouf, J. J. Morcrette, N. A. Rayner, R. W. Saunders, P. Simon, A. Sterl, K. E. Trenberth, A. Untch, D. Vasiljevic, P. Viterbo, and J. Woollen (2005), The ERA-40 re-analysis, *Quarterly Journal of the Royal Meteorological Society*, *131*(612), 2961-3012, Doi 10.1256/Qj.04.176.

Vestreng, V., G. Myhre, H. Fagerli, S. Reis, and L. Tarrason (2007), Twenty-five years of continuous sulphur dioxide emission reduction in Europe, *Atmospheric Chemistry and Physics*, *7*(13), 3663-3681.

von Hann, J. (1883), *Handbuch der Klimatologie*, 764 pp., J. Engelhorn, Stuttgart.

Vose, R. S., D. R. Easterling, and B. Gleason (2005), Maximum and minimum temperature trends for the globe: An update through 2004, *Geophysical Research Letters*, *32*(23), Artn L23822, Doi 10.1029/2005gl024379.

Wild, M., A. Ohmura, H. Gilgen, and E. Roeckner (1995), Validation of General-Circulation Model Radiative Fluxes Using Surface Observations, *Journal of Climate*, *8*(5), 1309-1324.

Wild, M., A. Ohmura, H. Gilgen, and D. Rosenfeld (2004), On the consistency of trends in radiation and temperature records and implications for the global hydrological cycle, *Geophysical Research Letters*, *31*(11), Artn L11201, Doi 10.1029/2003gl019188.

Wild, M., H. Gilgen, A. Roesch, A. Ohmura, C. N. Long, E. G. Dutton, B. Forgan, A. Kallis, V. Russak, and A. Tsvetkov (2005), From dimming to brightening: Decadal changes in solar radiation at Earth's surface, *Science*, *308*(5723), 847-850, DOI 10.1126/science.1103215.

Wild, M., A. Ohmura, and K. Makowski (2007), Impact of global dimming and brightening on global warming, *Geophysical Research Letters*, *34*(4), L04702, Doi 10.1029/2006gl028031.

Wong, T., B. A. Wielicki, R. B. Lee, ., G. L. Smith, K. A. Bush, and J. K. Willis (2006), Reexamination of the observed decadal variability of the earth radiation budget using altitude-corrected ERBE/ERBS nonscanner WFOV data, *Journal of Climate*, *19*(16), 4028-4040.

Zhou, L. M., R. Dickinson, P. Dirmeyer, H. S. Chen, Y. J. Dai, and Y. H. Tian (2008), Asymmetric response of maximum and minimum temperatures to soil emissivity change over the Northern African Sahel in a GCM, *Geophysical Research Letters*, *35*(5), Artn L05402, Doi 10.1029/2007gl032953.

Acknowledgments

Curriculum Vitae

Knut Makowski, Limmatstrasse 103, 8005 Zürich, Knut.Makowski@gmail.com

born on 2nd of October 1979 in Rheinfelden (D), citizen of Germany

Education

2006 - 2009	PhD student at ETH Zurich, Institute for Atmospheric and Climate Science (supervisor: Prof. T. Peter)
2002 – 2005	Study of Geography, Diploma, University Zurich
	Diploma Thesis: Changes in monthly mean maximum & minimum surface air temperature throughout northern hemisphere. (in German)
2000 – 2002	Study of Geography, Pre-degree, University Basel
1990 – 1999	Scheffel Gymnasium, Abitur, Bad Säckingen

Work Experience and Services

Since 2009	PostDoc at ETH Zurich, Institute for Atmospheric and Climate Science
2004 – 2005	student assistant, Institute of machine tools and manufacturing, ETH Zürich
2004 – 2006	student assistant, Institute for nonmetallic inorganic materials, ETH Zürich
2003 – 2004	student assistant, Fachgruppe Simulation, Informatik und Materialflusstechnik, ETH Zürich
2000 – 2002	Geoterra Inc., Büro für Ingenieurgeologie, Hydrologie & Umweltgeologie
1999 – 2000	Military service, Pfullendorf, Sigmaringen, Todtnau Fahl

Teaching

Supervision of Master Thesis:

- Stefan Stauber „DTR and surface solar radiation in ERA40 and ENSEMBLES Regional Climate Model simulations", 2009.

Teaching Assistant:

- Climate Systems, Prof. Reto Knutti, Fall 2008

- Radiation and Climate Change, Prof. Heinz Blatter & Dr. Martin Wild, Spring 2008

Publications

Makowski, K. and A. Ohmura (2009). Diurnal temperature range, periodic amplitude and surface solar radiation, submitted to International Journal of Climatology

Makowski, K., E. B. Jaeger, M. Chiacchio, M. Wild, T. Ewen, and A. Ohmura (2008). On the relationship between diurnal temperature range and surface solar radiation in Europe, JGR - Atmospheres, J. Geophys. Res., 114, D00D07, doi: 10.1029/2008JD011104

Makowski, K., M. Wild, A. Ohmura (2008). Diurnal temperature range over Europe between 1950 and 2005, Atmos. Chem. Phys., 8, 6483-6498, 2008

Vonder Muehll, D., Noetzli, J., Roer, I., Makowski, K. and Delaloye, R. 2007. Permafrost in Switzerland 2002/2003 and 2003/2004, Glaciological Report (Permafrost) No. 4/5 of the Cryospheric Commission (CC) of the Swiss Academy of Sciences (SCNAT) and Department of Geography, University of Zurich, 106 pp. Glaciological Report (Permafrost) No. 4/5

Wild, M., A. Ohmura, and K. Makowski (2007), Impact of global dimming and brightening on global warming, Geophys. Res. Lett., 34, L04702, doi:10.1029/2006GL028031

Vonder Muehll, D., Noetzli, J., Makowski, K. and Delaloye, R. 2004. Permafrost in Switzerland 2000/2001 and 2001/2002, Glaciological Report (Permafrost) No. 2/3 of the Glaciological Commission (GC) of the Swiss Academy of Sciences (SAS) and Department of Geography, University of Zurich, 86 pp. Glaciological Report (Permafrost) No. 2/3

Oral Presentations

"On the relationship between diurnal temperature range and surface solar radiation in Europe" - European Geosciences Union, General Assembly, Vienna, April 2009

"Diurnal temperature range over Europe between 1950 and 2005" - European Geosciences Union, General Assembly, Vienna, April 2008

"Kühlelemente für das Klima - Wie kleinste Teilchen nicht nur unsere Gesundheit sondern auch unser Klima beeinflussen" - Kantonsschule Trogen, Trogen, 23. January 2008

"Kühlelemente für das Klima - Wie kleinste Teilchen nicht nur unsere Gesundheit sondern auch unser Klima beeinflussen" - 20 Jahre Departement Umweltwissenschaften, Zurich, 3. November 2007

"Global Erwärmung und Klimawandel" - Klimagipfel der Zürcher Jungparteien, Zürich, 3. October 2007

Poster Presentations

EGU General Assembly, Vienna, Austria, April 2008

Global Dimming and Brightening workshop, Ein Gedi, Israel, March 2008

9th Swiss Global Change Day, Berne, Switzerland, April 2008

AGU Fall meeting, San Francisco, United States, December, 2007

EGU General Assembly, Vienna Austria, April 2007

Workshop Climate Variability and Extremes during the past 100 years, Thun/Gwatt, Switzerland, July 2006